Functional Consequences of Model Complexity in Hybrid Neural-Microelectronic Circuits.

A Thesis
Presented to
The Academic Faculty

by

Michael Elliott Sorensen

In Partial Fulfillment
of the Requirements for the Degree
Doctor of Philosophy

School of Biomedical Engineering
Georgia Institute of Technology
March 21, 2005

Functional Consequences of Model Complexity in Hybrid Neural-Microelectronic Circuits.

Approved by:

Professor Stephen DeWeerth, Advisor
Department of Biomedical Engineering
Georgia Institute of Technology

Professor Ron Calabrese, Co-Advisor
Department of Biology
Emory University

Associate Professor Robert Butera
School of Electrical and Computer Engineering
Georgia Institute of Technology

Assistant Professor Robert Lee
Department of Biomedical Engineering
Georgia Institute of Technology

Professor Kurt Wiesenfeld
School of Physics
Georgia Institute of Technology

Date Approved: February 2005

For my wife, Betsey.

If anyone tells you that fire is light,

pay no attention.

ACKNOWLEDGEMENTS

The past five years have been the most challenging, frustrating, and rewarding of my life. I could never have completed this thesis without the support of my family, friends, teachers, and colleagues; to all of you I give my sincere thanks and appreciation.

Before all others, I must thank my parents, Tom and Bobbi Sorensen. They instilled in me a sense of individualism, a love of learning, and a moral grounding that have served me well my entire life. Without their guidance, encouragement, and love, I would not be the person I am today. Thank you, Mom and Dad.

And my thanks also to the rest of my family, my sister, Cara Sorensen, and my grandparents, Tobe and Roberta Cogswell, and Janet and Mike Rothberg, for always being there for me, and providing me with their wisdom and examples.

My thanks also to Judy McElroy, who took me on my first trip through the "Kingdom of Read".

My deep and sincere thanks to Dr. Suzanne Mazur, who taught me far more than chemistry. You taught me to really care about being smart. You taught me to be intellectually honest.

My thanks to Rice University and Jones College, who gave me something to care about more than grades or a degree.

To Dr. Peter Saggau, who gave me my first exposure to scientific research, who gave me the opportunity, the challenge, and the satisfaction to handle a project of my own.

To Brian Williams and Amber Burris, our support staff in the Laboratory for Neuroengineering.

To all the members of the DeWeerth group and Calabrese Lab who have provided me with their help or advice: Mario Simoni, Tina Hudson, Chuck Wilson, Edgar Brown, Mike

Reid, Alex Bragg, Shane Migliore, Carrie Williams, Kate Williams, Jim and Kyla Ross, Paul Garcia, Gennady Cymbalyuk, Anne-Elise Tobin, Adam Weaver, and Angela Wenning.

To Dr. Rob Butera and Dr. Robert Lee, who provided a great deal of help and advice in guiding this research.

To Dr. Ron Calbrese, my co-advisor, for trying (I hope not in vain) to make a neuroscientist out of an electrical engineer. You opened my eyes to a different world, and changed the way I thought. For that, you have my deepest gratitude.

To my advisor, Dr. Steve DeWeerth, for his continuous support and mentorship. With you I have learned how to communicate my ideas. I have learned to think critically about my own conclusions. I have learned how to be an independent researcher. Most importantly, I have become a better scientist. For all these things, you have my sincere and profound thanks.

And finally, to my wife, Betsey. You are my purpose, and my reason. I love you, darling.

TABLE OF CONTENTS

LIST OF TABLES

LIST OF FIGURES

SUMMARY

Hybrid neural-microelectronic systems, systems composed of biological neural networks and neuronal models, have great potential for the treatment of neural injury and disease. The utility of such systems will be ultimately determined by the ability of the engineered component to correctly replicate the function of biological neural networks. These models can take the form of mechanistic models, which reproduce neural function by describing the physiologic mechanisms that produce neural activity, and empirical models, which reproduce neural function through more simplified mathematical expressions.

We present our research into the role of model complexity in creating robust and flexible behaviors in hybrid systems. Beginning with a complex mechanistic model of a leech heartbeat interneuron, we create a series of three systematically reduced models that incorporate both mechanistic and empirical components. We then evaluate the robustness of these models to parameter variation, and assess the flexibility of the models' activities. The modeling studies are validated by incorporating both mechanistic and semi-empirical models in hybrid systems with a living leech heartbeat interneuron. Our results indicate that model complexity serves to increase both the robustness of the system and the ability of the system to produce flexible outputs.

CHAPTER I

INTRODUCTION AND BACKGROUND

The machines and inventions of mankind — while impressive in their power and scale — appear crude and ugly when compared to the elegant creations of nature. Consider the capabilities of a simple worker ant. The ant can navigate based upon visual and chemical cues in its environment, can traverse uneven terrain while carrying over thirty times its own weight, and runs on sugar water. No creation of mankind can be said to meet any of these impressive feats.

Nature can therefore serve as an effective teacher, instructing us in how to design technologies that allow us to treat disease, repair injuries, interact with our environment, and increase our productivity.

This idea is not without precedent. For centuries, mankind has used the designs of nature to inspire his own creations. Leonarda da Vinci studied the anatomy of birds and bats in his efforts to design gliders. George Cayley noted that birds' wings performed two separate functions, lift and thrust, and used this knowledge to build a manned glider. Wilbur and Orville Wright observed how birds' wings change shape to alter their lateral movement. These studies of how biology solves the problem of flight were all critical to the development of the airplane.

In fact, many people view evolution as a sort of "perfect engineer" designing a solution ideally suited for a given goal and constraints. Whether evolution may or may not be a perfect engineer, it is certainly a very, very good engineer, producing systems that are extremely well suited to solving certain problems.

1.1 Introduction

The nervous systems of animals are able to integrate vast amounts of information from the animal's internal and external environment, and produce responses to regulate and control a wide variety of physiological processes. The power and flexibility of nervous systems is produced in part by the massive parallel structure and integrative capabilities of the system. But another key factor is that even small circuits of neurons, or individual neurons themselves, can demonstrate an amazing degree of complexity in their behavior. By studying the nervous system and basing new technologies on neural-like properties, we can develop new methods to treat neurodegenerative disease, repair traumatic neural injury, and create machines that better interact with the physical world.

In order to better understand the workings of the nervous system, however, it is necessary to develop a quantitative description of the workings of the nervous system: a neural model. Fortunately, although neurons demonstrate a great deal of functional and mechanistic complexity, their electrical activity can be approximated by simplified models. There are two basic types of neural models: empirical models and mechanistic models.

Empirical models take a "black box" approach to describing neural function. This approach assumes no underlying structure for relating a neuron's inputs to its output. The model is deemed "good" as long as its input-output relationship corresponds to that observed in biology. Empirical modeling therefore seeks to reproduce the function of a given neuron or neural system, often through the simplest means possible.

Mechanistic models reproduce the input-output relationships of biological neurons by describing the biophysical processes responsible for the generation of neuroelectric activity. The behavior of the model derives from a neuron-like structure. Mechanistic models are usually much more complex than their empirical counterparts. They are, however, able to provide insight into the inner workings of a neuron or neural system that are not possible with empirical models. Mechanistic modeling often assumes that the biophysical structure of the neuron is important to its function.

Ultimately, the choice of modeling strategy is dependent upon the context in which that model is to be used. Determining the “best” model for a given application requires evaluating the tradeoff between model *simplicity* and model *accuracy*. A simple model may not be able to provide the necessary functionality, while an overly complex model may inhibit one’s ability to study or control the system.

An emerging area in which model choice plays a crucial role is in the development of *hybrid neural microsystems*: systems in which neural models and living neurons interact in real-time. These systems exploit biology as part of the technology, creating a functional result that is a product of both the biology and the engineered construct. The assumed benefit of such a system is that the complex dynamics and functionality of the living neurons are left intact, while the model provides a means to manipulate and control the system. In such a system the model component needs both to correctly interpret signals coming from the living neurons and to produce a meaningful response to those signals. Obviously, the choice of model in such a system is of critical importance.

Two characteristics of neural systems that must be reproduced by such hybrid systems are *robustness* and *flexibility*. Robustness can be considered as the size of the system’s input/parameter space; the nervous system is able to function reliably despite the ever-present "noise" of physiologic processes: changing concentration gradients, errors in transcription, etc. Flexibility can be considered as the size of the system’s ouput/behavior space; neural systems are able to produce a rich variety of behaviors in order to achieve their function. In order for hybrid systems to accurately reproduce the function of neural systems, it is critical that the models employed in such systems contribute to operation that is both robust and flexible.

1.1.1 Specific Aims

Our *long-term goal* is to develop the techniques and methodologies for creating hybrid systems that accurately reproduce the function of biological neural networks. The *objective*

of this research is to determine how the performance of hybrid systems is affected as the complexity of the model is reduced. Our *hypothesis* is that reducing the complexity of the model will both decrease the *robustness* of the system and decrease the *flexibility* of the system. Towards this end, we propose the following specific aims:

1. **Create a hybrid half-center oscillator for investigating neural network properties.** As an initial step towards building hybrid neuro-microelectronic systems, we will create a hybrid system composed of a single biological neuron and an analog circuit model neuron already developed within our group. This aim will serve several goals. First, it will familiarize us with the neurophysiological and engineering techniques necessary to build hybrid neural circuits. Second, by using a physiological model neuron and basing the structure of the hybrid network on that of a biological network, we will be able to use the controllability of the model neuron to investigate neuronal properties responsible for generation of activity in the network.

2. **Construct a flexible platform for interfacing real-time model neurons to living neurons.** In order to interface a variety of neuronal models with living neurons, we need to construct a platform for modeling that meets several criteria. First, it must have a means to communicate with the equipment used for recording and stimulating living neurons. Second, it must allow all neuronal models to operate in real-time. Finally, the architecture of the platform must accommodate a variety of neuronal model structures — the underlying dynamics of the neuronal model must be modifiable.

3. **Develop a series of systematically reduced neural models.** Starting with a previously developed physiologically realistic neuron model, we will perform a series of systematic reductions in the complexity of the model. These reduced models will encompass both physiologic and empirical mechanisms. We will the evaluate the models for their ability to produce robust and flexible behavior.

4. **Validate neural models with hybrid systems.** Using the reduced models developed in Aim 3, we will construct at hybrid systems using our reduced model neurons, and evaluate the ability of these systems to produce robust and flexible behavior.

1.2 Background and Significance

This project draws from three subject areas: modeling neural systems, the dynamics of rhythmic neural networks, and the electrophysiological techniques to bring models and neurons together.

1.2.1 Modeling Neural Systems

Neurons display an incredible diversity of activities, behaviors, and functions. In most neurons, there are numerous ion channel types, modulatory agents, and spatial processing structures that contribute to the behavior of the neuron. Despite this extraordinary amount of complexity, the electrical activity of a neuron can often be described by a simplified system of equations — a neural model. Neural modeling seeks to relate neural function to a mathematical structure that provides insight to the operation of the system.

The rationale for modeling a neuron is the same as for modeling any physical system: a model allows the operator to better analyze or understand the physical system without the constraints of the physical system. In the case of the nervous system, analysis and understanding of neuronal properties are very compelling reasons to create a neural model because many neuronal properties are physically inaccessible with current technology. As an example, it is very difficult to record with high precision from numerous individual

neurons in a large neural network; a model neural network, however, can provide us with detailed information about the behavior of individual neurons. A model therefore provides us with a means to understand how a physical system works, what function it accomplishes, and what properties and parameters are necessary for its operation and control.

The requirements for a neural model are also the same as for any model of a physical system: the model must be simple enough to be understandable, but also accurately portray the relevant aspects of the physical system. Which aspects are relevant and what criteria constitutes a "good" model are left to the discretion of the modeler. While a simple model may produce the desired results, it may not provide enough insight into the workings of the system to be of much use. Alternatively, the detail of information in a complex model may prohibit effective analysis. This trade-off is the fundamental decision that must be made in modeling any physical system: model simplicity vs. model accuracy.

It is not surprising that there are a wide variety of neural models, from the extremely simple to the incredibly complex. At the risk of over-simplification, we will separate these models into two categories: empirical models and mechanistic models (Figure 1).

Empirical models, also known as nonparametric models, take a "black box" approach to describing neural function. This approach assumes no underlying structure for relating a neuron's inputs to its output. An empirical model is considered to be a "good" model as long as its input-output relationship corresponds to that observed in biology. An underlying assumption of empirical neural modeling is that the function of a neuron is distinct from the mechanisms used to produce that function. Given the constraints of physics, chemistry, and genetics, it is not surprising that complex mechanisms may be needed to achieve a functionally simple result. As an example, consider the transduction of light into electrical potentials by photoreceptors in the retina. This process is dependent on several complex biochemical reactions, involving numerous enzymes and proteins. The conversion of light energy to electric energy by a photodiode, in comparison, seems rather simple. Mathematical neuronal models, which are free from all physical constraints, can seek the most

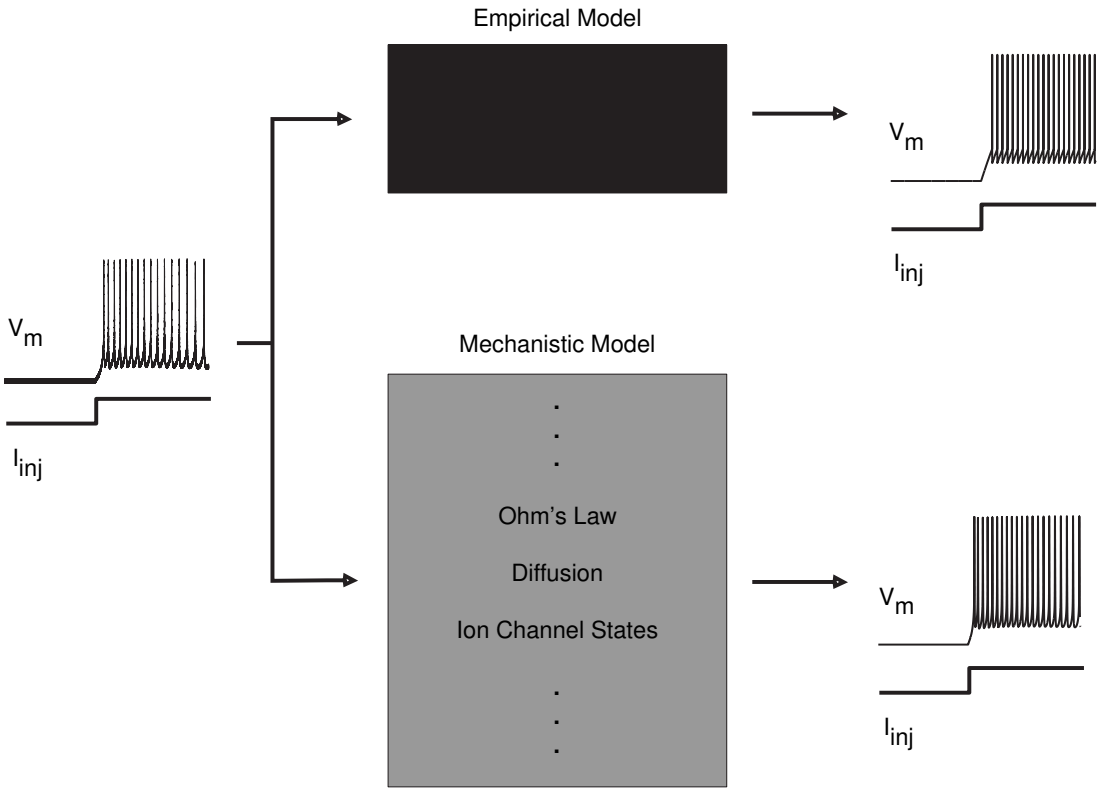

Figure 1: Empirical neural model (black box) utilize any convenient mathematical structure to describe neuronal function. Mechanistic neural models (grey box) utilize known physical properties of the system to describe neuronal function.

straightforward way to describe a neuron's activity. Empirical modeling therefore seeks to reproduce only the function of a given neuron or neural system, often through the simplest means possible.

The classical integrate-and-fire neuron model is an excellent example of an empirical neuron model [19]. In this model, the neuron simply integrates a current input until a certain threshold voltage is reached. The neuron then "spikes" , its voltage is reset to some value, and the integrate-and-fire process continues. The integrate-and-fire model thereby provides a good description of the relationship between current input and spiking frequency: as the magnitude of the current increases, the time required to reach firing threshold decreases, and therefore the spike frequency increases. The Fitzhugh-Nagumo and Hindmarsch-Rose models are other good examples of empirical neural models [8, 30]. Another excellent example of an empirical model is the resonate-and-fire model, which

describes how neurons can respond preferentially to stimuli given during a certain phase of their oscillation [17].

The distinct advantage of empirical models is that are relatively easy to analyze and require little computational overhead. The disadvantage of these models is that while they describe *what* a neuron does they do not explain *how* a neuron does it. For example, the integrate-and-fire model neuron would correctly predict that lowering the spike threshold would increase the resultant spike frequency but would not be able to explain how spike threshold could be lowered in a real neuron.

Mechanistic models, which are also known as also known as physiological or parametric models, reproduce the input-output relationships of biological neurons by describing the biophysical processes responsible for the generation of neuro-electric activity, and the behavior of the model derives from a neuron-like structure. They incorporate known physical and chemical laws to describe both the activity of a neuron and the process by which the neuron generates that activity. Mechanistic models are usually much more complex than their empirical counterparts. They are, however, able to provide insight into the inner workings of a neuron or neural system that are not possible with empirical models. Mechanistic modeling often assumes that the biophysical structure of the neuron is important to its function. As a result, they can not only *describe* a neuron's behavior but also *predict* the neuron's behavior under altered conditions.

The standard method for mechanistic neural modeling is based on the Hodgkin-Huxley formalism [16]. This method of mechanistic modeling describes the activation and inactivation of voltage-dependent ion channels in a neuron's membrane. Ions move across the membrane dependent upon the state of the channel and the chemical and electrical forces upon the ion; in turn, the movement of the ions across the capacitative membrane of the neuron changes the neuron's membrane potential, altering the state of the ion channels.

The advantage of mechanistic modeling is that the structure and parameters of the model correspond with physical properties of the neuron itself, and thus describe not only

what the neuron does, but also *how* the neuron does it. Continuing our spike threshold example, increasing the density of the fast sodium current would effectively lower spike threshold, leading to an increase in spike frequency for a spiking neuron. Because of the physiological approach to modeling, we know not only that lowering the spike threshold increases firing frequency, but also how a living neuron might accomplish this feat. Furthermore, because the interaction of different physiological processes is taken into account we often find that modifying one parameter has a significant effect on how *another* parameter effects the system. The disadvantage of mechanistic modeling is that it generally requires far more computational resources than a simplified empirical model. Furthermore, the large number of equations and parameters necessary often make effective analysis of the model very difficult.

These two neural modeling strategies illustrate the classic trade-off in modeling physical systems. The simplicity of empirical models facilitates implementation and analysis; the accuracy of mechanistic models provides greater insight into the the form and function of living neurons. Of course, *every* model is, at some point, a simplification of the physical system. A modeler who studies the physical biochemistry of ion chances might say that Hodgkin-Huxley type neural models are overly simplistic. Nonetheless, there is a significant difference between models that assume *no* underlying structure and models that incorporate *some* of the known structure of neurons into their operation; and as more of the neural structure is incroporated into the model, the model's accuracy increases, while the model's simplicity decreases.

Given this trade-off, it is not surprising that many modelers have sought to find an approach to modelling that bridges the empirical and mechanistic strategies. The goal of this approach is to reduce the complexity of mechanistic models while still retaining their physiological relevance and insight into neuronal function.

One of the simplest methods to reduce neural model complexity is to eliminate conductances to a smaller set that produce the desired feature or features of neural behavior.

The oscillatory Morris-Lecar model is good example of this type of model [28]. Although Morris and Lecar originally designed their model to describe slow action potentials in the barnacle muscle fiber, the reduced set of conductances they use has proven extremely useful for describe oscillatory phenomena in small neural networks. For example, this model has been used very effectively to demonstrate the "escape" and "release" mechanisms responsible for creating oscillations in a two-neuron network [45]. Other techniques for model reduction include combining several variables with similar dynamics into one variable [18, 10], separating the model into fast and slow subsystems and characterizing their interactions [3], or even replacing the fast variables with an integrate-and-fire model and quantifying the effects of spiking on the evolution of the slow variables [2]. All of these methods provide a means to reduce the complexity of a model while still retaining much of its physiological relevance.

1.2.2 Rhythmic Neural Networks and the Leech Heartbeat Timing Network

Rhythmic neurons and neural networks are characterized by the regular appearance of a particular pattern of activity. They are found in nearly all nervous systems, and are implicated in a diverse range of behaviors and activities. Although they are critical for the formation of locomotor actions and other movements, rhythmic pattern generating networks are also involved in such diverse phenomena as visual processing, olfaction, memory, and sleep.

There are therefore two extremely compelling reasons to study rhythmic neural networks. First, their production of a sterotypic activity pattern provides a well-defined baseline of activity. Applying a stimulus to the network often has a distinct effect on the timing relationship between the different elements of the network. Because we have a well-defined baseline of activity and a well-defined response, we can make strong conclusions about the relationship between the inputs and outputs of the network and how neural networks process information. Second, the ubiquity of rhythmic neural networks across numerous systems and species demonstrates that they are a critical component of animal life. In order

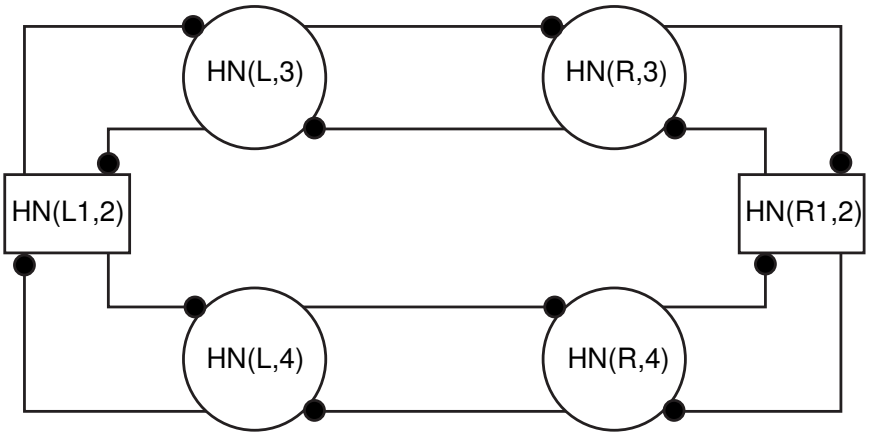

Figure 2: The Central pattern generator for the leech heartbeat timing network. Two heart interneurons in ganglia three and four (circles) are coupled via inhibitory synapses to form a half-center oscillator. Coordinating interneurons from ganglia one and two (rectangles) couple the two half-center oscillators.

to fully understand the behaviors and activities produced by these networks, it is critical to understand the mechanisms by which oscillatory circuits function [27].

One rhythmic network that has been particularly well studied is the network that paces the heartbeat in the medicinal leech. This network produces a pattern of activity that is relatively simple; the generation of this pattern, however, relies on the interaction of numerous complex mechanisms, both intrinsic and synaptic. The network has a very well-defined and symmetric synaptic structure, with a few core elements that produce a rhythmic pattern that paces the rest of the network. The central timing of this network is generated by two *elemental oscillators* in the third and fourth ganglia of the leech [14, 15]. Each elemental oscillator is composed of two *heart interneurons* (HN) that are connected by mutually inhibitory synapses. This two-cell network is generally referred to as a *half-center oscillator*. The two elemental oscillators are coupled by *coordinating fibers* that originate from heart interneurons in the first and second ganglia (Figure 2).

When one heart interneuron of an elemental oscillator fires, it inhibits the activity of its partner. Mechanisms within the inhibited neuron serve to drive the neuron out from inhibition, the neuron begins firing and then inhibits the activity of the first neuron, and the cycle repeats [1]. Thus, the neurons fire *bursts* of spiking activity separated by periods of silence.

Numerous intrinsic currents within the heart interneurons serve to determine the structure of the bursts . In particular, a hyperpolarization-activated inward current, I_{h}, and a slow calcium current, I_{CaS}, appear to interact to determine the period and duty cycle of bursting. I_{h} determinines the frequency of inhibitory stimuli from which an inhibited neuron can escape; I_{CaS} of the opposing cell, however, determines the time course of inhibitory stimuli [14]. In simpler terms, I_{h} determines the dynamics of the inhibited phase of activity, while I_{CaS} determines the dynamics of the active phase of activity.

The well-defined synaptic structure of the leech heartbeat timing network makes it ideal both for circuit analysis and for the creation of biologically realistic hybrid systems. Application of the pharmocological agent bicuculline blocks the inhibitory synapses in the network, effectively isolating individual neurons from all other neuronal activity. This facilitates the creation of a hybrid oscillator in which one of the neurons of the elemental oscillator is replaced by a model neuron.

1.2.3 Hybrid Neural-Microelectronic Systems

Modeling and experimentation have been viewed traditionally as separate, albeit complementary, fields. Data from neural models suggest new experimental directions; experiments, in turn, suggest refinements to the models.

Advances in technology, however, have led to the creation of models that operate in real time: the input given to the model is represented in the output of the model with a minimal delay. These real-time models can therefore perform an active role in an experiment. In such experiments, the features of the model — high degree of controllability, access to internal states, well-defined structure — can be used to investigate or control the neural system in ways that are impossible through traditional techniques. The neural system, on the other hand, provides a level of physical realism and complexity that modeling can not accomplish. Thus, a “hybrid” system is created that draws from the strengths of both the model and the physical system.

As described earlier, neuronal modeling is a diverse field, with many different types of models used investigating different phenomena. Given the diversity in both biology and biological modeling, it is not surprising that the development hybrid systems has taken many different directions.

In one of the first hybrid systems, four interconnected analog oscillator circuits were coupled to each other and to a single neuron from the mamallian inferior olive [48]. Oscillations in this hybrid network were triggered by a stimulus to either the neuron or one of the analog oscillators. These oscillations were sustained with activation of a low-threshold calcium current in the olivary neuron. This approach illustrates one of the primary strategies for building hybrid systems. With this approach, a relatively simple empirical model component is designed to reproduce some dynamical feature of the neuronal system's behavior. This approach is useful because a simplified modeling paradigm facilitates the investigation of the dynamical properties of the system. In this approach, precise physiologic modeling is neither required nor desired, as the complexity introduced by modeling physiological processes would hinder analysis of the system. This approach has shown that realistic activity can be generated between non-physiologic models and living neurons [40, 47].

A different strategy for building hybrid systems was made possible by the development of the dynamic clamp, a technique for creating computer-generated physiologic conductances in living neurons [41]. Shortly after the development of the dynamic clamp, a hybrid system was created wherein a Hodgkin-Huxley type model LP cell was introduced into the stomatogastric ganglion network of the crab [38]. In this system, it was shown that increasing the strength of model ionic currents could alter the behavior of the hybrid network. In further studies this network was used to investigate how both synaptic and cellular conductances contribute to network behavior [20]. This approach relies on physiology-based modeling paradigms, such as the Hodgkin-Huxley approach. While such systems are ostensibly more difficult to work with and harder to analyze, the advantage is that the physiologic

nature of the modeled system can be used to understand the mechanisms by which neuronal systems generate activity. This approach has been used extensively in recent years to investigate network activity in the stomatogastric ganglion, the leech heartbeat timing network, the thalamus, and the spinal cord [21, 6, 29, 26, 44].

Another, less significant, division within the field of hybrid systems is the choice of model implementation technology. Most hybrid systems have been constructed with digital microprocessors or digital signal processors as the implementation architecture for the neural model. Several other systems, however, have been implemented by using analog solutions, either discrete or integrated analog circuits. Each method offers several advantages and disadvantages. As a general rule, digital systems are easier to implement, and more flexible; however, they consume large amounts of power and often require much overhead in order to obtain real-time operation. Alternatively, analog systems possess the characteristics of automatic real-time operation and low power consumption, although they are usually more difficult to implement and characterize and are less flexible than digital systems [25, 33, 34, 7].

Ultimately, the choice of implementation technology is less important to the behavior of the hybrid network than the underlying structure of the model, and should be chosen based on the requirements of the particular project.

Hybrid neural systems have generally remained relatively small in scope. That is, they have involved only a few model neurons and a few living neurons. This is due to the limitations of both neural interfacing techniques and simulation methods. However, as both the technology for emulating networks and the technology simultaneously recording and stimulating from neurons improves we can expect hybrid neural networks to grow in both scale and complexity. Early signs of this trend are currently evident in projects that use microelectrode arrays to interface engineered systems to cultures of living neurons [35]. As the scale of these systems grows, we can expect that the complexity of the systems will grow as well. It is therefore important to assess how much computational complexity is

required in order to produce useful interactions with the nervous system.

CHAPTER II

HYBRID SYSTEMS DEVELOPMENT

This chapter presents our initial studies in developing hybrid systems composed of model neurons and living neurons. Our goal with these experiments was to demonstrate that we could generate biologically realistic activity with a hybrid system, and use the properties of the model to reveal the functional role of an ionic current [46]. Our interest in the consequences of model complexity grew out of these experiments.

The hybrid system used in these experiments is composed of a single leech heart interneuron and an analog circuit based "silicon neuron" connected by inhibitory synapses. The rhythmic activity produced by this hybrid half-center oscillator is qualitatively similar both to the activity of the rhythmic network in the leech, and to the activity of a mathematical model half-center oscillator.

We focused our studies on investigating the functional role of the hyperpolarization-activated inward current, I_h, on the oscillations produced by the network. We focused our studies on I_h because it has been implicated in the generation of rhythmic activity in numerous vertebrate and invertebrate systems [32, 42, 23, 39]. By inducing changes in $\bar{g}_h$, the maximal conductance of I_h, we show that $\bar{g}_h$ determines both the period of the oscillations and the balance of activity between the two neurons in the network. Moreover, we demonstrate that the model neuron is an effective replacement for a heart interneuron, and that changes made in the model can accurately mimic similar changes made in the living system. We also used a previously developed mathematical model the half-center oscillator to corroborate our findings. Our results demonstrate that this hybrid system technique is advantageous for investigating neuronal properties that are inaccessible with traditional techniques.

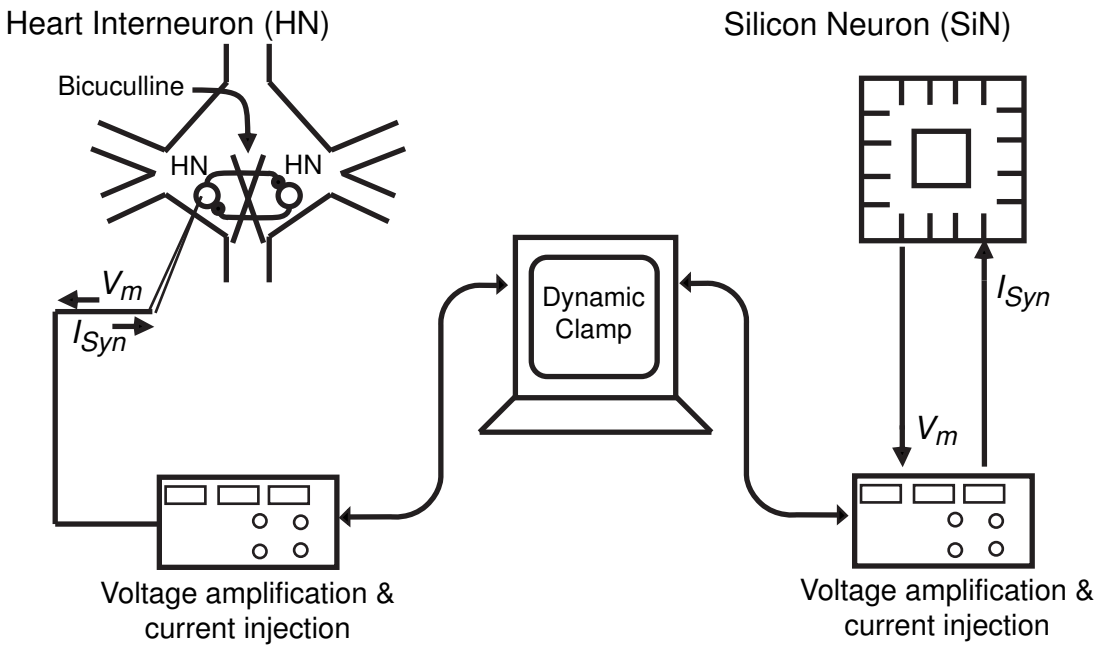

Figure 3: Schematic of hybrid half-center oscillator. A heart interneurons (HN) in the leech ganglia is pharmacologically isolated with bicuculline and impaled with a sharp microelectrode. Voltage/current-clamp amplifiers were used to record voltages and inject current into both the heart interneuron and the silicon neuron (HN). The dynamic clamp creates real-time model synaptic currents that couple the heart interneuron and silicon neuron.

2.1 Materials and Methods

The hybrid system used in these experiments consists of three components: the heart interneuron (HN), the silicon neuron (SiN), and the dynamic clamp (Figure 3). The specific methods used to create this hybrid system are described below.

2.1.1 Leech Heart Interneurons

Leeches (*hirudo medicinalis*) were obtained from a supplier (Leeches USA, Westbury, NY and Biopharm, NC) and maintained in artificial pond water at 15°C. The animals were anesthetized in ice-cold saline, and midbody segmental ganglia three and four were each isolated and pinned ventral-side-up in Petri dishes lined with Sylgard (bath volume 0.5 ml). The methods for preparing and maintaining leech ganglia and for identifying heart interneurons for electrophysiological recording are described elsewhere [31]. The ganglionic

sheath over the cell bodies was removed with fine microscissors or scalpels.

Ganglia were superfused continuously with normal leech saline containing (in mM): 115 NaCl, 4 KCl, 1.8 $CaCl_2$, 10 glucose, 10 HEPES buffer, pH adjusted to 7.4 using 2 M NaOH. Heart interneurons were isolated pharmacologically with $2.5x10^{-4}$ M bicuculline methiodide (Sigma, St. Louis, MO) added to normal saline. In some experiments, a 2 mM concentration of CsCl was added to the saline to block I_{h}.

Heart interneurons were penetrated with sharp microelectrodes made from borosilicate glass tubes (A-M Systems) 1 mm outer diameter, 0.75 mm inner diameter and filled with 4 M potassium acetate with 20 mM KCl. Microelectrode resistance was 25-30 MΩ. Membrane potential recording and current injection were performed using an Axoclamp 2A electrophysiology amplifier (Axon Instruments, Foster City, CA). All hybrid systems experiments were performed using discontinuous current clamp (DCC) mode. DCC sample rates were between 2.5 and 3 kHz. The electrode potential was monitored by an oscilloscope to ensure that it settled between current injection cycles. The input resistance (R_{in}) of the neurons was measured by injecting several short pulses of inhibitory current; only neurons with $R_{in} > 60M\Omega$ were accepted for hybrid experiments.

2.1.2 The Silicon Neuron Model

The silicon neuron was fabricated through an integrated-circuit brokerage service in the AMI $1.2\mu m$ process (MOSIS, Marina del Rey, CA). It was designed to produce electrical activity similar to a leech heart interneuron by emulating its major ionic currents with a Hodgkin-Huxley-like formalism [16, 43]. The silicon neuron provides emulation of several ionic currents: a passive leak current,I_{leak}, fast sodium current,I_{Na}, a fast inactivating potassium current,I_{K1}, a persistent potassium current, I_{K2}, persistent sodium current,I_{P}, slowly inactivating low-threshold calcium current,I_{CaS}, and a hyperpolarization-activated inward current, I_{h}. Parameter values of the silicon neuron were set using 16-bit, 4-channel digital to analog converters (Analog Devices, Inc., Norwood, MA). Digital to analog converters

were interfaced to a PC via PIC microcontrollers (Microchip, Inc., Chandler, AZ). A user interface and software to communicate with PIC microcontrollers was written with the Java programming language (Sun Microsystems, Santa Clara, CA). Membrane potential measurement of and current injection into the silicon neuron were accomplished by direct connection to the headstages of an Axoclamp-2A electrophysiology amplifier (Axon Instruments, Union City, CA). State variables were measured through a current preamplifier (Stanford Research System, Sunnyvale, CA).

The architecture of the silicon neuron was based on a previously published mathematical model of a heart interneuron [14]. There are three notable differences between the silicon neuron and this mathematical model. First, the silicon neuron does not emulate the potassium current I_{KA}, or the fast calcium current I_{CaF}. Second, there is no exponential power (other than 1) applied to the state variables of the silicon neuron. Third, the time constants of the silicon neuron are single-valued parameters, instead of voltage-dependent functions.

2.1.3 Dynamic Clamp

Dynamic clamp was used to implement artificial synaptic conductances between the silicon neuron and an intracellularly recorded oscillator heart interneuron [5]. Dynamic clamp synapses were implemented according the following equations [4]:

$$I_{\mathrm{Syn}} = \bar{g}_{\mathrm{Syn}} Y_{\mathrm{post}} M_{\mathrm{post}} (V_{\mathrm{post}} - E_{\mathrm{Syn}}) \tag{1}$$

$$\frac{dY_{\mathrm{post}}}{dt} = \frac{X_{\mathrm{post}} - Y_{\mathrm{post}}}{\tau_2} \tag{2}$$

$$\frac{dX_{\mathrm{post}}}{dt} = \frac{M_{\infty}(V_{\mathrm{pre}}) - M_{\mathrm{post}}}{0.2} \tag{3}$$

$$X_{\infty}(V_{\mathrm{pre}}) = \frac{1}{1 + e^{-1000(V_{\mathrm{pre}} + .01)}} \tag{4}$$

$$\frac{dM_{\text{post}}}{dt} = \frac{X_{\infty}(V_{\text{pre}}) - X_{\text{post}}}{\tau_1} \tag{5}$$

$$M_{\infty}(V_{\text{pre}}) = 0.1 + \frac{0.9}{1 + e^{-1000(V_{\text{pre}}+.04)}} \tag{6}$$

where $\tau_1 = .002$ s, $\tau_2 = .011$ s, $\bar{g}_{\text{Syn}} = 500$ nS, and $E_{\text{Syn}} = -0.062V$.

Dynamic clamp I_{h} was implemented as follows:

$$I_{\text{h}} = \bar{g}_{\text{h}} m_{\text{h}} (V_{\text{m}} - E_{\text{h}}) \tag{7}$$

$$\frac{m_{\text{h}}}{dt} = \frac{m_{\infty \text{h}} - m_{\text{h}}}{\tau_{m_{\text{h}}}} \tag{8}$$

$$m_{\infty}(V_{\text{m}}) = \frac{1}{1 + e^{180(V_{\text{m}}+.047)} + e^{500(V_{\text{m}}+.047)}} \tag{9}$$

$$\tau_{m_{\text{h}}} = 0.7 + \frac{1.7}{1 + e^{-100(V_{\text{m}}+.073)}} \tag{10}$$

where $E_{\text{h}} = -.02$ V.

All dynamic clamp calculations were performed on a dedicated real-time signal processing controller board (DS1104, DSPACE, Detroit, MI).

2.1.4 Data Acquisition and Analysis

All experimental data were digitized and stored using pCLAMP software (Axon Instruments, Union City, CA). For both hybrid experiments and mathematical modeling, analysis of burst characteristics were performed off-line with scripts written in Matlab (MathWorks, Natick, MA).

Action potentials (spikes) were detected by determining when the membrane potential rose and then fell across a threshold of -20mV. If this sequence of two crossings occurred

within a time window of .001 s, the event was taken to be spurious due to noise or digitization and discarded. All other such events were considered to be spikes.

The time of occurrence of the spike was taken as the time when the maximum membrane potential was reached. For all detected spikes in a continuous record, the mean and standard deviation of the inter-spike interval (ISI) was calculated. ISIs greater than 0.5 sec were used to mark the end of one burst and the beginning of the next burst, however when three successive ISIs were greater than 0.5 sec, the middle spike was considered to be spurious and was discarded. All ISIs within a burst had values within the mean ISI ± two standard deviations. We verified this method manually for 630 sec of recorded data and it was found to be highly accurate for detecting both spikes and bursts of spikes.

At least 8 burst cycles were detected and analyzed per experimental trial. For each experimental trial, cycle period, burst duration, duration of the inhibited phase, and final spike frequency at burst transition was calculated. Burst period was calculated as the time between the median spike of one burst and the median spike of the next burst. Determining cycle period in this fashion minimizes period variability due to spurious spikes at the beginning and end of a burst. Burst duration was calculated as the time between the first and last spike of a burst of spikes. Duration of the inhibited phase was calculated as the time between the last spike of a burst and the first spike of the next burst. The final spike frequency was defined as the instantaneous spike frequency for the last two spikes of a burst.

In experiments where the maximal conductance of I_{h} was varied directly in the silicon neuron or in the heart interneuron with dynamic clamp, we measured the activation variable, m_{h}, and determined the percent of the inhibited phase at which it first reached it maximal value. For heart interneurons, even when $\bar{g}_{\mathrm{h}}$ was set to zero or a negative value in dynamic clamp, m_{h} was calculated and this point of maximal activation was determined to estimate when endogenous I_{h} would activate.

Values reported here are the mean and standard deviation across experiments, except

as indicated. Statistical significance was assessed by performing a one-way ANOVA and a multiple comparison of means using the Bonferroni t-test. A cutoff of $p = 0.05$ was used to evaluate statistical significance.

2.2 The Hybrid Half-Center Oscillator

We discovered after several trials that cell input resistance (R_{in}) after sharp electrode penetration was critical to the success of establishing rhythmic bursting in the hybrid system. Poorly penetrated heart interneurons, $R_{in} < 60M\Omega$, fired at a high frequency and dominated the silicon neuron in the hybrid half-center. Moreover, the low input resistance resulted in a fast membrane time constant and therefore poor synaptic integration. We thereby decided to accept only cells with $R_{in} > 60M\Omega$ for the experiments described here.

To determine appropriate synaptic strength for hybrid oscillations, the maximal synaptic conductance, $\bar{g}_{Syn}$, for both artificial synapses was varied between 0 nS and 625 nS in twelve equal steps for four separate preparations. When isolated ($\bar{g}_{Syn} = 0$) both the silicon neuron and heart interneuron fired tonically (Figure 4A). For low values of synaptic conductance, the two neurons continued to fire tonically, with occasional lapses in activity (Figure 4B). Once sufficient synaptic strength had been reached, the neurons began alternating oscillations (Figure 4C). Once stable oscillations were established, their period varied little with increasing $\bar{g}_{Syn}$ (Figure 4D). The oscillations observed at $\bar{g}_{Syn} = 511$ nS were regular; the coefficient of variation of the period ranged from 3.7% to 11.5% with a mean of 6.8% for the four preparations shown. We selected 500nS as the canonical value of $\bar{g}_{Syn}$ for all further experiments.

Using canonical parameters for the silicon neuron and with $\bar{g}_{Syn}$ set at 500nS, rhythmic antiphasic bursting was obtained with all heart interneurons where $R_{in} > 60M\Omega$. To initiate antiphasic bursting, the synapses were activated by moving their maximal conductances from 0 to 500 nS (Figure 5). Activating the synapses caused one of the neurons to be inhibited while the other continued to fire tonically. Once a neuron was inhibited, its I_h

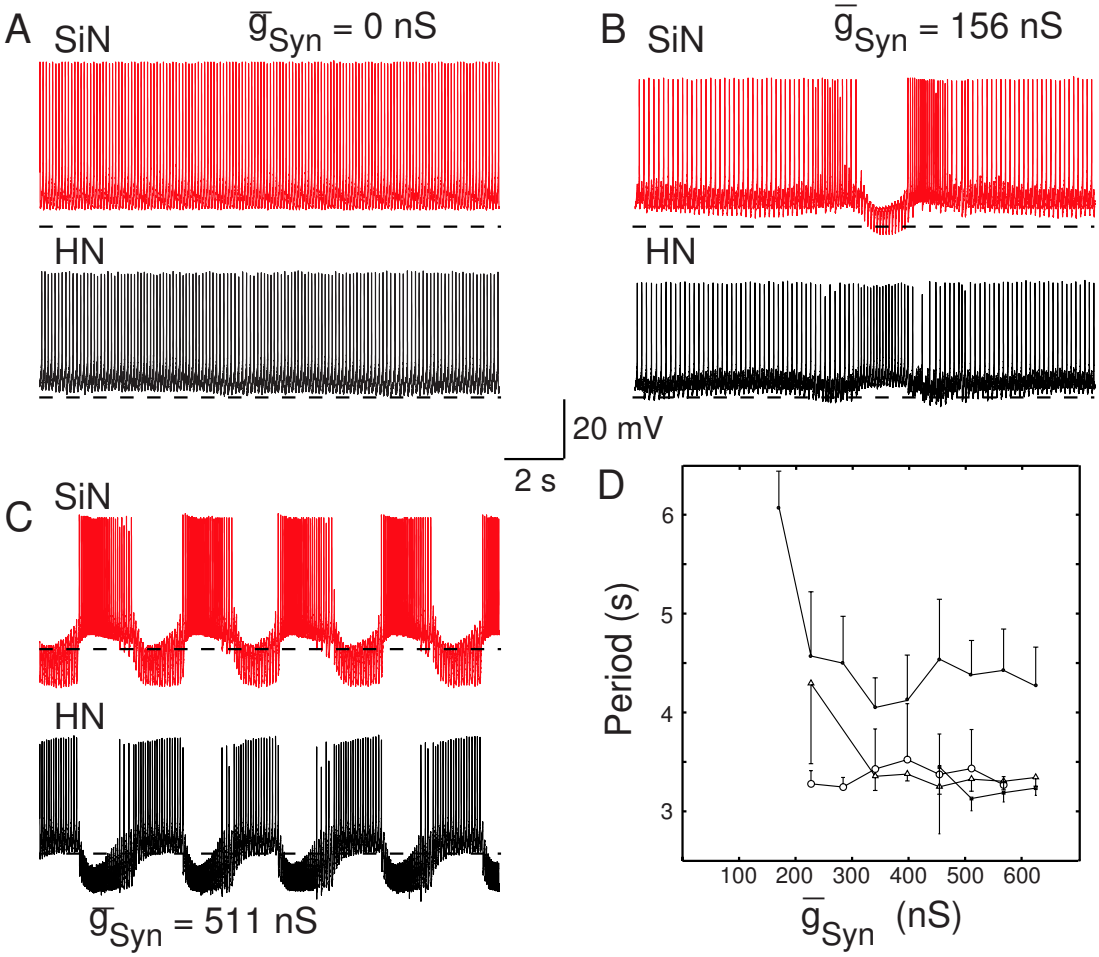

Figure 4: Variation of $\bar{g}_{\mathrm{Syn}}$ in hybrid half-center oscillator. **A.** In isolation, both the heart interneuron (HN, black) and silicon neuron (SiN, red) are tonically firing. **B.** Weak synapses will cause occasional inhibition, but not half-center oscillation. **C.** Synapses of sufficient strength cause sustained half-center oscillations. **D.** Changes in $\bar{g}_{\mathrm{Syn}}$ do not significantly alter the period of half-center oscillations.

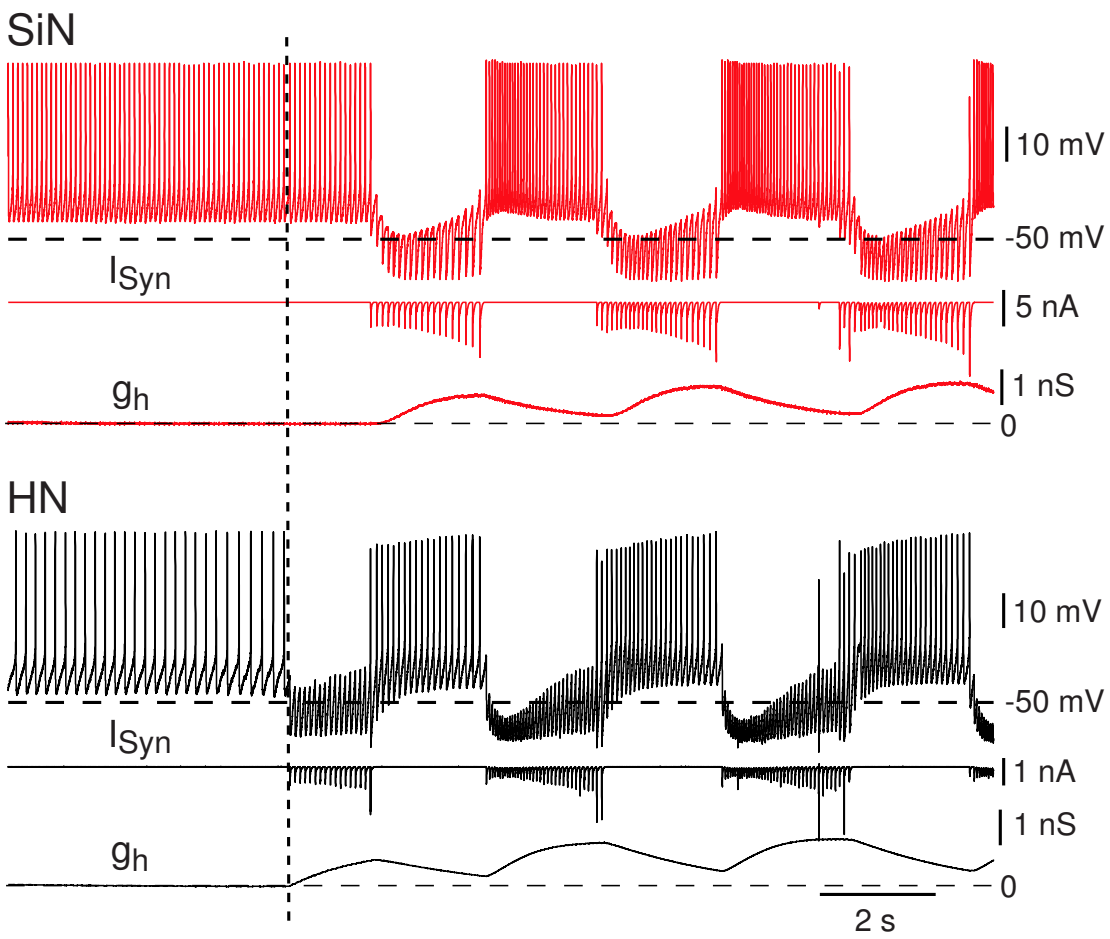

Figure 5: Strong artificial inhibitory synapses cause an immediate transition from tonic firing to rhythmic bursting in a hybrid half-center oscillator. Membrane potential (V_m), synaptic current (I_{Syn}), and h-current conductance (g_h)) are shown for the silicon neuron (SiN, red) and the heart interneuron (HN, black). The vertical dashed line indicates the time at which the dynamic clamp was activated to enable the mutual inhibitory synapses. When one of the neurons is inhibited, its I_h activates, driving it back toward the firing threshold. Once it begins to fire, the other neuron is inhibited, its I_h activates, driving it back toward firing threshold so that it inhibits the first neuron, and the cycle repeats.

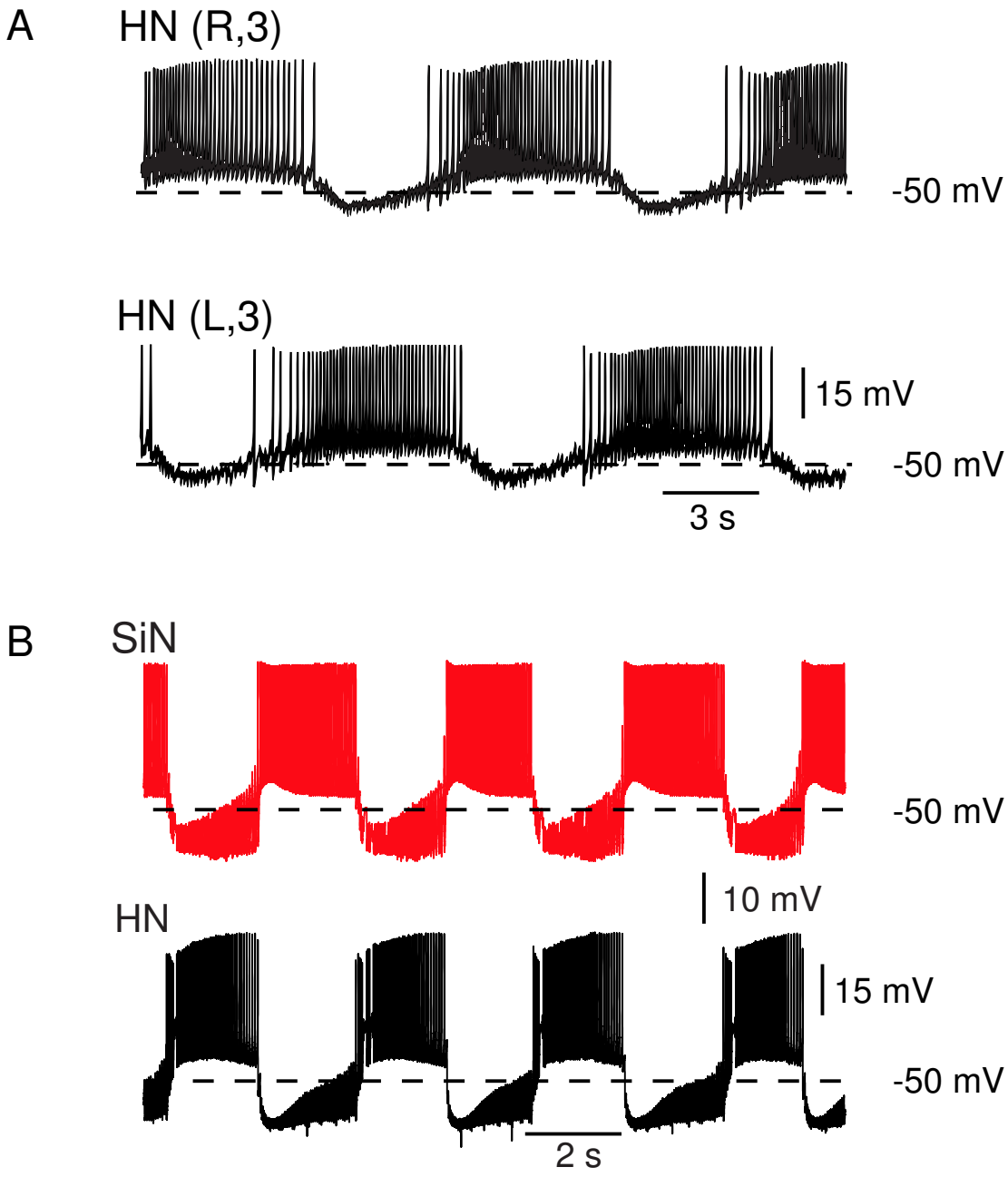

Figure 6: Comparison of biological and hybrid half-center oscillators. **A.** Biological half-center oscillator. **B.** Hybrid half-center oscillator. Membrane potential of the silicon neuron is shown in red. Membrane potential of the biological neuron is shown in black.

activated; meanwhile, the spike rate of the active neuron rapidly increased and then slowly decreased due to the activation and subsequent inactivation of I_{CaS}. Once the spike rate in the active neuron was low enough, the inhibited neuron escaped from inhibition and began firing, inhibiting the other neuron. This process then repeated, resulting in antiphasic bursting that was similar to that observed in the biological oscillator (Figure 6).

2.2.1 Unilateral Variation of $\bar{g}_h$ in the Silicon Neuron

To assess experimentally the effects of varying $\bar{g}_h$ of the silicon neuron (SiN $\bar{g}_h$), we established rhythmic antiphasic bursting between the silicon neuron and an isolated heart interneuron. In five separate experimental preparations, we varied SiN $\bar{g}_h$ from 0 to 8 nS in increments of 2 nS (canonical SiN $\bar{g}_h$ = 4 nS). At each interval we assessed the cycle period, the burst duration, and the final spike frequency for each neuron. Typical activity is shown in Figure 7, and results are summarized in Figure 8.

With canonical parameter values, the cycle period was 4.7 ± 0.4 s. This period is is considerably shorter than both the average period observed in the biological system and the period of the mathematical model mathematical model (8.8s and 8.6s, respectively), although the period is close to the low end of the range observed in the biological system (6.4s) [4]. There are several possible factors that might explain this difference. For example, sharp microelectrode penetration of the heart interneuron causes a decrease in the membrane time constant, reducing the efficacy of spike-mediated synaptic transmission. Limitations in the silicon neuron, such as the lack of voltage-dependent time constants, or in the dynamic clamp synapses, such as the lack of graded synaptic transmission, could also play a role.

With increasing SiN $\bar{g}_h$, the oscillator cycle period decreased (Figure 8A); there was a statistically significant effect of varying SiN $\bar{g}_h$ on the period of the system. With complete removal of I_h (SiN $\bar{g}_h$ = 0), the silicon neuron was not always able to escape from inhibition (n = 2); in the cases where it was able to escape (n=3), the cycle period was greatly

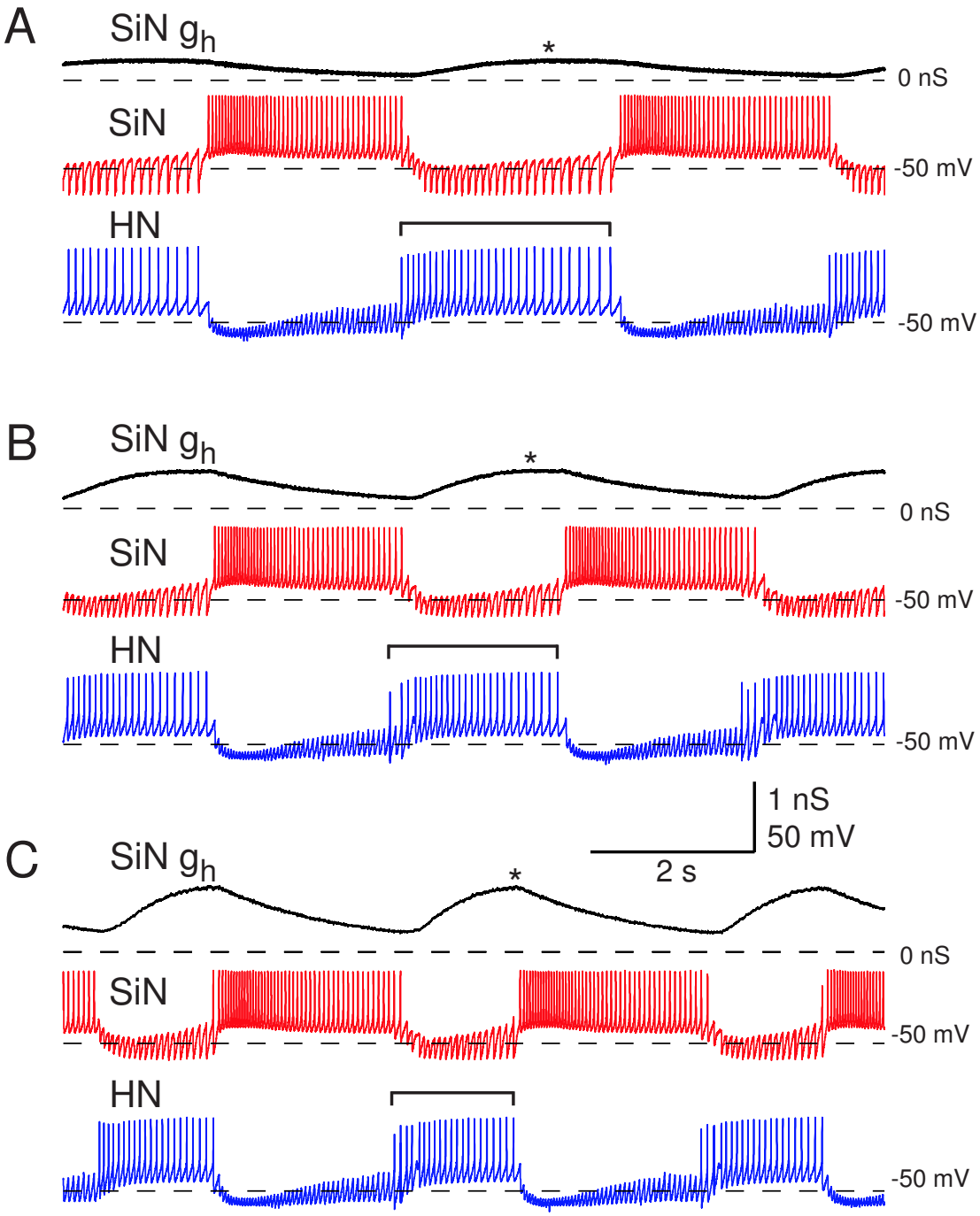

Figure 7: Half-center oscillator activity with variation of $\bar{g}_h$ in SiN. Membrane potential traces for SiN (red) and HN (blue). g_h for the silicon neuron is shown in black above the SiN membrane potential trace. Asterisks indicate when g_h reaches its maximal level of activation. **A.** SiN $\bar{g}_h$ = 2 nS. **B.** SiN $\bar{g}_h$ = 4 nS. **C.** SiN $\bar{g}_h$ = 8 nS.

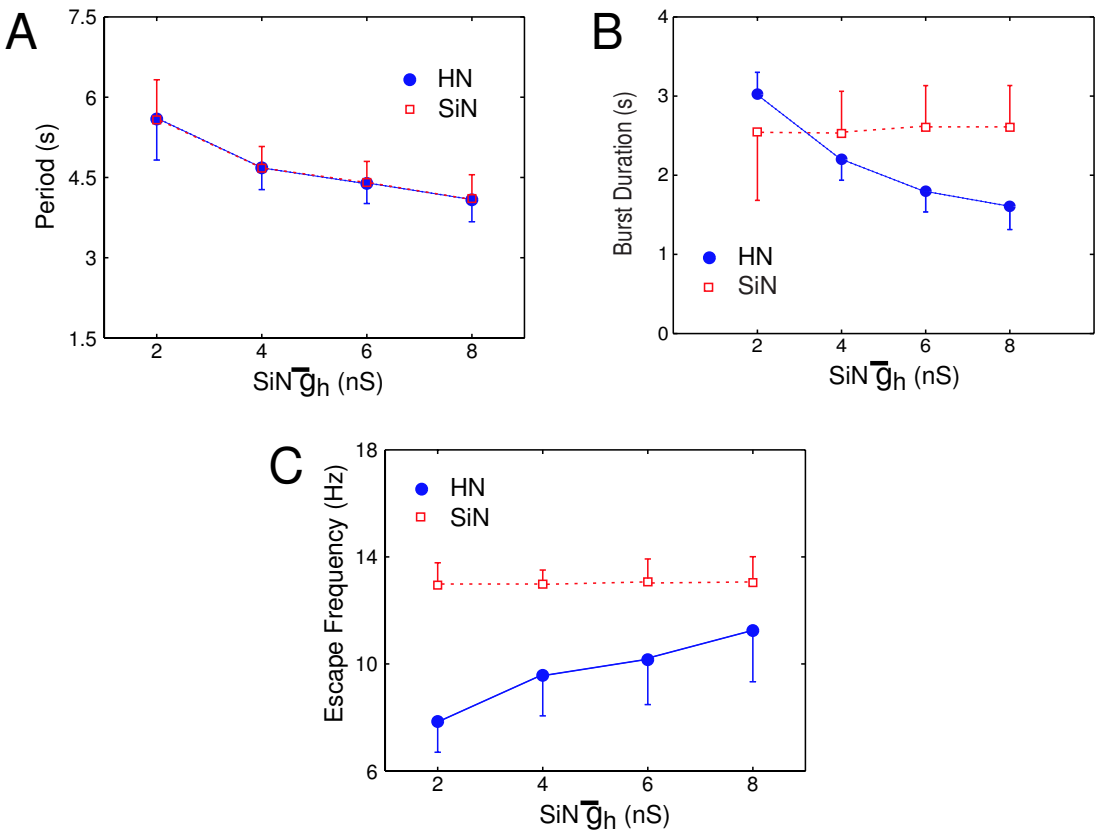

Figure 8: Results of varying $\bar{g}_h$ in silicon neuron. Data for SiN are shown in red and data for the HN are shown in blue. **A.** Oscillator period. **B.** Burst duration of SiN and HN. **C.** Escape frequency (final spike frequency of the opposing cell).

elongated (13.3 ± 1.8 s). When SiN $\bar{g}_h$ is varied, the change in the cycle period of the hybrid half-center oscillator is largely accounted for by the change in the duration of the inhibited phase of the silicon neuron.

In this hybrid half-center oscillator, the duration of the inhibited phase of one cell is approximately equal to the burst duration of the opposing cell. With canonical parameters, the burst duration of the silicon neuron and the burst duration of the heart interneuron were similar (2.5 ± 0.5 s and 2.2 ± 0.2 s, respectively). With increasing SiN $\bar{g}_h$ the burst duration of the heart interneuron decreased, corresponding to a decrease in the inhibited phase of the silicon neuron (Figure 8B). The final spike frequency of the heart interneuron also increased (Figure 8D). There was a statistically significant effect of varying SiN $\bar{g}_h$ on the burst duration and final spike frequency of the heart interneuron but no apparent effect on

these characteristics in the silicon neuron. The absence of a significant change in the burst duration of the silicon neuron indicates that variations in SiN $\bar{g}_{\mathrm{h}}$ selectively influence the inhibited phase of the oscillation. The increase in the final spike frequency of the heart interneuron indicates that with a higher $\bar{g}_{\mathrm{h}}$ the silicon neuron is able to overcome a higher frequency of inhibition from the heart interneuron and escape into its burst. Variations in SiN $\bar{g}_{\mathrm{h}}$ thereby change the balance of oscillations; with higher values of SiN $\bar{g}_{\mathrm{h}}$ the silicon neuron has an increased duty cycle, and with lower values of SiN $\bar{g}_{\mathrm{h}}$ the heart interneuron has an increased duty cycle.

With canonical parameters, the final spike frequency is noticeably higher for the silicon neuron than for the heart interneuron; the heart interneuron is generally able to escape from a higher frequency of inhibition. This difference is most likely due to the difference in membrane time constants and input resistance, which determine the efficacy of dynamic-clamp synaptic currents in altering membrane potential.

At low values of SiN $\bar{g}_{\mathrm{h}}$, the time point during the inhibited phase of the burst cycle at which I_{h} attained it maximal level of activation was well before the burst transition occurred. We expressed this time point as a percent of the inhibited phase. This observation indicates that the silicon neuron was "waiting" for a decrease in the inhibition it receives from the heart interneuron before it could begin firing. Therefore, the dynamics of spike frequency adaptation in the heart interneuron were determining the duration of the inhibited phase of the silicon neuron rather than the dynamics of I_{h} activation. As SiN $\bar{g}_{\mathrm{h}}$ increased, I_{h} attained its maximal level of activation at relatively later and later time points in the inhibited phase. The absolute amount of time necessary to attain maximal activation was nearly invariant but this maximal activation occurred at a greater percent of the inhibited phase. At high values of SiN $\bar{g}_{\mathrm{h}}$, I_{h} attained it maximal level of activation practically at the end of the inhibited phase. This observation indicates that at high values of SiN $\bar{g}_{\mathrm{h}}$ the dynamics of I_{h} activation were determining the duration of the inhibited phase of the silicon neuron rather than the dynamics of spike frequency adaptation in the heart interneuron.

2.2.2 Unilateral Variation of $\bar{g}_h$ in the Heart Interneuron

To vary the strength of I_h in the heart interneuron, we used dynamic clamp to create a model I_h, which could be used in conjunction with the endogenous I_h of the heart interneuron. By setting the maximal conductance of the dynamic clamp I_h, HN $\bar{g}_h$, to be greater than zero, we added to the endogenous I_h. We subtracted from the endogenous I_h by setting HN $\bar{g}_h$ to negative values. Subtracting I_h in excess of the effective endogenous I_h created a positive feedback system, driving the cell to an extremely hyperpolarized state. Several cells were tested, and it was found that an artificial maximal conductance of -16 nS would almost always cause this undesirable condition to occur, but -12 nS would not; -12 nS was therefore chosen as the maximal "negative conductance". Furthermore, the heart interneuron required a larger variation in I_h than did the silicon neuron to observe similar effects, so HN $\bar{g}_h$ was varied over a larger range than in the case for the silicon neuron.

In five experiments, hybrid oscillations were established and HN was varied between -12 nS and +16 nS. SiN $\bar{g}_h$ was kept constant at the canonical value of 4nS. Typical activity for different levels of HN $\bar{g}_h$ is shown in Figure 9. With no addition or subtraction to the endogenous I_h (HN $\bar{g}_h$ = 0 nS), the cycle period of the hybrid oscillator was 4.24 ± 0.6 s, and the burst duration of the silicon neuron (2.1 ± 0.3 s) was similar to the burst duration of the heart interneuron (2.2 ± 0.4 s). With increasing HN $\bar{g}_h$ the period of the system decreased (Figure 10A); there was a statistically significant effect of varying HN $\bar{g}_h$ on period. Moreover, with increasing HN $\bar{g}_h$ the burst duration of the silicon neuron decreased, corresponding to a decrease in the inhibited phase of the heart interneuron, and the final spike frequency of the silicon neuron increased (Figure 10B-C). There was a statistically significant effect of varying HN $\bar{g}_h$ on the burst duration of the silicon neuron, but the effect on final spike frequency of the silicon neuron was not statistically significant ($p = 0.08$). There was no apparent effect of varying HN $\bar{g}_h$ on burst duration or final spike frequency in the heart interneuron.

As observed when varying SiN $\bar{g}_h$, the change in period when varying HN $\bar{g}_h$ was due

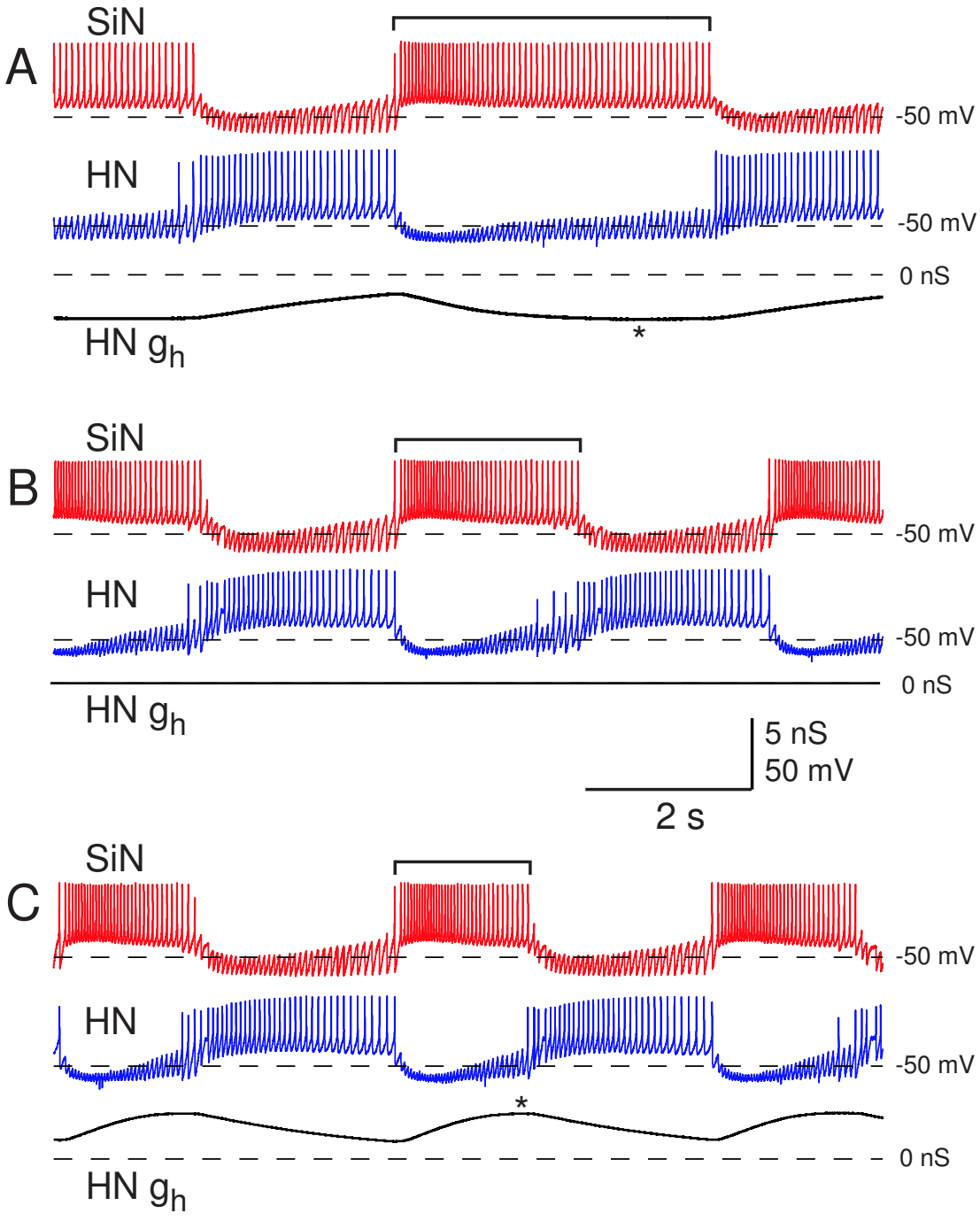

Figure 9: Half-center oscillator activity with variation of $\bar{g}_h$ in HN. Membrane potential traces for SiN (red) and HN (blue). g_h for the silicon neuron is shown in black below the HN membrane potential trace. Asterisks indicate when g_h reaches its maximal level of activation. **A.** HN $\bar{g}_h = -12$ nS. **B.** HN $\bar{g}_h = 0$ nS. **C.** HN $\bar{g}_h = 16$ nS.

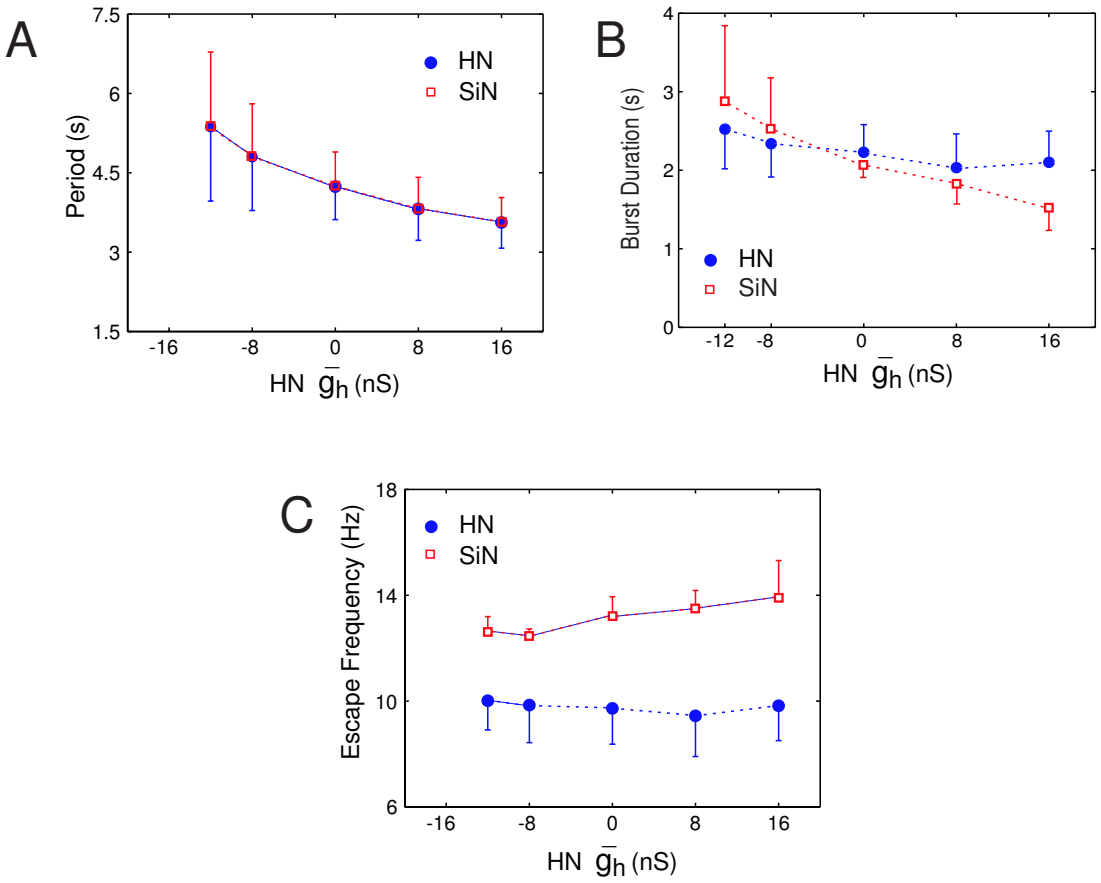

Figure 10: Results of varying $\bar{g}_h$ in heart interneuron. Data for SiN are shown in red and data for the HN are shown in blue. **A.** Oscillator period. **B.** Burst duration of SiN and HN. **C.** Escape frequency (final spike frequency of the opposing cell).

to a change in the duration of the inhibited phase of the modified neuron. The duration of the inhibited phase of the heart interneuron, which is equivalent to the burst duration of the silicon neuron, decreased, while the burst duration of the heart interneuron remained relatively constant. These results are remarkably similar to the case when SiN $\bar{g}_h$, was varied; increasing HN $\bar{g}_h$ caused I_h to attain its maximal level of activation at a relatively later point of the inactive phase of the burst cycle. Although the effect here is not as striking as in the SiN $\bar{g}_h$ case, it is still apparent.

In six additional experiments, we blocked the endogenous I_h of the heart interneuron with 2mM Cs+ and the dynamic clamp was then used to reintroduce a completely artificial I_h into the heart interneuron. HN $\bar{g}_h$ was then varied from 0nS to 32 nS in 8 nS increments. Typical activity for different levels of HN $\bar{g}_h$ is shown in (Figure 11). As observed in the other experiments where $\bar{g}_h$ was varied, increasing HN $\bar{g}_h$ decreased the cycle period of the system (Figure 12A); there was a statistically significant effect of varying HN $\bar{g}_h$ on the period. Moreover, with increasing HN $\bar{g}_h$ the burst duration of the silicon neuron decreased, corresponding to a decrease in the inhibited phase of the heart interneuron, and the final spike frequency of the silicon neuron increased (Figure 12B-C). There was a statistically significant effect of varying HN $\bar{g}_h$ on the burst duration and final spike frequency of the silicon neuron but no apparent effect on these characteristics in the heart interneuron. As in the previous experiments, the change in period was due to a change in the duration of the inhibited phase of the modified neuron (Figure 13D). Increasing HN $\bar{g}_h$ also led to an increase in the percent of the inhibited phase at which I_h attained it maximal level of activation in the heart interneuron (Figure 13C), which was very similar to when $\bar{g}_h$ was varied in the silicon neuron.

The remarkable similarity in results when $\bar{g}_h$ was varied in the silicon neuron and the living heart interneuron, both with endogenous I_h present and when it was blocked by Cs+, demonstrates that the dynamics of dynamic clamp I_h are compatible with the intrinsic currents in the living neuron and that I_h serves a similar function in both the heart interneuron

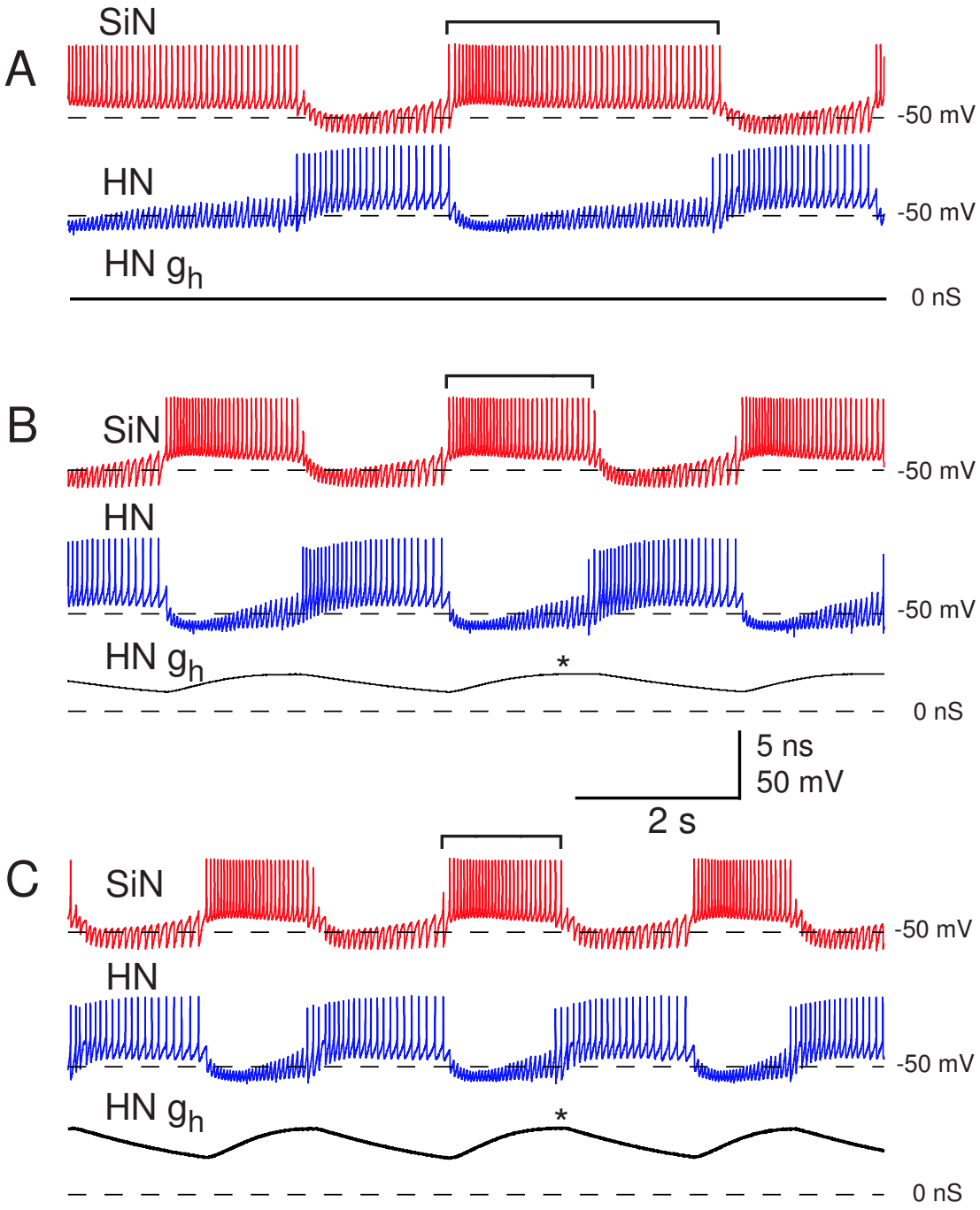

Figure 11: Half-center oscillator activity with variation of $\bar{g}_h$ in HN when endogenous I_h is blocked by Cs2+. Membrane potential traces for SiN (red) and HN (blue). g_h for the silicon neuron is shown in black below the HN membrane potential trace. Asterisks indicate when g_h reaches its maximal level of activation. **A.** HN $\bar{g}_h$ = 0 nS. **B.** HN $\bar{g}_h$ = 16 nS. **C.** HN $\bar{g}_h$ = 32 nS.

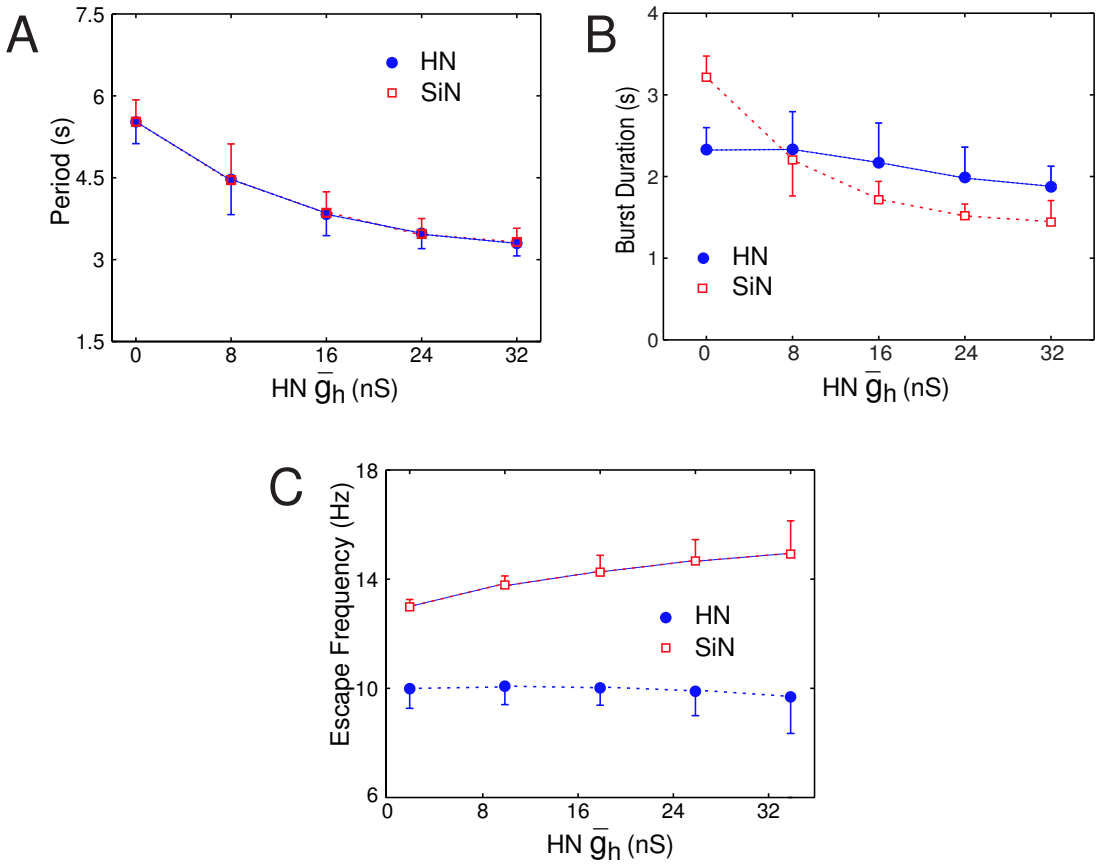

Figure 12: Results of varying $\bar{g}_h$ in heart interneuron when endogenous I_h is block by Cs2+. Data for SiN are shown in red and data for the HN are shown in blue. **A.** Oscillator period. **B.** Burst duration of SiN and HN. **C.** Escape frequency (final spike frequency of the opposing cell).

and the silicon neuron.

2.3 Comparison with Mathematical Modeling

To corroborate our results from the hybrid systems analysis, we investigated the effects of unilateral variation in a mathematical model of a leech heartbeat half-center oscillator. This additional mathematical modeling of the half-center oscillator was performed in the GENESIS simulation environment (freely available from *http://www.genesis-sim.org/*), running under Mandrake Linux v8.1. The model half-center oscillator consisted of two single-compartment heart interneurons connected by inhibitory synapses. Differential equations were integrated using the exponential Euler method with a time step of 10^{-4} s. For each simulation, the model was run for 100 s to allow the activity to settle, and then 400 sec of data were recorded. Details of the model structure and simulation parameters are found in Hill et al. [14].

Previous modeling studies indicated that $\bar{g}_{\mathrm{h}}$ determines the final spike frequency, the firing frequency at which a heart interneuron escapes the inhibition of the other neuron in the half-center oscillator. However, these studies investigated only the effects of bilateral variation of parameters not the unilateral variations that we employed in our hybrid systems analysis. We varied $\bar{g}_{\mathrm{h}}$ of one model neuron of a model half-center oscillator from 0 to 8 nS (4 nS canonical) in 0.5 nS increments. We then assessed the resultant activity for cycle period, burst duration, duration of the inhibited phase, and final spike frequency.

Unilateral variation of $\bar{g}_{\mathrm{h}}$ in the model revealed effects similar to those observed in the hybrid system. Increasing $\bar{g}_{\mathrm{h}}$ unilaterally resulted in a decrease in the burst duration of the unmodified (constant) model cell corresponding to a decrease in the duration of the inactive phase of the modified model neuron (Figure 14A). The burst duration of the modified model neuron, however, exhibited virtually no change. This selectivity for influencing the inactive phase of the burst was not apparent when was varied bilaterally (Figure 14B, inset). Final spike frequency increased nearly linearly for the constant model

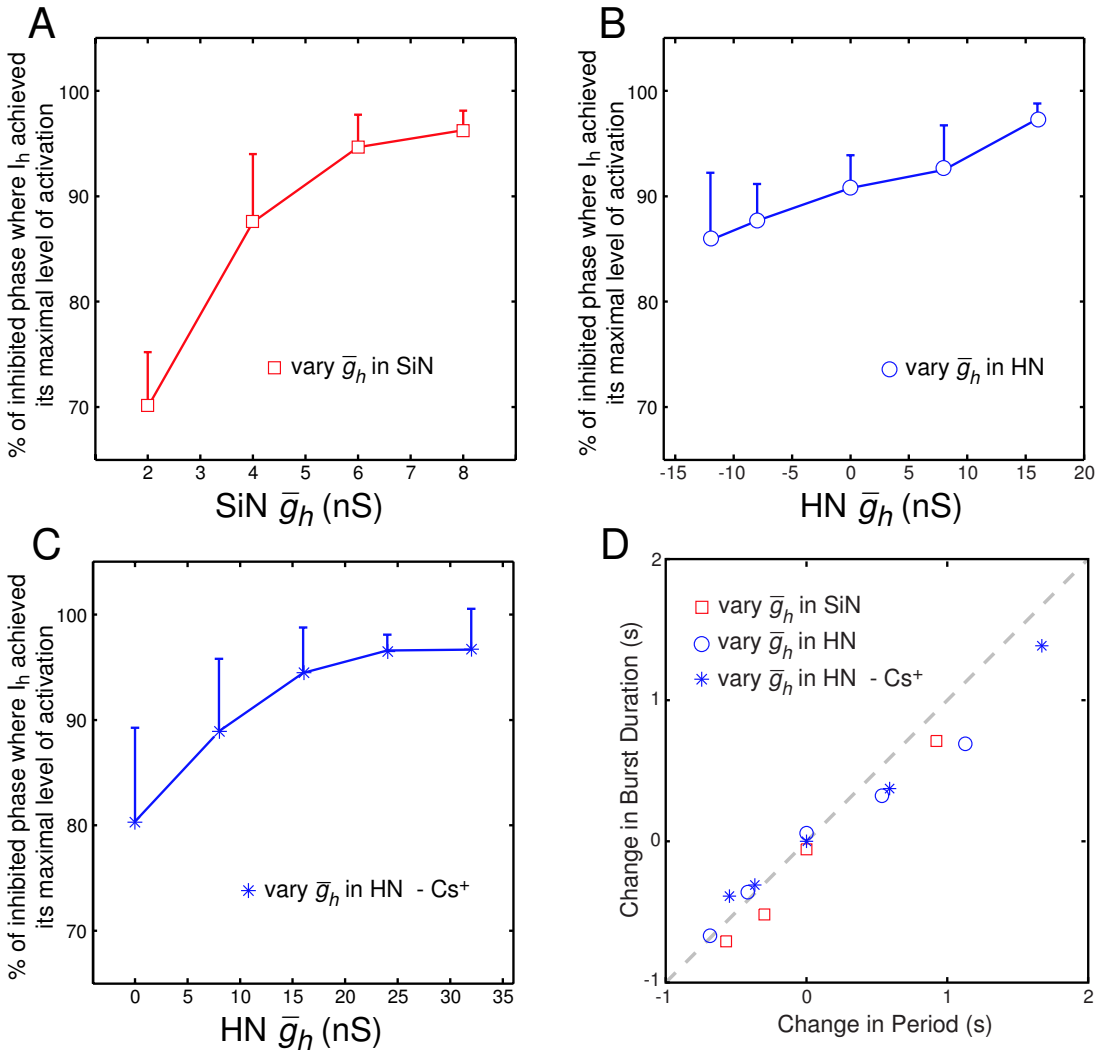

Figure 13: Other effects of varying $\bar{g}_{\mathrm{h}}$ in hybrid half-center oscillator. **A.** Percent of inhibited phase where g_{h} achieved its maximal activation vs $\bar{g}_{\mathrm{h}}$ of SiN. **B.** Percent of inhibited phase where g_{h} achieved its maximal activation vs $\bar{g}_{\mathrm{h}}$ of HN with endogenous I_{h} present. **C.** Percent of inhibited phase where g_{h} achieved its maximal activation vs $\bar{g}_{\mathrm{h}}$ of HN with endogenous I_{h} blocked. **D.** Change in oscillator period is due to change in burst duration of unmodified cell.

neuron but remained constant for the varied model neuron (Figure 14C). The changes in final spike frequency in the unmodified model neuron for unilateral variation of $\bar{g}_h$ corresponded closely to the changes in final spike frequency observed for symmetric variation of $\bar{g}_h$ (Figure 14C, inset)). These modeling results for asymmetric variation of further support the hypothesis developed from symmetric variation of $\bar{g}_h$ in the model and from our hybrid system analysis that $\bar{g}_h$ sets the final spike frequency from which an inhibited neuron escapes.

Finally, the changes in cycle period of the model half-center oscillator observed under bilateral and unilateral variation of are qualitatively very similar (Figure 15). Essentially, the change in period for a bilateral change in $\bar{g}_h$ is double that for a unilateral change in $\bar{g}_h$.

2.4 Discussion

These experiments provide three findings that are important for the rest of this thesis. First, they demonstrate that biologically realistic activity can be generated using a hybrid oscillator. Second, they demonstrate that the parameters of the model can be used to manipulate the output of the hybrid network. Third, they demonstrate that a hybrid system built from a reduced model can produce results that are very similar to the predictions of a complex mathematical model.

2.4.1 Functional role of I_h in the Hybrid Half-Center Oscillator

We investigated the role of the hyperpolarization-activated inward current, I_h, in rhythm generation and the control of period and burst duration. We varied the maximal conductance of I_h, $\bar{g}_h$, in the silicon neuron and, by using dynamic clamp, in the heart interneuron, both with endogenous I_h present and with endogenous I_h blocked. In all three of these studies, Increasing $\bar{g}_h$ increased the firing frequency of the active (unvaried) neuron at which the inhibited (varied) neuron escaped from inhibition. As a result, increasing $\bar{g}_h$ decreased the duration of the inhibited phase in the varied neuron, and decreased the cycle period.

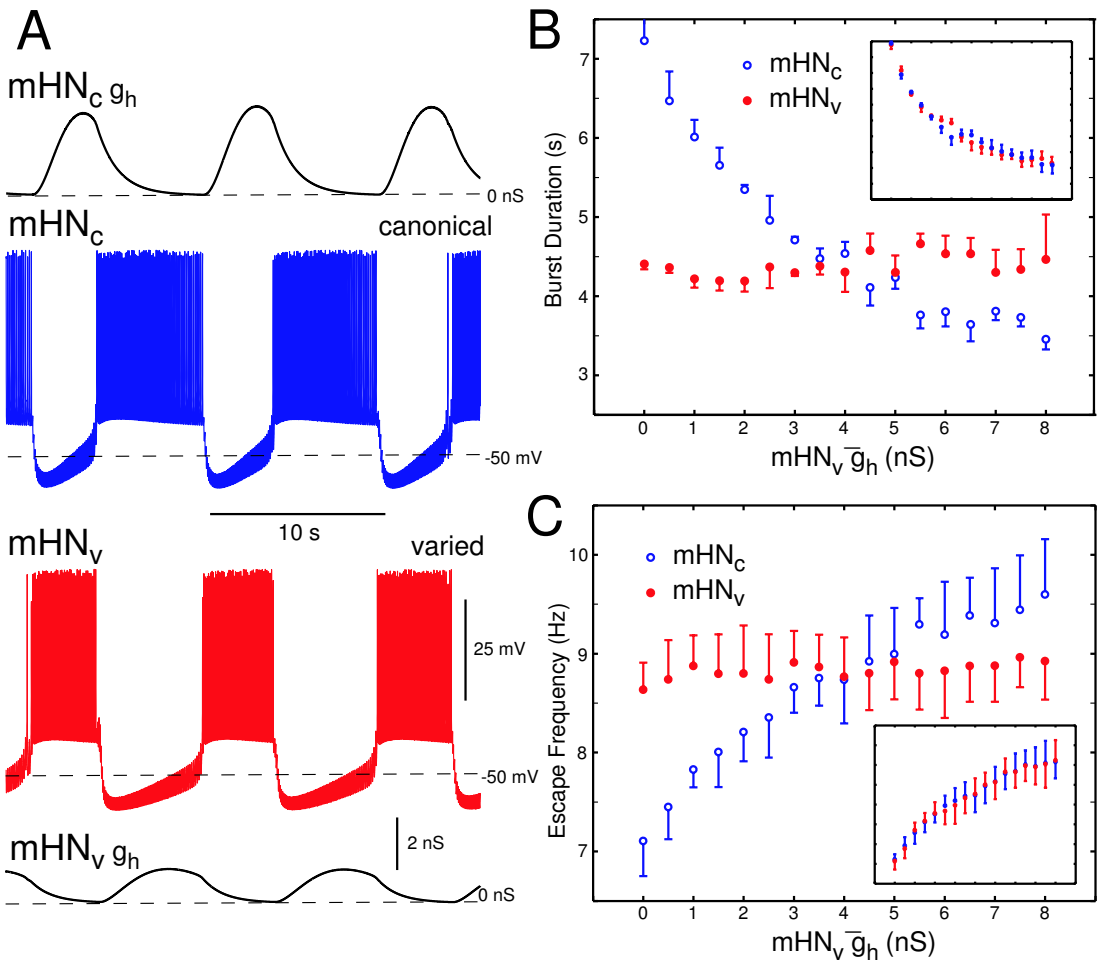

Figure 14: Unilateral variation of $\bar{g}_h$ in mathematical model half-center oscillator. **A.** Activity of model oscillator with asymmetric $\bar{g}_h$. Membrane potential of control model HN (mHN$_c$, $\bar{g}_h$ = 4 nS) is shown in blue. Membrane potential of variable model HN mHN$_v$, $\bar{g}_h$ = 1 nS) is shown in red. g_h for each neuron is shown in black. **B.** Burst duration vs. mHN$_v$ $\bar{g}_h$. *inset*: results for bilateral variation of $\bar{g}_h$. **C.** Escape frequency vs. mHN$_v$ $\bar{g}_h$. *inset*: results for bilateral variation of $\bar{g}_h$.

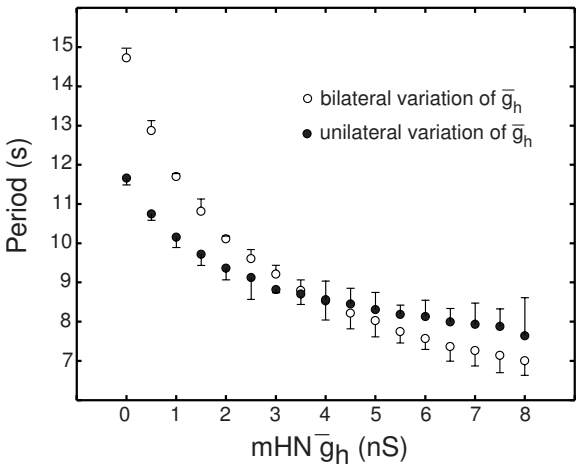

Figure 15: Oscillator period vs. unilateral and bilateral variation of $\bar{g}_{\mathrm{h}}$ in mathematical model half-center oscillator.

Previous modeling and physiological studies have indicated that I_{h} exerts an important control on period in heart interneuron half-center oscillators [31, 14]. By making unilateral changes in this analysis, we have supplemented the previous work to demonstrate the selectivity of I_{h} in controlling the inhibited phase of the heart interneuron burst cycle. In both the mathematical model and the hybrid system, modulation of I_{h} by $\bar{g}_{\mathrm{h}}$ substantially effects the duration of the inhibited phase of the oscillation, with little or no effect on burst duration of the varied neuron. Thus, in addition to its role as a period regulator, I_{h} can also alter the balance of activity in a half-center oscillator. Our results are consistent with other investigations into the functional role of I_{h}, which demonstrated that increasing I_{h} decreases cycle period and increases the duty cycle of modified cell [24]. Because leech heartbeat half-center oscillators always produce equally balanced rhythmic oscillations, any modulatory process which acts on $\bar{g}_{\mathrm{h}}$ would either have to either act bilaterally or additionally effect some other property in order to maintain an appropriate balance of activity.

These results demonstrate that the hybrid systems technique is useful for investigating the role of neuronal properties in the generation of neural activity. The accessibility of the model provides a degree of control that is not possible with traditional experimental methodologies; the neural component, however, provides a level of realism and relevance

greater than with modeling alone.

2.4.2 Validity of the Hybrid Neural Network

For several years, numerous efforts have been made to construct hybrid networks for neuronal network investigations. The goal of such investigations has been to use the controllability and well-defined structure of a model to better understand neuronal function, while still retaining the realism provided by living neurons. In general, these efforts have taken two different approaches. The first approach has employed non-physiological models, such as nonlinear oscillators or phenomenological model neurons, coupled to a neuron or a neuronal network [48, 47]. The relative simplicity of these models facilitates the study of dynamical properties; such study is extremely difficult with more complicated models. The second approach has been to use physiologically realistic, conductance-based model neurons. This approach facilitates the investigation of both the mechanisms by which activity is produced and the functional role of different conductances [38, 20, 29, 26, 21, 6].

Our hybrid system used an analog silicon neuron that implemented a realistic conductance-based model based on the Hodgkin-Huxley formalism [16, 43]. This mechanistic approach to modeling was necessary because we were interested in studying how intrinsic ionic currents contribute to generating rhythmic oscillatory activity. When the tonically firing model neuron and tonically firing biological neuron were coupled with inhibitory synapses using dynamic clamp, they produced alternating rhythmic bursting. This transformation in activity is analogous to results observed when inhibitory synaptic transmission is reversibly blocked in heart interneurons recorded by sharp microelectrode penetration [4].

The oscillations produced by our hybrid system were qualitatively similar to those observed in the living heart interneuron half-center oscillator. We demonstrated that alterations of $\bar{g}_{\mathrm{h}}$ in the silicon neuron and heart interneuron produced similar affects on cycle period, burst duration, and escape frequency. This demonstration of symmetry in observed effects between the model neuron and the heart interneuron indicates that conclusions drawn

from the model can be applied confidently to the living system.

2.4.3 Reduced Models in Hybrid Systems

The silicon neuron used in these experiments is a reduced version of a physiologically realistic mathematical model of a heart interneuron. As compared to the mathematical model, the silicon neuron implemented a reduced set of ionic currents, the time constants of the silicon neuron were single-value parameters rather than voltage-dependent functions, and the state variables were not raised to powers.

In spite of the reduced nature of the model, however, the results produced by experiments with the hybrid system were very similar to the results observed in simulations with the more complex mathematical model. The one prominent difference was that the hybrid system oscillated at a substantially shorter period than the mathematical model; the effects of $\bar{g}_{\mathrm{h}}$ on period, burst duration, and escape frequency, however, were the same in both the hybrid system and in the mathematical model.

It appears, therefore, that the function of $\bar{g}_{\mathrm{h}}$ was not affected by the reduced nature of the silicon neuron. This finding led us to question the functional consequences of model complexity in hybrid systems.

CHAPTER III

REDUCTION OF THE HN MODEL

In the previous chapter, we demonstrated our ability to generate realistic half-center oscillations with a hybrid system, and we demonstrated how these oscillations could be controlled through the parameters of the model neuron. Our ultimate goal is to evaluate how model complexity contributes to the performance of such hybrid systems. In order to address this goal, we must first create a series of reduced models based on the heart interneuron.

We begin with a previously developed mechanistic model of the leech heartbeat interneuron, referred to hereafter as the FULL model [14]. We then use a variety of model reduction techniques to eliminate state variables and ionic currents in this model, creating a simplified mechanistic model referred to as the R1 model. In the next reduction stage, we will replace the Hodgkin-Huxley style spiking mechanisms with integrate-and-fire type dynamics, creating a model with both mechanistic and empirical components, referred to as the R2 model. In the final reduction stage, we will replace several active ionic currents with a passive current; this final model is referred to as the R3 model.

In the following chapters, we will evaluate the robustness and flexibility of these reduced models in model half-center oscillators. We will then validate our reduced models using hybrid half-center oscillators. These studies will produce both an understanding of how model complexity contributes to the robustness and flexibility of model systems and an understanding of how well our reduced models predict the behavior of hybrid systems.

3.1 FPGA Implementation of Neuronal Models

Before reducing our model, we must consider our simulation platform. The silicon neuron used in Chapter 2 is not an effective platform for evaluating model reduction. Although the

silicon neuron provides control over a model's parameters, it does not provide control over the model's structure. Utilizing the silicon neuron would therefore allow only specific kinds of reduction techniques. For example, while a particular state variable could be eliminated from the model by adjusting its parameters, a more structural change, such as replacing Hodgkin-Huxley style dynamics with integrate-and-fire type dynamics, would be very difficult. Although different circuits could implement structurally different models, the long fabrication time makes this strategy rather onerous. Additionally, the silicon neuron's real-time performance can be a hinderance in modeling; platforms capable of running a given model faster than real-time provide a distinct advantage when investigating the parameter space of a model.

In order to address these deficiencies with the silicon neuron, we implemented our neuron models on a field-programmable gate array (FPGA). The FPGA provides several distinct advantages over the silicon neuron: the model structure can be easily altered, the time required to physically implement a given model design is minimal, and FPGAs are capable of incredibly fast running speeds [13, 12]. We will describe here the basics of modeling neurons on FPGAs, and provide the specifics of our FPGA-based neuronal model design.

3.1.1 FPGAs

FPGAs are programmable digital logic devices. In their simplest form, FPGAs consist of two elements: logic cells and interconnects. The logic cells are small circuits consisting of a small look-up table, binary logic gates, and flip-flops. The interconnects consist of wires and multiplexors placed around the logic cells; they allow different logic cells to be hooked up to each other, and also allow communication with devices outside of the FPGA. Although the functionality of a single logic cell is quite limited, when several logic cells are hooked together they are capable of implementing much more complicated functions, such as counters, adders, or multipliers. Because a single FPGA device can contain millions of

logic cells, an FPGA is capable of extremely complex functionality. Furthermore, advanced FPGAs contain additional logic elements, such as block RAM or dedicated multipliers, augmenting the capabilities of an FPGA even further.

The user of an FPGA creates a description of the desired function of the FPGA either by using a hardware description language (such as VHDL or Verilog), or by designing a logic schematic. Computer software is then used to turn the code or schematic into a binary file that can be downloaded to the FPGA. This binary file defines how the the logic cells are interconnected to each other, and how the communicate with external devices. Once this binary description has been downloaded to the FPGA, the FPGA will implement the described logic as long as the device remains powered.

3.1.2 Modeling Neurons on FPGAs

There are several important differences between FPGAs and digital computers to consider when modeling neurons on FPGAs. The first major difference is that FPGAs utilize fixed-point representation for all numbers, rather than floating-point representation. This difference means that the model must be analyzed ahead of time in order to determine how much precision is needed for each signal or parameter within the model.

For example, consider the following equation describing an ionic current in a Hodgkin-Huxley style model:

$$I_{\text{ion}} = \bar{g}_{\text{ion}} m_{\text{ion}}^2 h_{\text{ion}} (V_{\text{m}} - E_{\text{ion}}) \tag{11}$$

We then make the following assumptions: The membrane potential V_{m}, ranges from -80 to $+20$ mV, and requires a resolution of at least .1 mV. The reversal potential E_{ion} will be -20 mV, requires similar resolution to the membrane potential. The state variables m_{ion} and h_{ion} range from 0 to 1, and require resolution of at least .001. The maximal conductance, $\bar{g}_{\text{ion}}$, will be varied from 20 to 200 nS, with a resolution of 0.25 nS. The current, I_{ion}, would therefore be expected to range from -12 to 8 nA.

If SI units are used to represent these signals in Volts, Siemens, and Amps, the voltage signals would require 15 bits (including the sign bit), the state variables would require 10 bits, and the maximal conductance would require 32 bits. If we wish to resolve the current to .01 nA, we would require 38 bits of precision. If we utilize non-SI units (mV, nS, nA), however, we can obtain similar resolution using 12 bits for the voltage signals, 10 bits for the maximal conductance, and 12 bits for the current (the state variables are unitless, and therefore their requirement is unchanged). By changing the units of our signals, we have conserved FPGA resources without losing any numerical resolution.

The second factor to consider when implementing a neuron model on an FPGA is that certain mathematical operations — namely exponential functions and divisions — are extremely resource intensive. When such resource-intensive functions are required by the model, it is necessary to utilize look-up tables stored in memory to implement the function. For example, the steady-state activation function

$$m_\infty = \frac{1}{1 + e^{a(V_m+b)}} \tag{12}$$

would be extraordinarily difficult to implement using standard logic elements. However, if the parameters a and b are known, the signal V_m can easily be turned into an index into a look-up-table (LUT) whose values correspond to m_∞. This method, unfortunately, means that the parameters a and b must be set at compile time, and cannot be altered while the FPGA is running.

The third consideration when implementing a design using FPGAs is that not all parameters or signals are externally accessible. The number of inputs and outputs of the FPGA are limited; in addition, due to the operation mode in which the FPGA was used, increasing the number of inputs and outputs of the model decreased the speed at which the FPGA could run. Although the inputs and outputs of the model can be time multiplexed, or buffered, it adds a level of design complexity that we were not able to address during this project. We therefore had to choose which model parameters and signals were externally

accessible.

As a final consideration, we note that not all FPGA operations are instantaneous. For example, accessing a stored value from memory requires one FPGA clock cycle to complete; utilizing a dedicated multiplier to multiply two signals requires three FPGA clock cycles. Many FPGA clock cycles are therefore necessary to compute one model simulation step. This latency provides an opportunity to increase the performance of the FPGA. By changing the parameters of the model with each FPGA clock step, several models with different parameters can be run simultaneously. This technique is known as *pipelining*.

3.1.3 Specific Methods Used for HN Models on FPGAs

Our HN HCO models were implemented on a BenADDA FPGA development board from Nallatech, Inc. (Eldersburg, MD). We chose this development package because it contained a powerful FPGA and converters for interfacing to external analog devices. At the center of this board is a Xilix Virtex-II FPGA. The Virtex-II provides 3 million logic gates, 96 dedicated 18x18 multipliers, and 96 1-KB units of block RAM. In addition, the BenADDA board provides two analog-to-digital converters (ADCs) and two digital-to-analog converters (DACs) that can be used to interface the FPGA with external devices.

The logic design for the FPGA was performed using the Xtreme DSP development kit from Xilinx. This kit allows the logic for the FPGA to be designed and compiled within the Simulink modeling environment (Mathworks, Cambridge, MA). Different Simulink blocks are provided for different logic structures: such as counters, adders, multipliers, etc. Model design is accomplished graphically by connecting these block together. Once the model has been designed, it can be compiled into FPGA-usable code; furthermore, the code can be linked into a new Simulink block that can be used in other Simulink models. This new block will use the FPGA as a computational resource, a functionality known as *hardware co-simulation*.

The hardware-co-simulation functionality facilitates utilizing the FPGA as a modeling

tool. Once the neuron model has been compiled into a hardware co-simulation block, a new Simulink model is created that contains the neuron model block, and Simulink constant blocks for the input parameters. The output of the neuron model block is sent to the Matlab workspace or to a file. Using the matlab *set_param* and *sim* commands, scripted simulations of the neuron model can be run that utilize the FPGA for solving the model equations. The functionality, however, comes at a price; in order to synchronize data transfer between Matlab/Simulink and the FPGA, it is necessary to the Simulink and FPGA clocks to be matched (known as *single-step mode* within Simulink). This clock-matching causes significant computational overhead, and limits the performance of the FPGA. In our model, the FPGA was clocked at approximately 200 kHz in single-step mode, whereas when the FPGA could generate its own clock (know as *free-running* mode), clock speeds of over 40 MHz were possible. Even with this limitation, however, the FPGA was still able to run the model at very fast speeds; data were produced at a rate approximately 36 times real-time.

All ionic current state variables in the model were implemented as 28 bit unsigned signals with their binary point at the 28th bit. The membrane potential was represented in mV using a 28 bit signed 2s-complement signal with the binary point at the 20th bit. This permitted an effective range of ±128 mV with a resolution of $2^{-18} = 3.8 \times 10^{-6}$ mV. All state variables were integrated using Euler-type integrators with a simulation step size, $T = 1 \times 10^{-4}$ s.

Time constants were implemented using look-up tables. Each look up table consisted of 2048 entries, with each entry consisting of an 18-bit unsigned value with 18 fractional bits. The values stored in the look-up tables corresponded to $T/\tau_{\mathrm{i}}(V_{\mathrm{m}})$, with entry 0 corresponded to a membrane potential of -80 mV and entry 2047 corresponded to a membrane potential of 48 mV. The time constant look-up table were therefore able to resolve time constant values from 1×10^{-4} to 26.2 s, in 1/16 mV increments, with a numerical precision that varied from 0.38×10^{-9} s at the low end to 13.1 s at the high end (because of

the inverse function there is more precision for smaller values and less precision for larger values). Eight bits of extra precision were added to the values for the look-up tables for $\tau_{h_{\mathrm{CaS}}}$ and $\tau_{m_{\mathrm{h}}}$, in order to provide better resolution of their larger time constants.

Steady-state activation and inactivation functions were also implemented with look-up tables. As with the time constant look-up tables, each table consisted of 2048 entries that spanned the voltage range from -80 to 48 mV. Each entry contained a 14-bit unsigned value with 14 fractional bits. This precision provides a resolution of the steady-state value to $6. \times 10^{-5}$.

A concession to resource conservation must be made when modeling synaptic currents. Spike mediated synaptic currents are described in the original model by the following equations:

$$I_{\mathrm{Syn}}(t, V) = (V_{\mathrm{post}} - E_{\mathrm{Syn}}) \times \sum_{s=1}^{N} M_i \bar{g}_{\mathrm{Syn}} f_{\mathrm{Syn}}(t - t_s) \tag{13}$$

$$f_{\mathrm{Syn}}(t) = a(e^{-(t-t_s)/.011} - e^{-(t-t_s)/.002}) \tag{14}$$

$$\frac{dM_{\mathrm{post}}}{dt} = \frac{M_\infty(V_{\mathrm{pre}}) - M}{0.2} \tag{15}$$

$$M_\infty(V_{\mathrm{pre}}) = 0.1 + \frac{0.9}{1 + e^{-1000(V_{\mathrm{pre}}+.04)}} \tag{16}$$

where $a = 1.785$, $E_{\mathrm{Syn}} = -62.5$ mV, $\bar{g}_{\mathrm{Syn}} = 60$ nS, and t_s is the time of occurrence of presynaptic spike s. V_{pre} and V_{post} are the pre- and post-synaptic membrane potentials, respectively.

Because the exponential function $f_{\mathrm{Syn}}(t)$ is implemented using a look-up table, $t - t_s \leq$ 102.4 msec. At the end of this time range, however, $f_{\mathrm{Syn}}(t)$ has decayed to $1.5e-4$, several orders of magnitude below its peak value of 1, so we do not think this limitation impacts the efficacy of a single synaptic event.

Furthermore, due to the limitation of resources on the FPGA, we cannot consider *every* presynaptic spike as in equation 13. In order to conserve resources on the FPGA we restrict the number of presynaptic spikes considered when calculation I_{Syn} to the previous four:

$$I_{\text{Syn}}(t, V) = (V_{\text{post}} - E_{\text{Syn}}) \times \sum_{s=N-3}^{N} M_i \bar{g}_{\text{Syn}} f_{\text{Syn}}(t - t_s) \tag{17}$$

Taking this limitation and the time limitation of $f_{Syn}(t)$ together, we could possibly encounter problems when the spike frequency of the presynaptic cell is greater than 39 Hz, although given the exponential drop off of $f_{\text{Syn}}(t)$, we think this will only pose a problem when the frequency exceeds 115 Hz. At this rate, an additional spike will "interrupt" more than 5% of the last synaptic event in the queue of four. This condition only occurred during a few of our hybrid systems experiments, and we do not think that it caused any significant alteration of the system's activity.

Eighteen simultaneous models were pipelined through the FPGA; we could therefore run eighteen simultaneous single-cell models, or nine simultaneous half-center oscillator models.

The input parameters to the FPGA consisted of a *base* and *space* value for the maximal conductances of the ionic currents. For example if the base $\bar{g}_{\text{h}}$ value were set to 4, and the space $\bar{g}_{\text{h}}$ value were set to 0.5, the first neuron model in the pipeline would have $\bar{g}_{\text{h}} = 4$, the second model would have $\bar{g}_{\text{h}} = 4.5$, the third would have $\bar{g}_{\text{h}} = 5$, and so on. In some of the reduction stages, it was necessary to include other model parameters as FPGA inputs. These differences are noted in the sections on model reduction.

The output of the FPGA was limited to the membrane potential of the models. The membrane potentials of the eighteen model neurons were multiplexed together and output as a single signal in order to optimize the FPGA speed during single-stepped hardware co-simulation. Because of this multiplexing, the time spacing between output samples for a single model was 1.9 msec, even though the model was simulated with a step size of .1 msec. Given the width of the spikes produced by all our models, we do not think this

downsampling caused any problems for our analysis.

3.2 Model Descriptions

We now turn our attention to the reduction of the original HN model. Beginning with the FULL model, we will perform three reductions to the model. The first reduced model (R1) will be created by eliminating state variables and ionic currents from the FULL model. The second reduced model (R2) will be created by replacing the Hodgkin-Huxley style spiking mechanisms with integrate-and-fire mechanisms. The final reduced model (R3) will be created by replacing active ionic currents with a passive ionic current. All results reported in this section are from neuron models running on the FPGA.

3.2.1 Parameter Tuning

One of the primary problems with model reduction (and with neuronal modeling in general) is the phase of model development known as the tuning or *parameter estimation* phase. In this phase, the parameters of the model are adjusted so that a desired activity is produced by the model.

One of the primary problems of tuning the model is that multiple sets of parameter can produce the same activity [22, 9, 11, 37, 36]. This *non-uniqueness problem* poses a serious challenge for the model developer because although the same activity may be produced by the model at distinct point in parameter space, the response of the model to parameter variation at these points may be very different. Unfortunately, no current method exists to determine the "correct" parameter set for a given activity, and developing such a method is beyond the scope of this thesis.

With all of our reductions, the parameters were tuned in the context of an asymmetric half-center oscillator. That is, once the *structure* of a reduced model had been determined, the reduced model was coupled via inhibitory synapses to a FULL model neuron. The

parameters of the reduced model were then tuned with the goal of achieving an approximately equal duty cycle between the two neurons in the oscillator. Specifics as to which parameters were tuned are included with the details of each reduction.

3.2.2 FULL Model

The FULL model is taken from Hill et al [14]. This model is a single isopotential compartment following the Hodgkin-Huxley formalism. In addition to the details cited in the section on FPGA neuronal modeling, the FULL model differs from the original published model in three ways. First, we have eliminated the FMRF-amide activated current I_{KF}. Second, we have eliminated the externally injected current I_{inj}. Third, we did not include the graded synaptic current I_{SynG}. Both I_{KF} and I_{inj} were not required for any of our simulations, so their removal had no impact on any of our studies. I_{SynG} has been shown to have little effect on the half-center oscillations, so we do not think its elimination impacts any of our studies.

As implemented on the FPGA, the FULL – FULL model half-center oscillator (a FULL model coupled to a FULL model) produces oscillations that are very similar to those produced in the original published model (Table 1). This similarity demonstrates that our FPGA model was able to accurately reproduce previous modeling results obtained through a conventional modeling system. The FULL model is capable of producing both tonic spiking (Figure 16) and intrinsic rhythmic bursting (Figure 17).

3.2.3 R1 Model

The first reduction stage combines state variables and ionic currents with similar dynamics into a single variable or current. The R1 model therefore retains the Hodgkin-Huxley formalism used in the FULL model; only the number of state variables emulated has been reduced.

In an attempt to uncover similarities between different ionic currents and state variables, we performed a multi-dimensional parameter sweep of each state variable. These sweeps

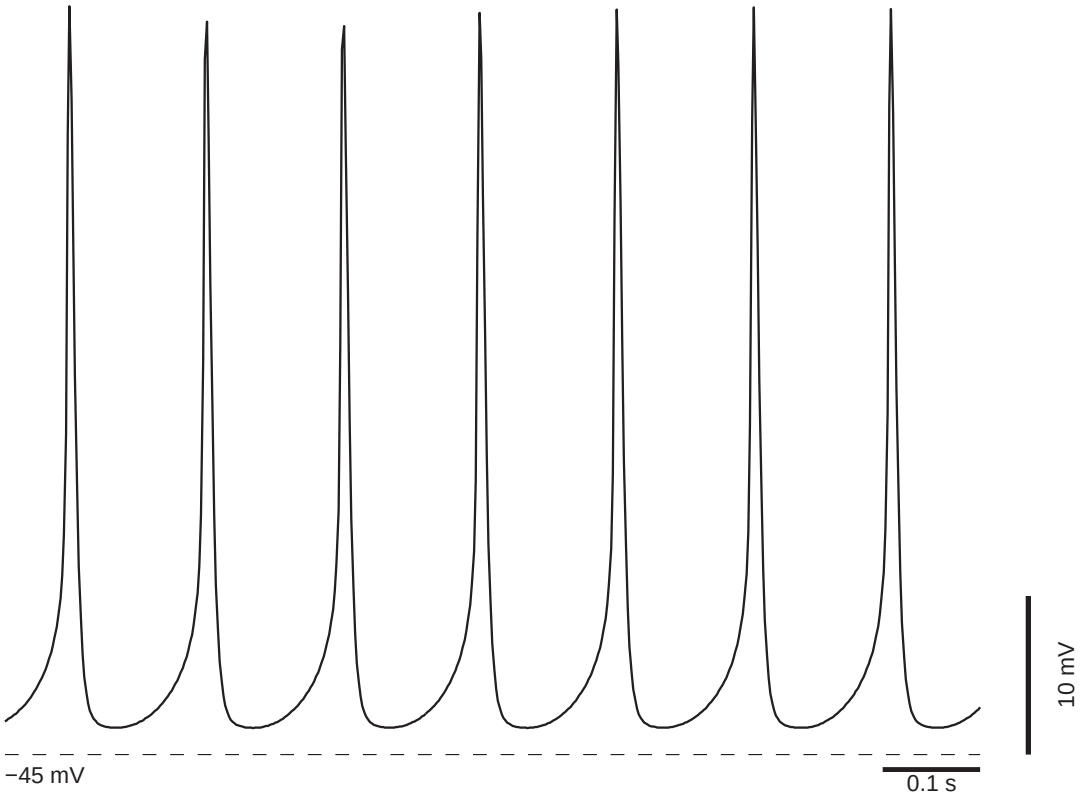

Figure 16: Tonic firing in the FULL model.

were performed on the FULL model in single cell configuration, and they covered a plane of the parameter space described by the half-maximal activation voltage $b_{m_{\text{ion}}}$ and the maximal conductance $\bar{g}_{\text{ion}}$. For ionic currents with inactivation variables, two additional parameter planes were investigated: the $b_{h_{\text{ion}}}$ – gbarion plane and the $b_{m_{\text{ion}}}$ – $b_{h_{\text{ion}}}$ plane. We analyzed the regions of these planes where the model produced intrinsic bursting behavior in order to determine where the model could be reduced.

We first recognized that the inactivation of I_{K1}, h_{K1} is largely unimportant in the behavior of the model (Figure 18). Increasing $b_{h_{\text{K1}}}$ shifts the steady-state inactivation curve to a point where there is little or no inactivation of I_{K1}; this change had little effect on the period, duty cycle, or spike frequency characteristics of the model.

By eliminating h_{K1}, we now have

$$I_{\text{K1}} = \bar{g}_{\text{K1}} m_{\text{K1}}^2 (V_m - E_{\text{K}}) \tag{18}$$

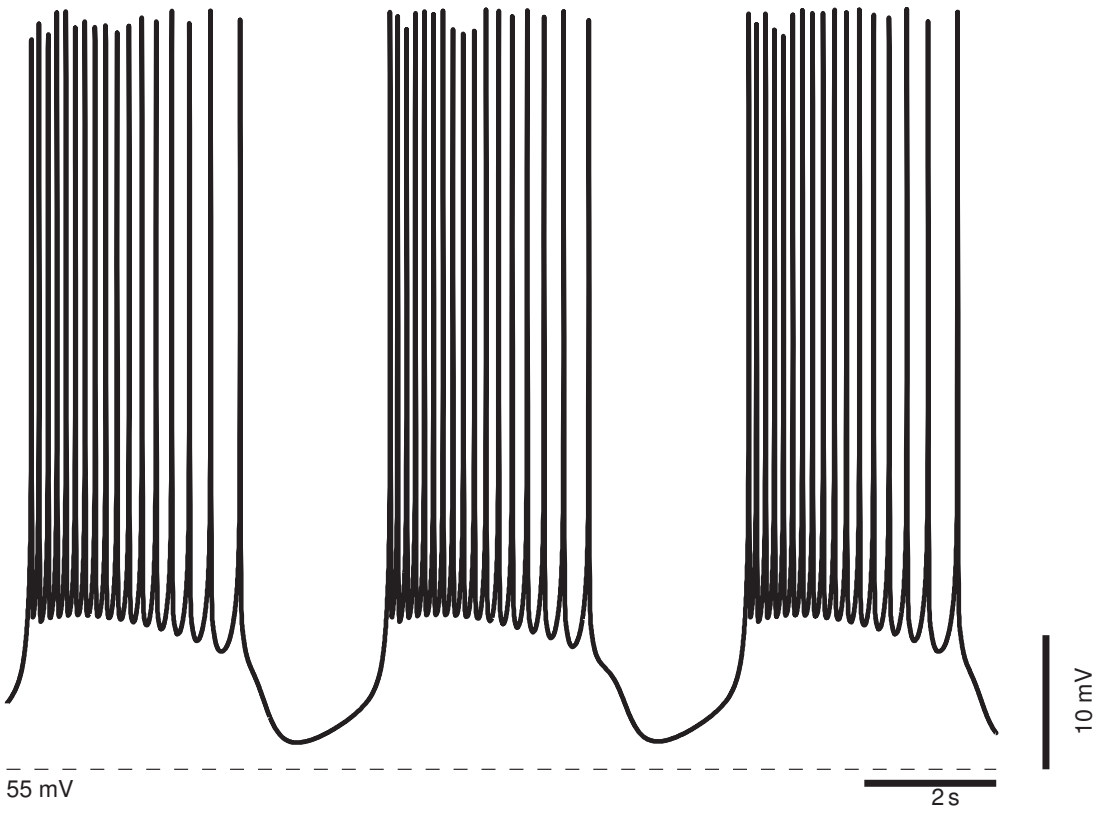

Figure 17: Intrinsic bursting in the FULL model.

In asymmetric half-center oscillator configuration, there was a slight imbalance in duty cycle due to elimination of h_{K1}. $\bar{g}_{K1}$ was tuned from 100 to 71 nS in order to compensate for this imbalance.

Next, we discovered that the fast calcium current, I_{CaF} is functionally very similar to the slow calcium current, I_{CaS} (Figure 19); the period, duty cycle and spike frequency characteristics of the model respond similarly to changes in the half-maximal activation and maximal conductance of both I_{CaF} and I_{CaS}. This similarity is surprising, because I_{CaF} and I_{CaS} evolve on very different time scales. I_{CaF} was therefore eliminated by setting $\bar{g}_{CaF} = 0$ nS, and $\bar{g}_{CaS}$ was tuned from 3.2 nS to 4.0 nS to compensate for the change in activity.

These two reductions, the elimination of h_{K1} and I_{CaF} were discovered through examination of the model's parameter space. To supplement this method, we employed the method

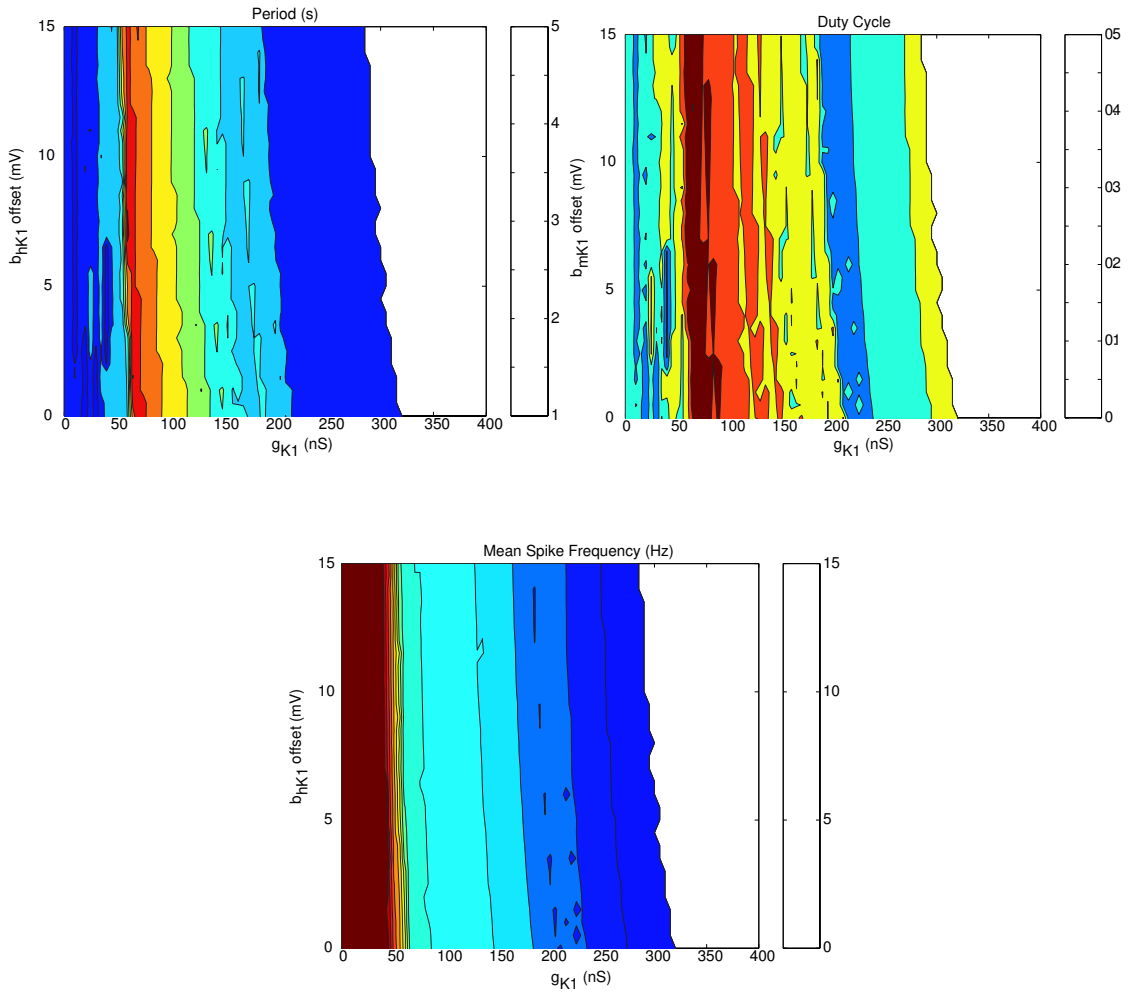

Figure 18: Effect of h_{K1} and $\bar{g}_{K1}$ on period, duty cycle, and mean spike frequency of bursting. As the half-maximal inactivation voltage of h_{K1} increases, there is little change in the period, duty cycle, or mean spike frequency of bursting.

of equivalent potentials to reveal similarities among the state variables (Figure 20) [18, 10]. The equivalent potential of a state variable is the value of the membrane potential at which the state variable's steady-state value would be equal to its current value. The steady-state function, f_∞, for the state variables (except $m_{h\infty}$) in the FULL model always takes the form of the sigmoidal function:

$$f_\infty(a, b, V_m) = \frac{1}{1 + e^{a(V_m + b)}} \tag{19}$$

the equivalent potential, U_m of a state variable m is therefore given by

$$U_m(m, a, b) = \frac{ln(\frac{1}{m} - 1)}{a} - b \tag{20}$$

where b is the half-maximal activation (or inactivation) voltage, a is the slope of the function at the half-maximal voltage, and V_m is the membrane potential. We compute the equivalent potentials for all remaining state variables over one oscillation period of the FULL – FULL half-center oscillator. We then compare the equivalent potentials to each other, and make reductions for state variables whose equivalent potentials are correlated. The equivalent potential for m_{h} was not computed because its steady-state function is non-invertible.

The equivalent potentials method shows us two further reductions that can be made to the FULL model. First, the activation of the fast sodium current, m_{Na}, is linearly correlated with V_m. This relationship means that we can eliminate m_{Na} as a state variable, replacing it with its steady-state activation function

$$m_{\mathrm{Na}} = m_{\mathrm{Na}\infty} \tag{21}$$

Second, we assume a linear relationship between $U_{m_{\mathrm{KA}}}$ and $U_{m_{\mathrm{P}}}$, and a quadratic correlation between $U_{h_{\mathrm{KA}}}$ and $U_{m_{\mathrm{P}}}$. These assumptions initially led us to model I_{KA} as a quadratic function of m_{P}; further investigations, however, revealed that the net activation of I_{KA} ($m_{\mathrm{KA}}^2 h_{\mathrm{KA}}$) could be closely approximated by m_{P} itself (Figure 21). We set $\bar{g}_{\mathrm{KA}} = 0$, and $\bar{g}_{\mathrm{P}}$ was tuned from 7 to 6.3 nS in order to compensate for the change in activity induced by this reduction.

All of these reductions taken together constitute the R1 model. This reduced model is very similar to the FULL model; it is capable of both tonic firing and intrinsic bursting. The spike shape is very similar (Figure 22) to the FULL model, as is the waveform of the intrinsic bursting (Figure 23). The behavior of the FULL – R1 half-center oscillator is very similar to the FULL – FULL half-center oscillator (Table 1).

This reduction has greatly simplified the FULL model. The number of state variables

has been reduced from 14 to 8, and the number of ionic currents emulated has been reduced from 9 to 7.

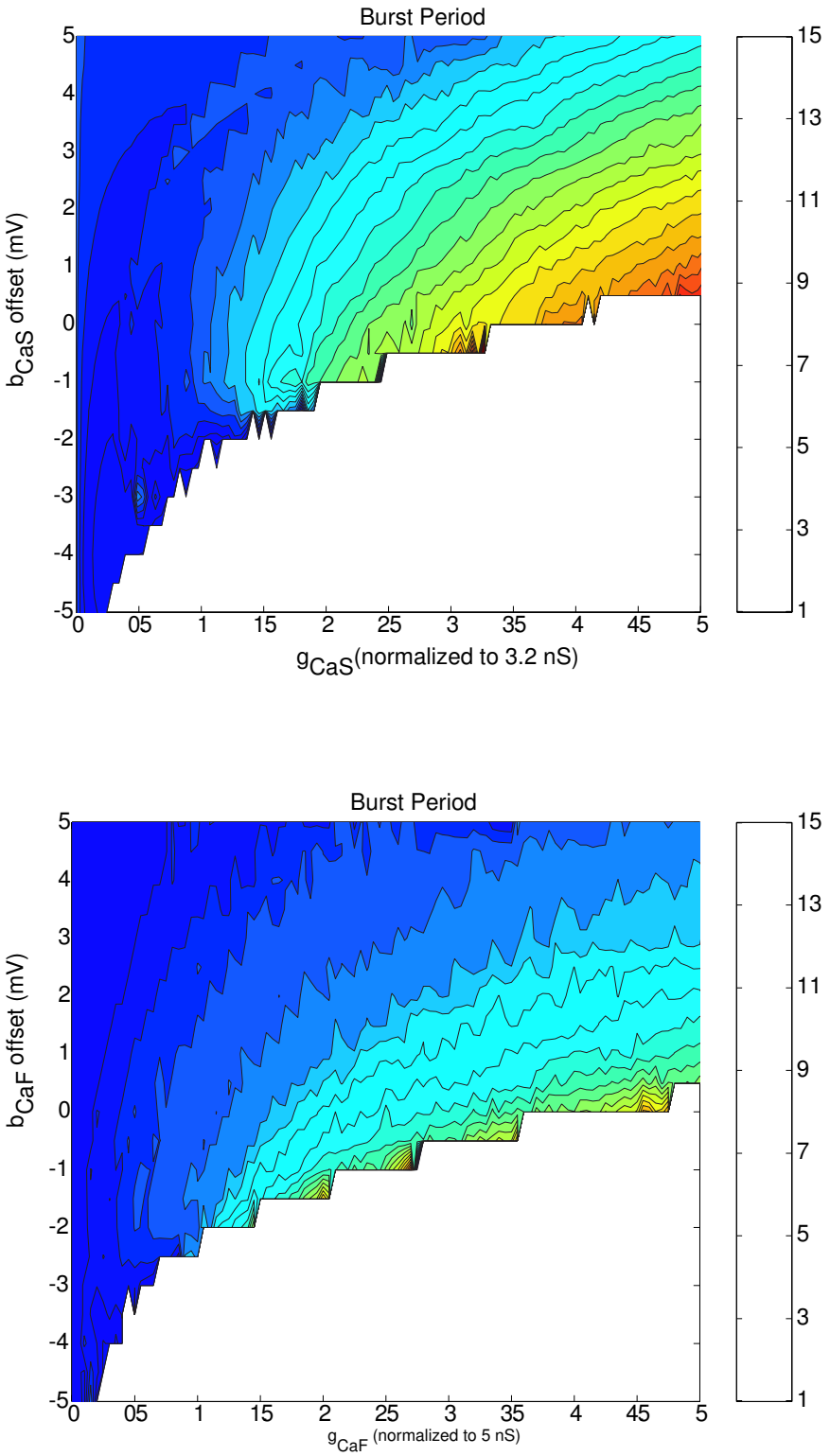

Figure 19: Modulation of I_{CaS} and I_{CaF} have similar effect on burst period. The period of the model responds similarly to changes in the half-maximal activation voltage and maximal conductances of I_{CaS} and I_{CaF}.

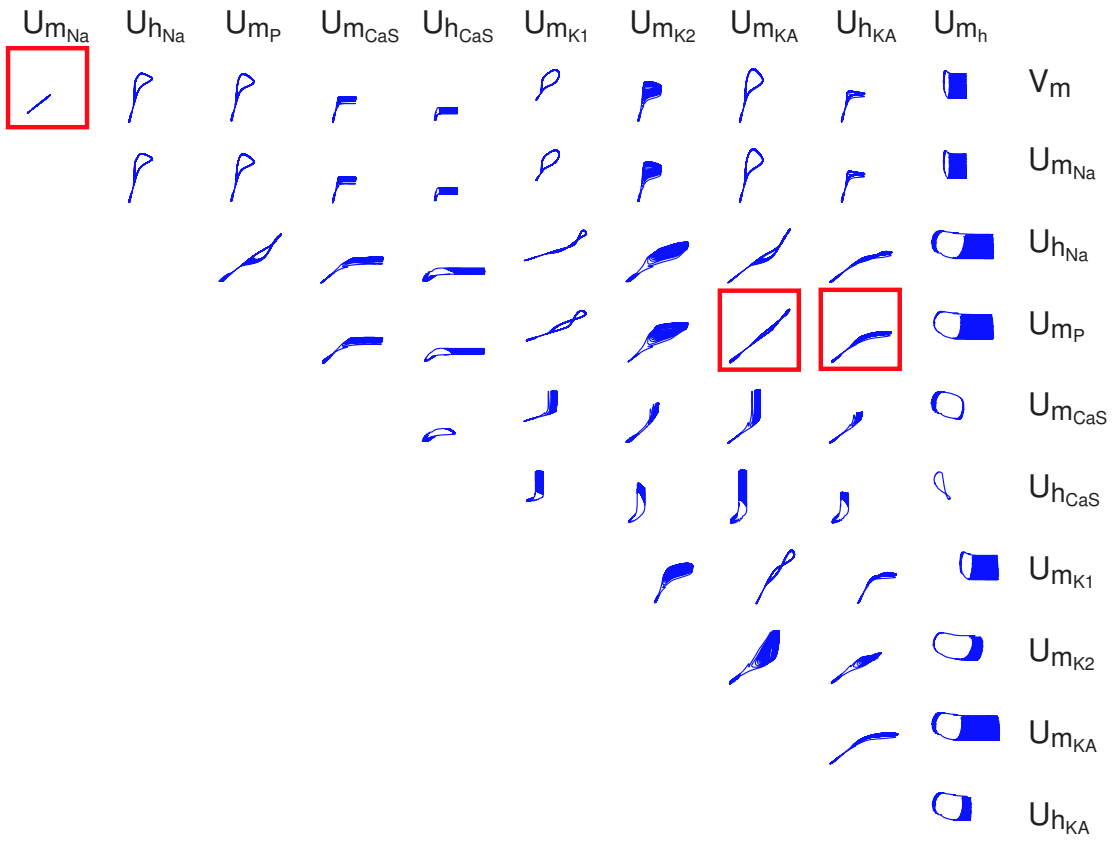

Figure 20: Comparing equivalent potentials in first stage reduction. Equivalent potentials for the FULL model over one oscillation period are plotted against each other. Red boxes indicate where reductions in the model were made.

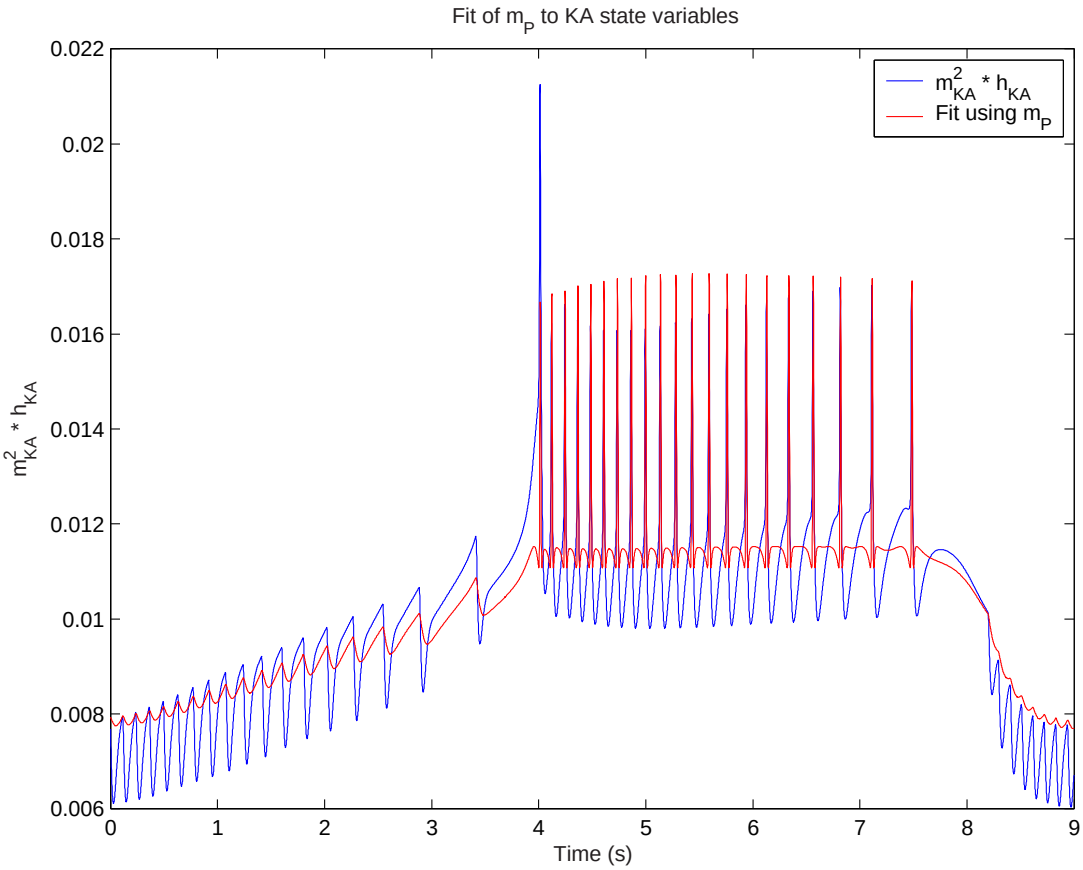

Figure 21: Approximating I_{KA} with m_P.

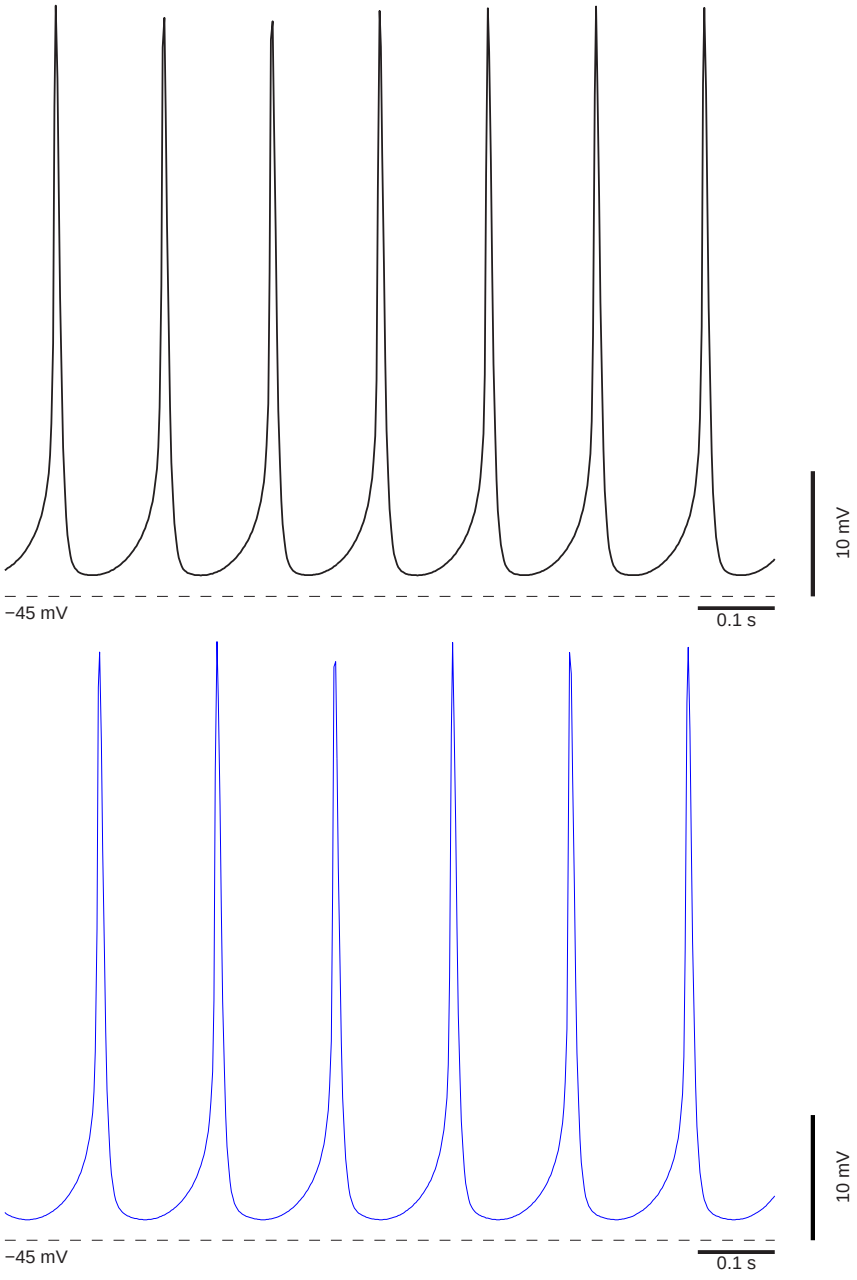

Figure 22: Comparing FULL and R1 models tonic firing.

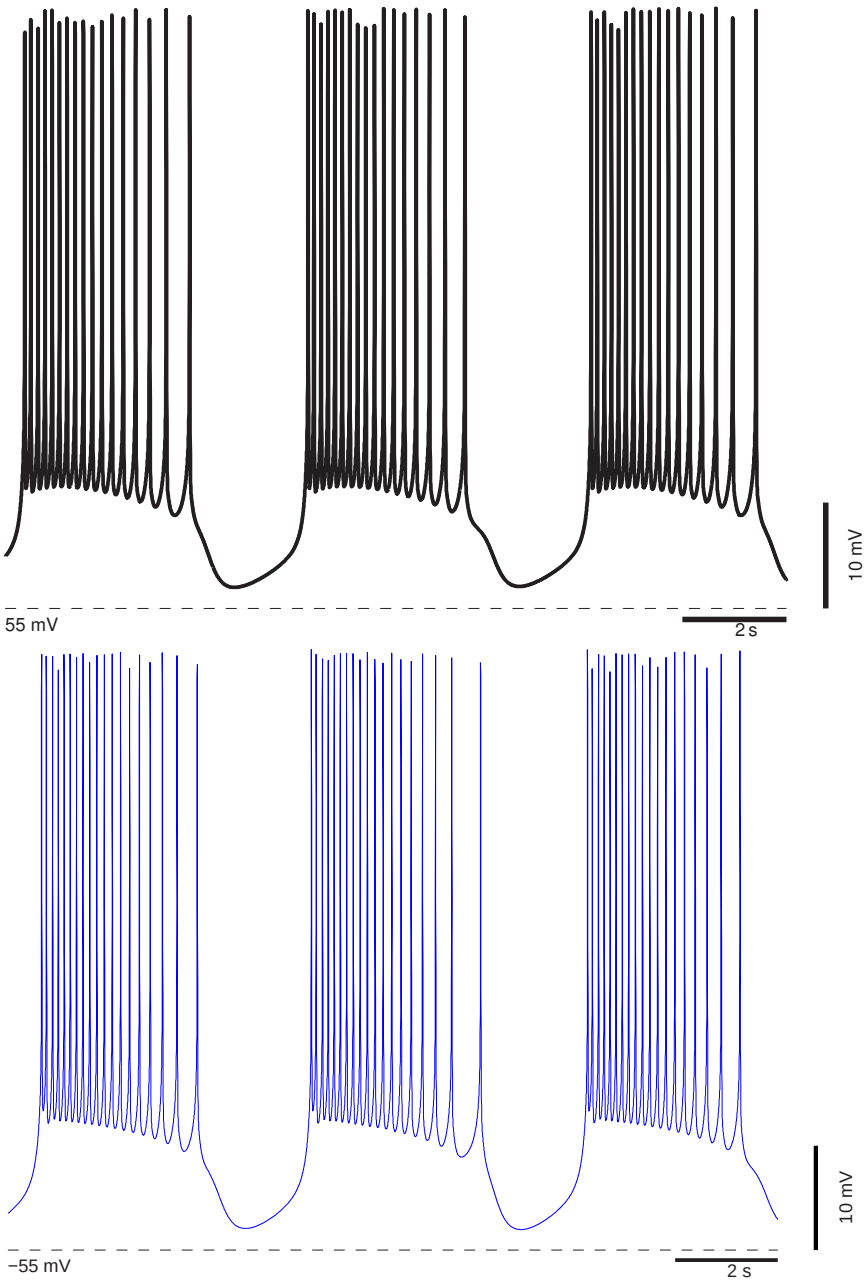

Figure 23: Comparing FULL and R1 models intrinsic bursting.

3.2.4 R2 Model

In the second stage reduction, we replace the fast spiking currents I_{Na} and I_{K1} with integrate-and-fire (IAF) mechanisms [2]. In this hybrid integrate-and-fire model, the integrate-and-fire parameters V_{thresh}, the firing threshold, and V_{reset}, the reset potential, are functions of the slow calcium inactivation variable h_{CaS}.

In order to make this reduction, we first characterize the relationship between h_{CaS} and V_{reset}. We do this by making h_{CaS} a parameter of the R1 model, varying h_{CaS} from 0 to 1 in increments of $1/128$, and then analyzing the activity of the model at each value of h_{CaS}. The model was given 30 seconds to settle and then 30 seconds of data were recorded. We calculate V_{reset} as the average minimum voltage between spikes (Figure 24); additionally, we calculate the spike frequency for each value of h_{CaS} (Figure 25).

Next, we removed the spike generating currents I_{Na} and I_{K1}, and replace them with IAF mechanisms that are described by V_{reset} and V_{thresh}. V_{reset} is a function of h_{CaS} based on the results shown in Figure 24, and implemented as a 128-entry look-up table with h_{CaS} as the index into the table. We made h_{CaS} and V_{thresh} model parameters, and examined the spike frequency of the model at different points in the $V_{thresh} - -h_{\mathrm{CaS}}$ parameter plane (Figure 26). Using these values, we then calculated what values of V_{thresh} (as a function of h_{CaS}) would best reproduce the relationship between spike frequency and h_{CaS}. Overall, the hybrid IAF model produces spike frequencies that are higher than R1 model. We were unable to lower the spike frequency by raising V_{thresh}; doing so caused the model to fall silent.

The final step in creating our hybrid IAF model is to consider the effect of a spike on the slow variable h_{CaS}. In an IAF model, the membrane potential transitions instantly from V_{thresh} to V_{reset}; this transition ignores the effect of a spike waveform on the evolution of the state variable h_{CaS}. In order to compensate for this effect, we calculated the perturbational effect of a spike on h_{CaS} by integrating h_{CaS} over a typical spike waveform from the R1 model (Figure 27).

Our new "hybrid" IAF model is therefore described by:

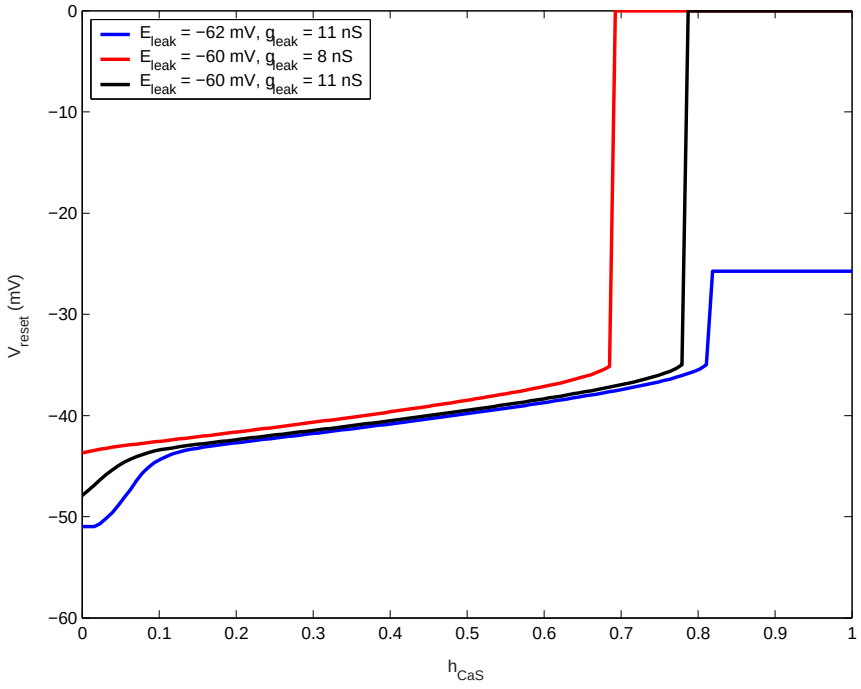

Figure 24: V_{reset} as a function of h_{CaS} in the R1 model. Changes is E_{leak} and g_{leak} affect V_{reset}.

$$\frac{dV_m}{dt} = \begin{cases} -\frac{1}{C}(I_{\mathrm{P}} + I_{\mathrm{K2}} + I_{\mathrm{CaS}} + I_{\mathrm{h}} + I_{\mathrm{leak}}) & : \quad V_m < V_{thresh}(h_{\mathrm{CaS}}) \\ V_{reset}(h_{\mathrm{CaS}}) - Vm & : \quad V_m \geq V_{thresh}(h_{\mathrm{CaS}}) \end{cases} \tag{22}$$

$$\frac{dh_{\mathrm{CaS}}}{dt} = \begin{cases} \frac{m_{\mathrm{hCaS}\infty}(\mathrm{Vm}) - m_{\mathrm{hCaS}}}{\tau_{\mathrm{CaS}}(V_m)} & : \quad V_m < V_{thresh}(h_{\mathrm{CaS}}) \\ D_{h_{\mathrm{CaS}}}(h_{\mathrm{CaS}}) - h_{\mathrm{CaS}} & : \quad V_m \geq V_{thresh}(h_{\mathrm{CaS}}) \end{cases} \tag{23}$$

and all other equations are as in the R1 model.

Two problems were encountered with this model. First, the model was not able to produce intrinsic bursting behavior. Second, the model did not produce half-center oscillations.

To address the first problem, we investigated how changes in E_{leak} and g_{leak} affect the reset voltage and spike frequency, as E_{leak} and g_{leak} are associated with changes in the intrinsic behavior of the model. The results are shown in Figures 24 and 25. These figures show that a decrease in E_{leak} or an increase in g_{leak} is essentially equivalent to an increase in h_{CaS}. Changes in E_{leak} and g_{leak} had little effect on the perturbation of h_{CaS} by a spike.

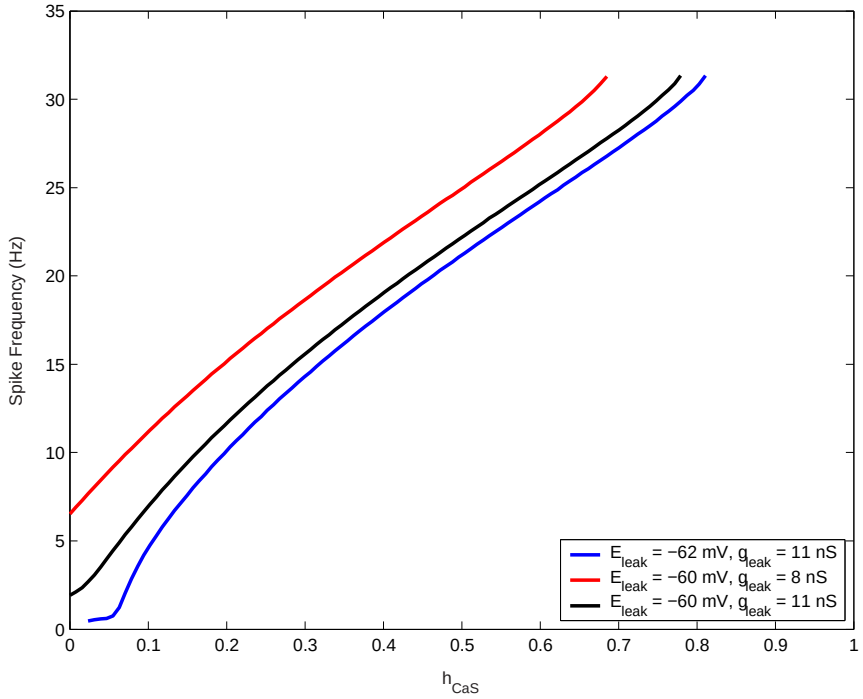

Figure 25: Spike frequency as a function of h_{CaS} in the R1 model. Changes is E_{leak} and g_{leak} affect the spike frequency.

We therefore changed the structure of the model to account for this effect:

$$\frac{dV_m}{dt} = \begin{cases} -\frac{1}{C}(I_{\text{P}} + I_{\text{K2}} + I_{\text{CaS}} + I_{\text{h}} + I_{\text{leak}}) & : \quad V_m < V_{thresh}(h'_{\text{CaS}}) \\ V_{reset}(h'_{\text{CaS}}) - Vm & : \quad V_m \geq V_{thresh}(h'_{\text{CaS}}) \end{cases} \tag{24}$$

$$\frac{dh_{\text{CaS}}}{dt} = \begin{cases} \frac{m_{\text{hCaS}\infty}(V_m) - m_{\text{hCaS}}}{\tau_{\text{CaS}}(V_m)} & : \quad V_m < V_{thresh}(h'_{\text{CaS}}) \\ D_{h_{\text{CaS}}}(h_{\text{CaS}}) - h_{\text{CaS}} & : \quad V_m \geq V_{thresh}(h'_{\text{CaS}}) \end{cases} \tag{25}$$

$$h'_{\text{CaS}} = h_{\text{CaS}} + .016 \times (E_{\text{leak}} - 62) + 0.029 \times (g_{\text{leak}} - 11) \tag{26}$$

This change adequately reproduced the relationship between spike frequency and h_{CaS} (Figure 28), and allowed the model to produce both tonic firing (Figure 29) and intrinsic bursting activity (Figure 30).

To account for the second problem, the inability of this model to produce half-center oscillations, we theorized that the elimination of I_{Na} was preventing our hybrid IAF model

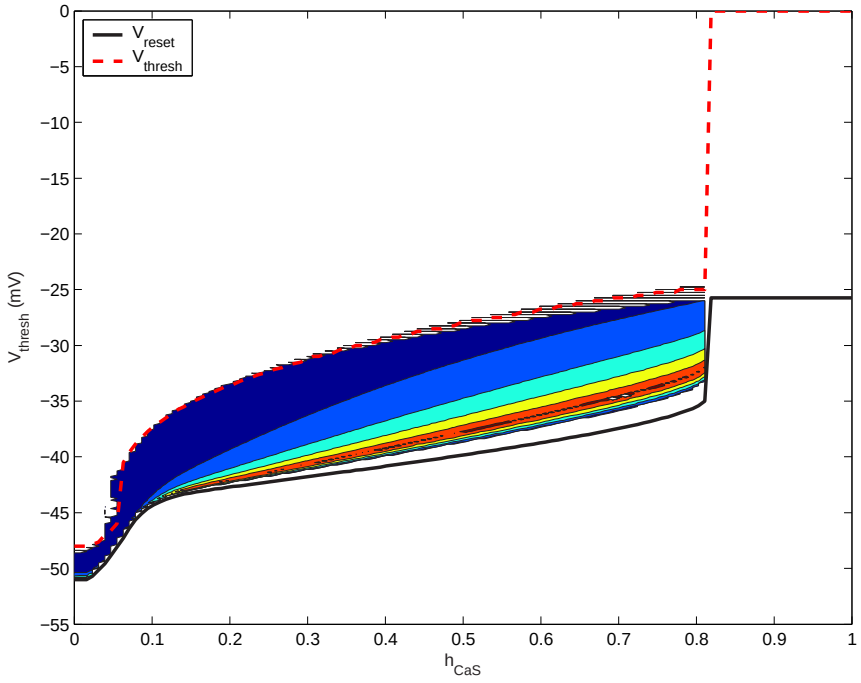

Figure 26: Calculating V_{thresh} as a function of h_{CaS}. The black line indicates the reset potential, V_{reset}. The dashed red line indicates the values of V_{thresh} that best reproduce the spike frequency relationship of Figure 25

from reaching firing threshold. We based this theory on the fact that the steady-state activation function for m_{Na}, $m_{\infty\mathrm{Na}}$ has a relatively shallow slope. Without the slight contribution of I_{Na} at subthreshold voltages, the model was unable to reach firing threshold. We tested three approaches to solving this problem: First, we tried increasing the magnitude of the hyperpolarization-activated current I_{h} by increasing $\bar{g}_{\mathrm{h}}$; a two-fold increase in $\bar{g}_{\mathrm{h}}$ was unable to elicit half-center oscillations, so we abandoned this approach. We tried both increasing $\bar{g}_{\mathrm{P}}$ and decreasing g_{leak}; both of these approaches produced half-center oscillations, but the oscillations were unequal, with the R3 model dominating the activity of the FULL model. Finally, we tried increasing $\bar{g}_{\mathrm{CaS}}$ to 5.375 nS. This approach was successful: the increase in $\bar{g}_{\mathrm{CaS}}$ caused the hybrid IAF model to escape inhibition, and an increase in g_{leak} from 8 to 8.75 nS created approximately equal duty cycles between the two neurons.

The introduction of integrate-and-fire dynamics has eliminated the formation of physiologic action potentials. In the data shown here, "spikes" are overlayed on top of the

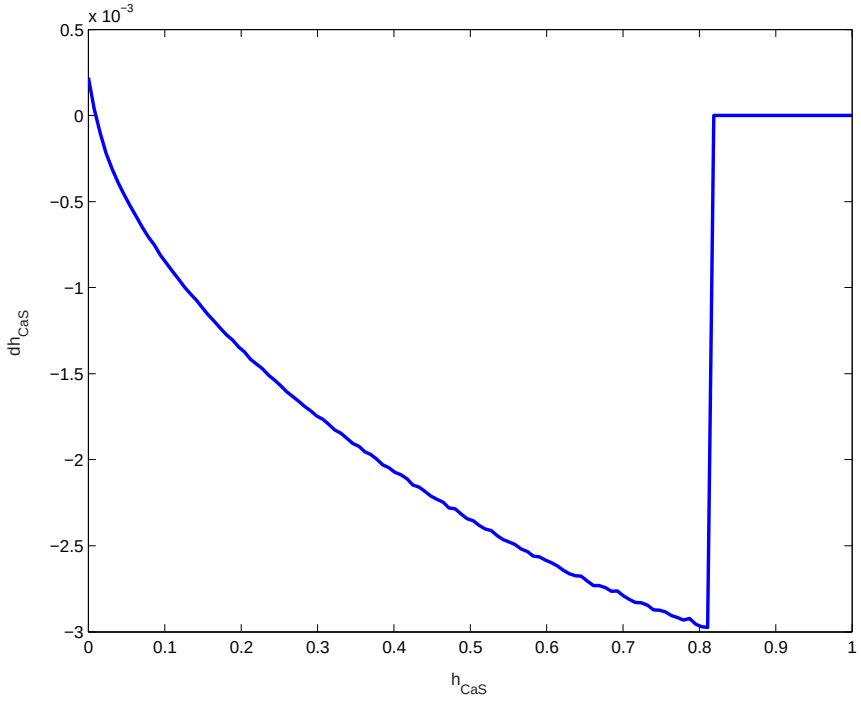

Figure 27: Change in h_{CaS}, $D_{h_{\mathrm{CaS}}}$ due to a spike.

membrane potential waveform in order to aid comparisons between the models. The spike is created by setting the external membrane potential of the model (that is, the membrane potential output by the FPGA) to 0 mV for 1.9 msec after a spike event occurs. The "internal" membrane potential of the model does not have this spike overlay.

The spike shape of the R2 model is obviously quite different from the FULL and R1 models. Even with this significant change in the structure of the model, however, the period, duty cycle, and slow-wave characteristics of the FULL-R2 half-center oscillator are very similar to FULL-FULL half-center oscillator (Table 1). Only the spike frequency characteristics of the R2 model are noticeably different from the FULL-FULL half-center (Table 2).

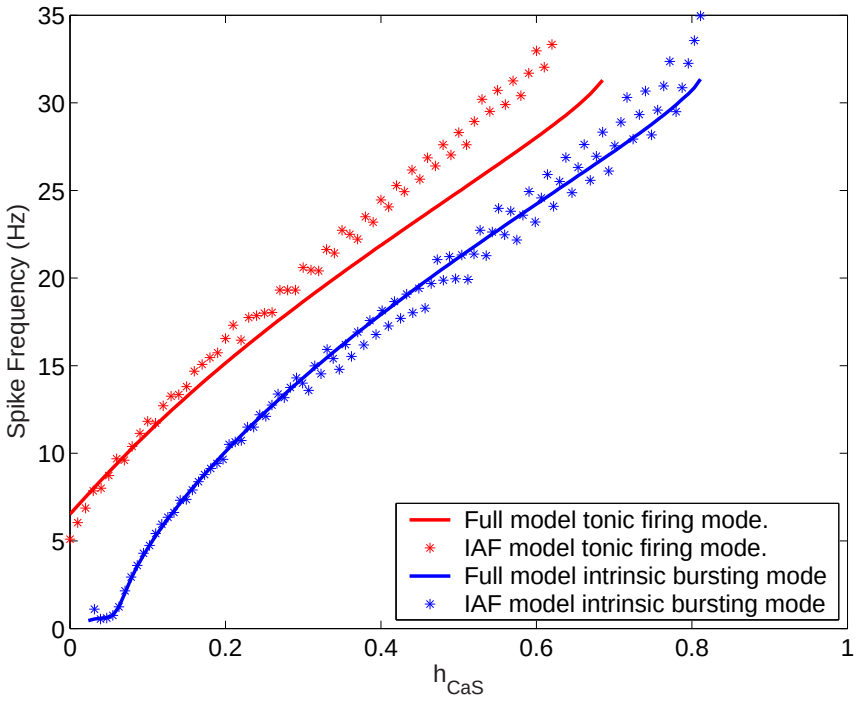

Figure 28: Spike frequency as a function of h_{CaS} in hybrid IAF model.

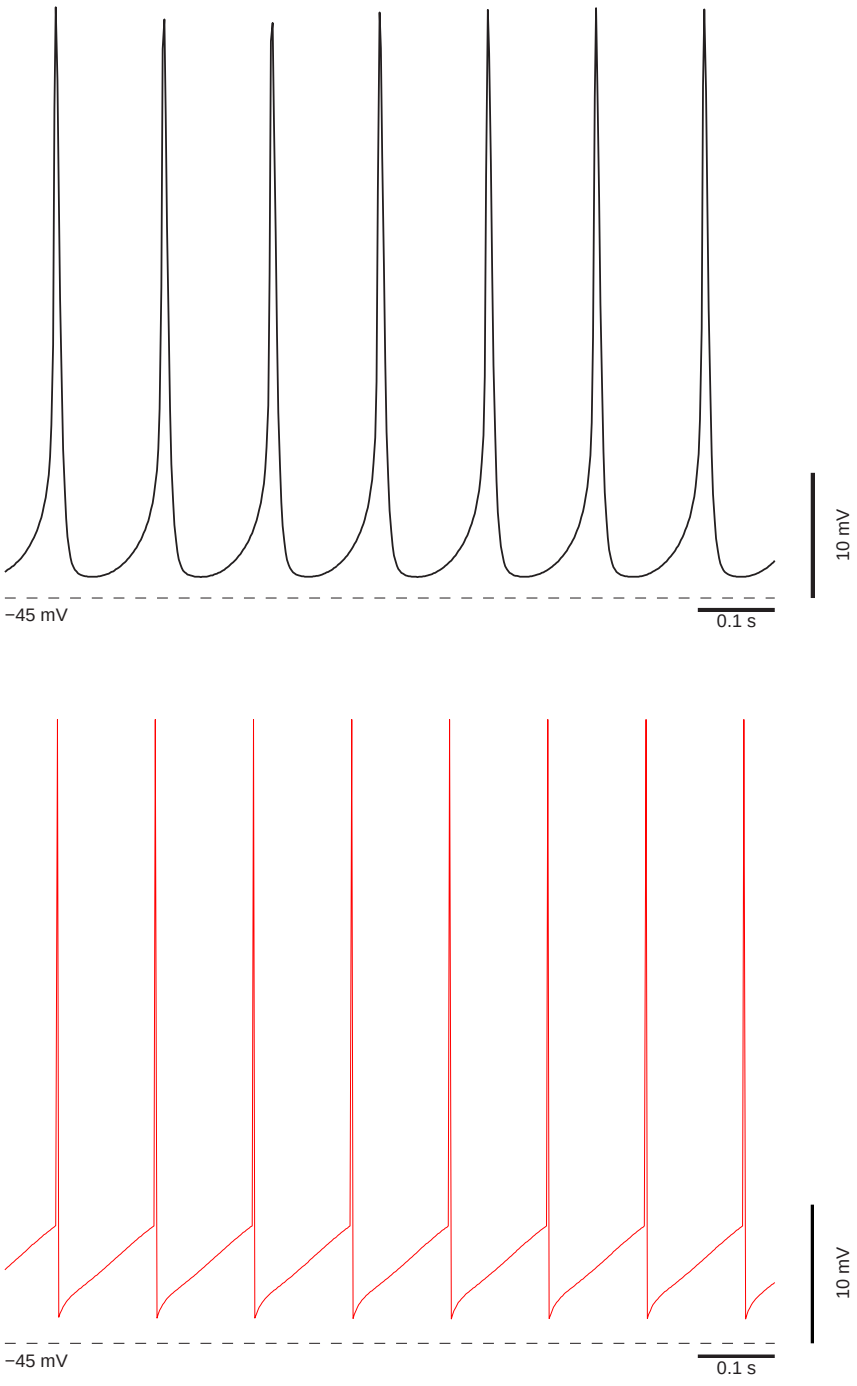

Figure 29: Comparing FULL and R2 models tonic firing.

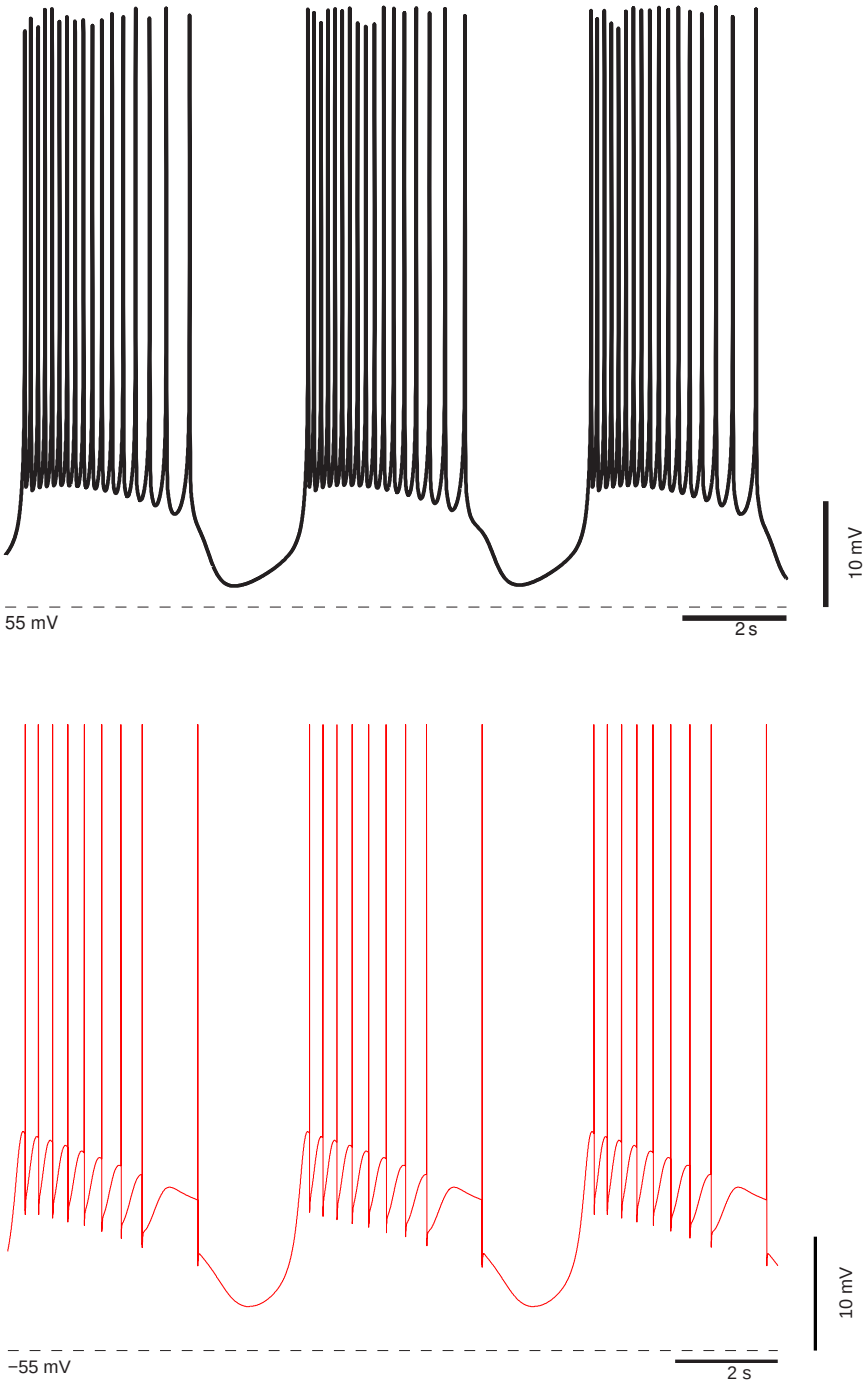

Figure 30: Comparing FULL and R2 models intrinsic bursting.

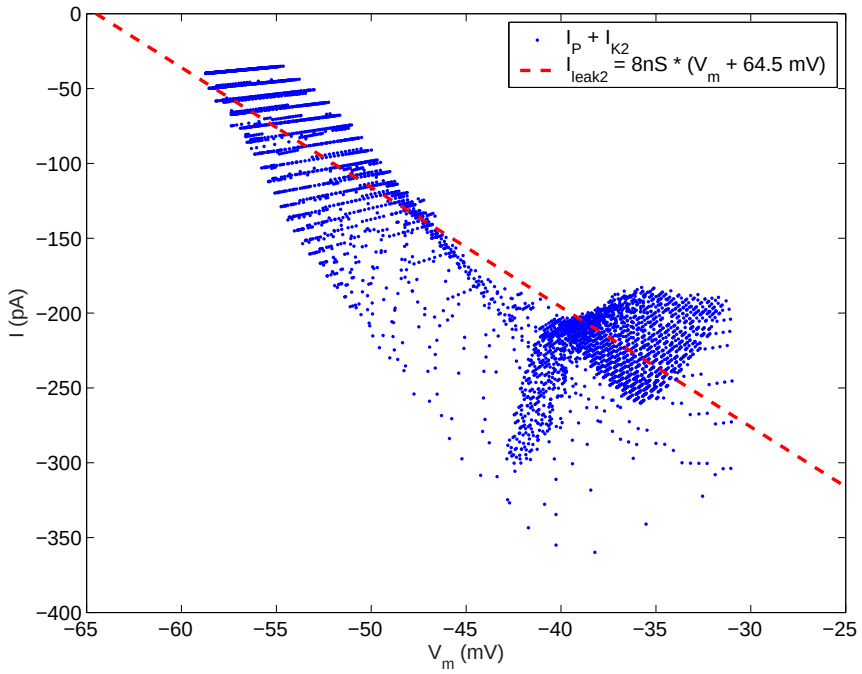

Figure 31: Third stage reduction. I_{P} and I_{K2} are replaced with a single passive current I_{leak2}.

3.2.5 R3 Model

In the third and final reduction of the HN model, we replace the persistent sodium current, I_{P}, and the persistent potassium current, I_{K2}, with a single passive current I_{leak2} (Figure 31).

$$I_{\mathrm{leak2}} = g_{\mathrm{leak2}}(V_{\mathrm{m}} - E_{\mathrm{leak2}}) \tag{27}$$

where $g_{\mathrm{leak2}} = -7.875$ nS and $E_{\mathrm{leak2}} = -64.5$ mV.

This reduction was not possible before the introduction of integrate-and-fire mechanisms because in the superthreshold region the combination of I_{P} and I_{K2} was not nearly linear.

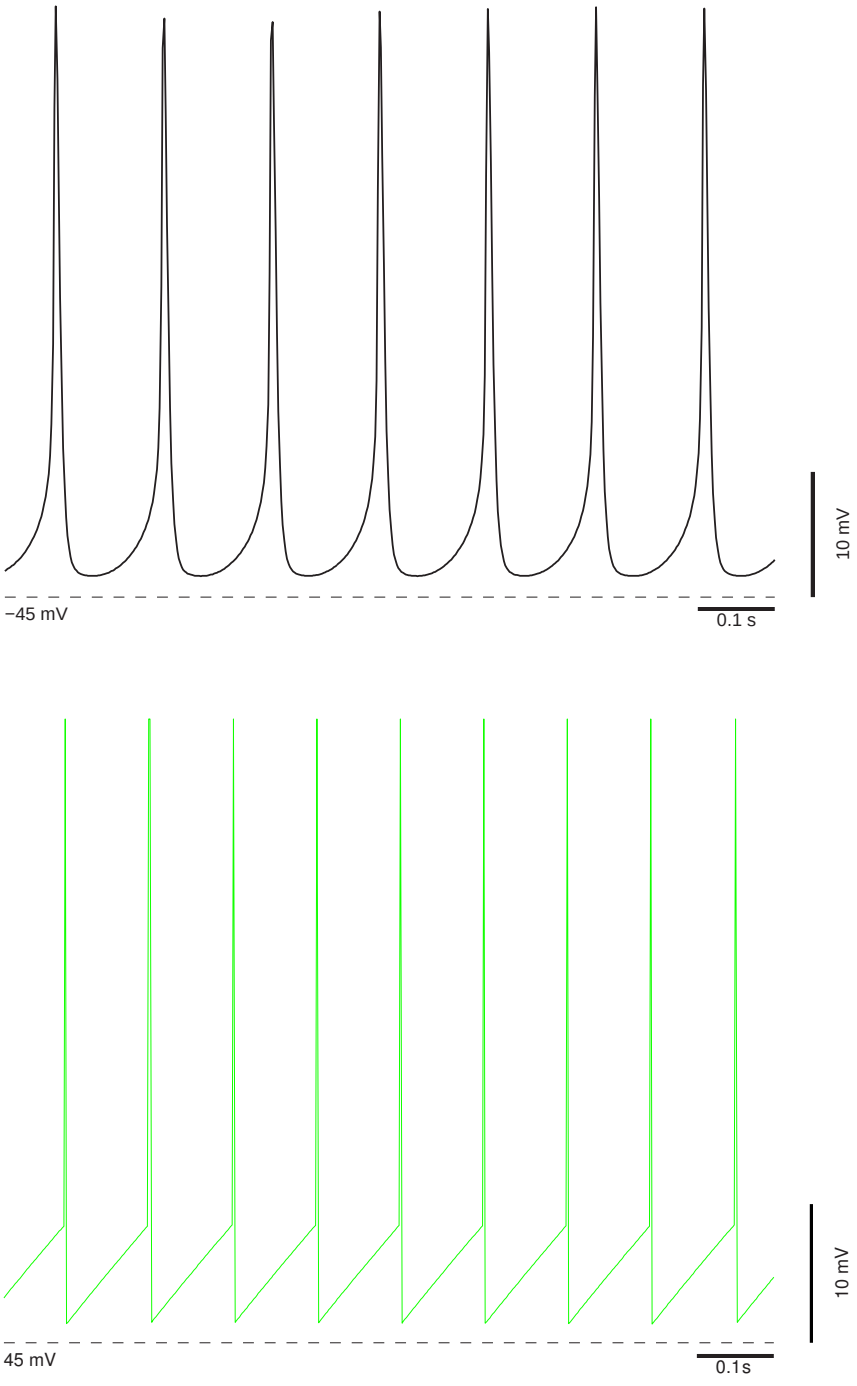

Figure 32: Comparing FULL and R3 models tonic firing.

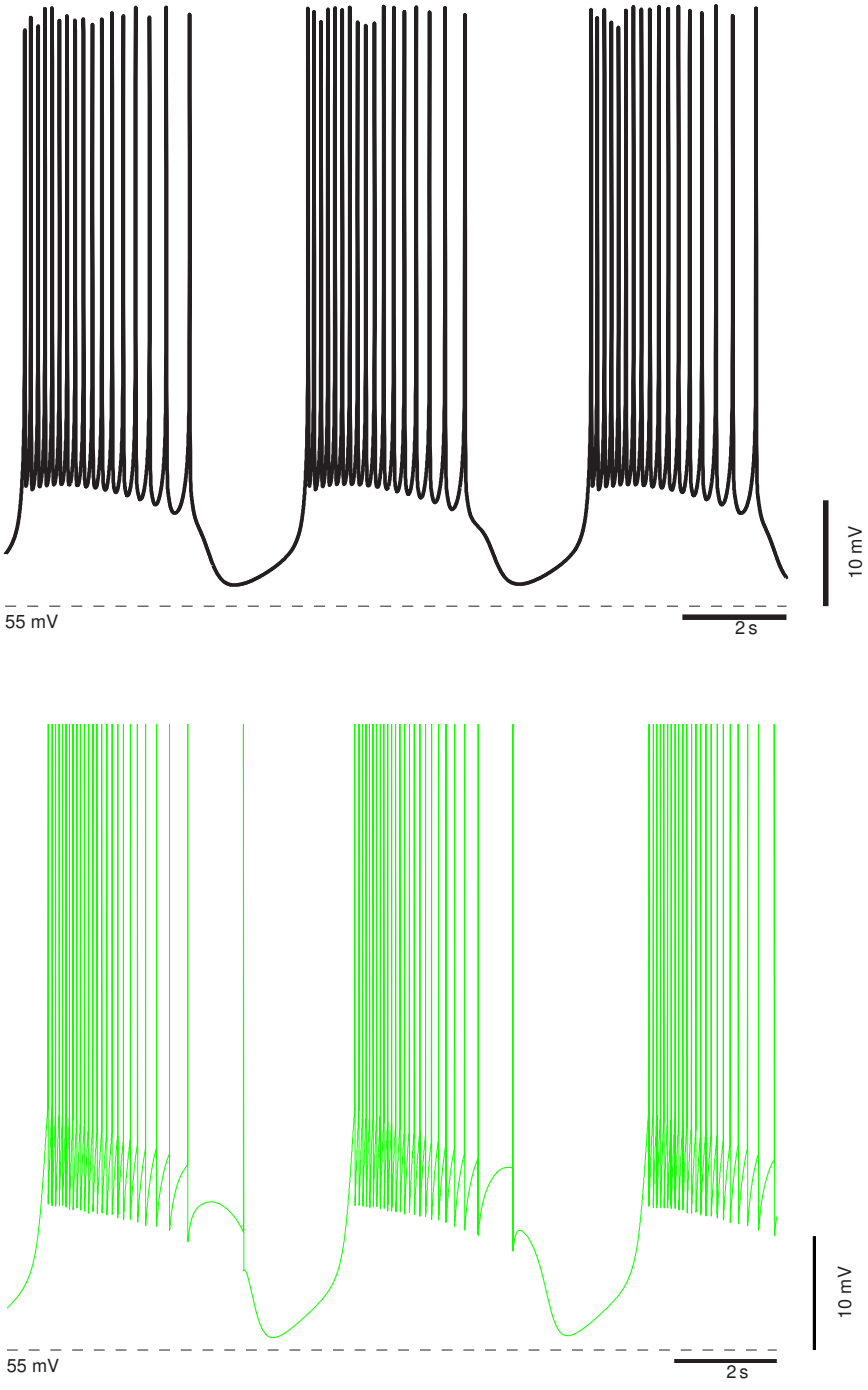

Figure 33: Comparing FULL and R3 models intrinsic bursting.

g_{leak} was set to 8.5 nS in order to create balanced oscillations in the FULL-R3 half-center oscillator.

This reduced model was able to produce both tonic firing (Figure 32) and intrinsic bursting (Figure 33) that were very similar to the R2 model. The period, duty cycle, and slow-wave characteristics in the FULL – R3 half-center oscillator were very similar to the FULL – FULL half-center. As in the FULL – R2 half-center oscillator, the spike frequency characteristics of the reduced model were noticeable higher than those of the the FULL model.

3.2.6 Discussion

We have successfully reduced our FULL neuron model to create three reduced neuron models: R1, R2, and R3. The R1 model retains the physiologic character of the FULL model, albeit with a smaller set of state variables and ionic currents. The R2 model replaces the physiologic spiking mechanisms with integrate-and-fire mechanisms, creating a model with both mechanistic and empirical components. The R3 model replaces two active ionic currents with a single passive current.

All three reduced models were able to produce both intrinsic bursting and tonic spiking activities, similar to the FULL model. In this sense, all three reductions are "good" reductions of the original model. In the following chapter, we will investigate the ability of the models to produce robust and flexible activity in half-center oscillators, we will investigate how parameter variation effects the reduced models, and we will validate our modeling studies using a hybrid half-center oscillator.

CHAPTER IV

FUNCTIONAL ROLE OF MODEL COMPLEXITY IN HALF-CENTER OSCILLATORS

Neural systems are presumed to produce activity that is both *robust* and *flexible*. They are robust in the sense that they function despite changes in their environment, such as changes in temperature, ionic concentrations, transcription errors, etc. They are flexible in that they are able to produce a rich variety of behaviors in order to achieve their function.

In order to accurately reproduce the function of neural systems, a neuronal model system must also be robust and flexible. In a hybrid neural system, robustness and flexibility are necessary because without them the functionality of the system will be extremely limited. The primary goal of this thesis is to evaluate how model complexity contributes to the functionality of hybrid systems built from both model neurons and living neurons; robustness and flexibility are our metrics for evaluating the functional performance of the system.

Unfortunately, given the experimental overhead involved, we cannot fully evaluate these metrics within the context of our hybrid system. Instead, we will create three *asymmetric* model oscillators that emulate a hybrid system. In these asymmetric oscillators, a reduced model neuron will be coupled to a FULL model neuron; the FULL model neuron will serve as the "biological equivalent" in the system. We will then perform a first-order parameter sweep of the maximal conductances in each asymmetric oscillator, and evaluate the robustness and flexibility of each model system. We will then use the hybrid system to validate a subset of our simulations of asymmetric model oscillators.

4.1 Robustness and Flexibility Metrics

Neural systems are considered to be *robust*: they function despite changing input conditions. For example, all neural systems are subject to biological "noise": internal variations in ion concentrations, errors in protein transcription, the presence of modulatory agents, varying synaptic input, etc. A neural system must be able to function in spite of these ever-changing conditions.

Neural systems are also considered to be *flexible*: they produce a rich variety of outputs in order to achieve their function. In a locomotor system, for example, the network may produce different patterns of activity depending on whether the animal is walking or running.

In order to assess the robustness and flexibility in our model networks, we must first define quantitative measurements of robustness and flexibility. Our robustness metric will describe the range of inputs over which the model functions, an approximation of the size of the system's input space. Our flexibility metric will describe variability in the model's outputs over its functional range, an approximation of the size of the system's output space.

4.1.1 Robustness Metric

The robustness of a system describes the size of the systems input space over which the system functions. We assume that the function of a half-center oscillator is to produce half-center oscillations. The inputs to our system are the system parameters: maximal conductances, reversal potentials, time constants, etc. Our robustness metric therefore describes the range of model parameters over which the system produces half-center oscillations.

For each parameter p investigated, we will produce a *robustness score*, r:

$$r = 50 \times \left(\log \left(\frac{p_{max}}{p_{min}} \right) \right) \tag{28}$$

where p_{min} is the lowest value of the parameter where the system produces half-center

oscillations, and p_{max} is the largest value where the system produces half-center oscillations. p_{min} is greater than or equal to 0.1 times the canocial paramter value. A score of 100 indicates that the model produces half-center oscillations from 0.1 times the canonical parameter value to 10 times the canonical parameter value.

4.1.2 Flexibility Metric

The flexibility of a system describes the variability in the system's output over its functional range. The functional range is determined by the range of parameters over which the system produces half-center oscillations. The output of our system is taken to be the measurements of the burst characteristics: period, duty cycle, etc. In order to assess variability of the system's output, we will use a statistical method known as principal component analysis (PCA).

PCA is a data reduction method in which a number of possibly correlated variables are transformed into a new set of uncorrelated variables, which are called the *principal components*. The first principal component will account for as much of the variance between the variables as possible; it is often a weighted mean of all the variables. The second principal component accounts for as much of the remaining variance as possible, and so on, until all the variance in the data is accounted for.

Although the number of principal components returned is equal to the original number of variables, most of the variance in the data will often be explained by the first few principal components. PCA thereby gives us a method to assess the overall amount of correlation in the data, an approximation of the size of the space spanned by the data. In the case of our neuron models, it gives us an approximation of the number of independent outputs that the system can produce. For example, if the oscillator period, duty cycle, and mean spike frequency could all be controlled independently, we would expect more principal components would be needed to explain the variance of the model's output than if the period and mean spike frequency were correlated.

We must note that there is no standard method for interpreting the results of PCA. In order to turn the results of PCA into a measure of oscillator performance, we chose to use the 95% level of variance explained; that is, how many principal components are needed to explain 95% of the variance in the data. A data set where three principal components are needed to explain 95% of the variance in the data is judged to have fewer modes of operation than a data set where five principal components are needed. Therefore, the more principal components needed to explain 95% of the variance, the less *flexible* we will consider the model to be.

We perform PCA on twelve measures of the half-center oscillator activity: period, duty cycle, burst duration, inhibited duration, mean spike frequency, median spike frequency, initial spike frequency, peak spike frequency, final spike frequency, phase of peak spike occurrence, number of spikes per burst, peak of the slow-wave, and trough of the slow-wave. The PCA was performed on the combined data set from the FULL and reduced neuron in the oscillator, for a total of 25 measures (period is identical for both neurons in a half-center oscillator).

4.2 Asymmetric Half-Center Oscillators

Our ultimate goal is to determine how model complexity effects the robustness and flexibility of a hybrid half-center oscillator. Unfortunately, assessing robustness and flexibility within the context of a hybrid system would be very difficult, if not impossible. Our present interfacing techniques have several problems associated with them: the time required for dissection and preparation of the ganglia, the low probability of an electrode stick of sufficiently high resistance, and the limited life of a heart interneuron after microelectrode penetration. This overhead prohibits the large-scale parameter variations needed to fully assess the robustness and flexibility of the system. Furthermore, because our measurement of flexibility is based on the variability of the data, it is likely that the inherent variability between biological preparations, which is considerable, may overshadow any effect due to

model reduction.

In order to assess how model reduction might affect the robustness and flexibility of hybrid systems, we will utilize a model system that emulates a hybrid system. We will construct *asymmetric* model half-center oscillators. In each of these oscillators, one of the reduced models will be coupled to a FULL model neuron; the FULL model will serve as a "biological analogue". We will then vary the maximal conductances of both the FULL and reduced model in each oscillator, and evaluate how the robustness and the flexibility of the oscillators change as the model complexity is reduced. We will then use the the hybrid system to validate a subset of these studies. If the hybrid system reproduces the results of these studies, we can be reasonably well assured that the conclusions drawn from the models can be adequately applied to the hybrid system.

4.2.1 Asymmetric Model Half-Center Oscillators with Canonical Parameters

Using the models described in the previous chapter, we constructed four asymmetric half-center oscillators. In each model half-center, a FULL model neuron was coupled to another model neuron, either another FULL model neuron or one of the three reduced model neurons. As described in the previous chapter, the parameters of each reduced model were tuned in order to produce balanced oscillations with the FULL model; for each reduced model, this set of parameters is referred to as the canonical parameter set.

The canonical activity of all four oscillators is shown in Figure 34. The most notable difference between the model oscillators is that the period increases from 8.3 s in the FULL – FULL oscillator to 10.8 s in the FULL – R3 oscillator. Because of the use of IAF mechanisms in the R2 and R3 models, the spike shape of the R2 and R3 models is noticeably different than in the FULL and R1 models. The shape of the underlying slow-wave, however, is largely unchanged as the model complexity is reduced, indicating that our reductions have not significantly effected the models' slow variables.

The measured characteristics of the model oscillators are compared in Tables 1 and

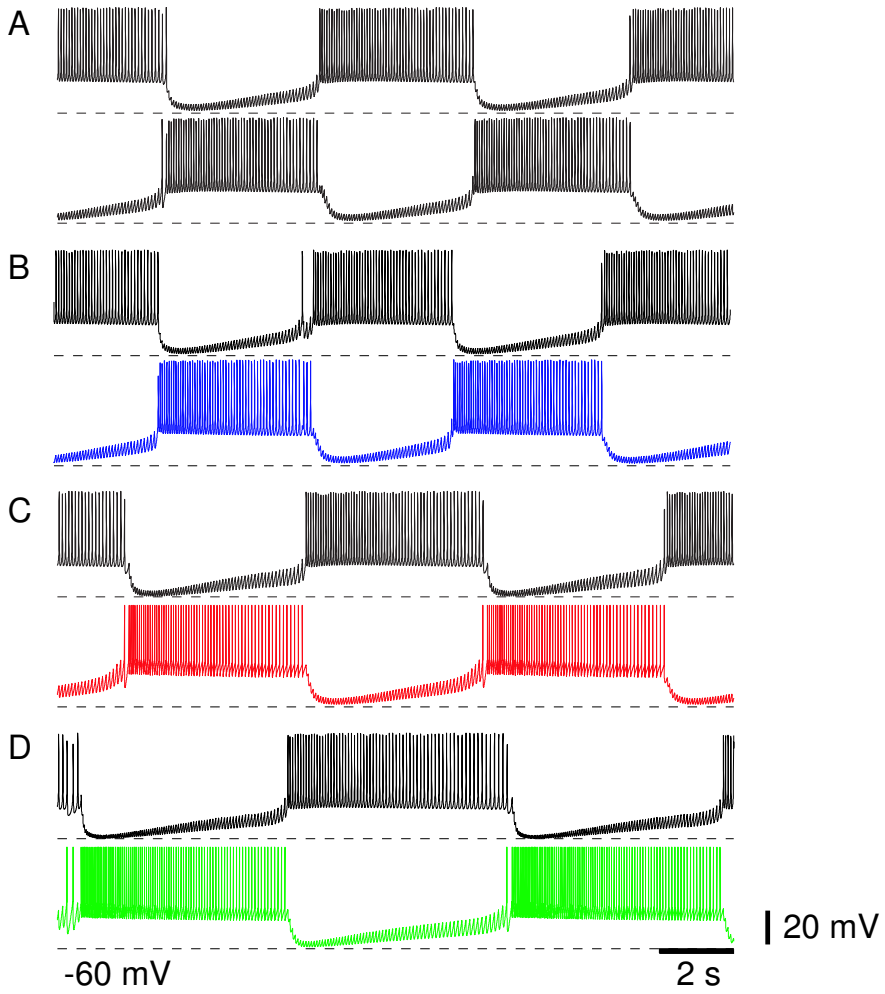

Figure 34: Comparing full and reduced half-center oscillators at canonical parameter values. **A.** FULL – FULL half-center oscillator. **B.** FULL – R1 half-center oscillator. **C.** FULL – R2 half-center oscillator. **D.** FULL – R3 half-center oscillator.

2. For both the FULL and the R1 model in the FULL – R1 oscillator, the period, duty cycle, spike frequencies, and slow wave characteristics are very similar to those observed in the FULL – FULL oscillator. In addition, these characteristics are all very similar to the previously published modeling studies [14], indicating that our FPGA implementation has not significantly altered the behavior of the model.

As compared to the FULL – FULL and FULL – R1 oscillator, the period of the FULL – R2 oscillator is increased. The spike frequency characteristics of the R2 neuron are increased as well; the mean, peak, and initial spike frequency of the R2 neuron are noticeably higher than for the FULL and R1 neurons. The escape frequency of the R2 neuron (the

Table 1: Canonical oscillation for different half-center oscillators. Data are taken from the FULL model of the asymmetric half-center oscillators.

	Original Model[14]	FULL – FULL HCO	FULL – R1 HCO	FULL – R2 HCO	FULL – R3 HCO
period (s)	8.6 ± 0.1	8.3 ± 0.2	8.0 ± 0.2	9.6 ± 0.0	10.8 ± 0.0
duty cycle	0.50 ± 0.02	0.51 ± 0.29	0.53 ± 0.25	0.50 ± 0.05	0.50 ± 0.0
mean f (Hz)	12.9 ± 0.6	13.0 ± 0.6	13.4 ± 0.5	13.4 ± 0.1	12.4 ± 0.0
initial f (Hz)	12.4 ± 5.9	13.0 ± 5.8	15.5 ± 4.8	17.4 ± 2.3	17.2 ± 2.4
peak f (Hz)	17.6 ± 1.0	17.5 ± 1.0	18.0 ± 1.1	18.2 ± 0.6	18.0 ± 0.9
escape f (Hz)	10.3 ± 0.7	10.3 ± 0.9	10.6 ± 0.9	10.3 ± 0.1	10.3 ± 0.1
sw peak (mV)	−41	−40.5 ± 1.6	−40.5 ± 1.3	−40.7 ± 0.6	−41.1 ± 0.3
sw trough (mV)	−59	−58.2 ± 0.2	−58.7 ± 0.1	−60.1 ± 0.0	−60.4 ± 0.0

spike frequency of the opposing cell at which the R2 neuron begins its burst) is unchanged in the FULL – R2 model. The spike frequency characteristics of the FULL neuron in the FULL – R2 oscillator are essentially unchanged from the FULL – FULL and FULL – R1 oscillators. The trough of the slow wave for the FULL neuron decreases slightly in the FULL – R2 oscillator, most likely due to the increased spike frequency in the R2 neuron. Finally, the standard deviations of all measurements except the initial spike frequency decrease in the R2 model; the activity of the FULL – R2 oscillator is less variable than in the FULL – FULL and FULL – R1 oscillators.

The FULL – R3 model has the longest period of all four oscillators, and the R3 model has the highest mean and peak spike frequencies of all four models. The escape frequency of the R3 is lower than in the other models, indicating that the R3 model can not as easily escape from inhibition as the other modelsThe spike frequency and slow-wave characteristics of the FULL model in the FULL – R3 oscillator are all essentially unchanged from the FULL – R2 oscillator.

These data demonstrate that the R1, R2, and R3 reduced models are all able to form half-center oscillators with the FULL model. The membrane potential waveforms of all four oscillators have a qualitatively similar structure, although there is an increased period in the FULL – R2 and FULL – R3 oscillators. The measured characteristics of the FULL

Table 2: Canonical oscillation data for reduced model in asymmetric half-center oscillators.

	Original Model[14]	FULL – FULL HCO	FULL – R1 HCO	FULL – R2 HCO	FULL – R3 HCO
period (s)	8.6 ± 0.1	8.3 ± 0.2	8.0 ± 0.2	9.6 ± 0.0	10.8 ± 0.0
duty cycle	0.50 ± 0.02	0.51 ± 0.03	0.49 ± 0.03	0.49 ± 0.01	0.49 ± 0.0
mean f (Hz)	12.9 ± 0.6	13.0 ± 0.6	13.6 ± 0.4	18.2 ± 0.2	23.0 ± 0.2
initial f (Hz)	12.4 ± 5.9	13.0 ± 5.8	14.6 ± 7.0	24.1 ± 6.5	22.8 ± 8.5
peak f (Hz)	17.6 ± 1.0	17.5 ± 1.0	20.6 ± 1.4	26.9 ± 0.8	35.3 ± 0.7
escape f (Hz)	10.3 ± 0.7	10.3 ± 0.9	10.5 ± 1.0	10.2 ± 0.1	9.3 ± 0.3
sw peak (mV)	−41	−40.5 ± 1.6	−40.5 ± 1.3	−40 ± 1.3	−40.6 ± 0.1
sw trough (mV)	−59	−58.2 ± 0.2	−58.7 ± 0.1	−58.4 ± 0.2	−59.1 ± 0.0

model in these oscillators are all generally unchanged as the complexity of the opposing neuron is reduced. In the FULL – R2 and FULL – R3 oscillators, the spike frequency characteristics of the reduced model is noticeably higher than in the FULL –R1 oscillator. Overall, we think that these data demonstrate that the asymmetric reduced model oscillators are all able to reasonably reproduce the characteristics of the FULL – FULL model oscillator, at least at canonical parameters. We will now examine the performance of the reduced oscillators when the parameters of the model are varied.

Table 3: Robustness scores for parameter variation in FULL model. For each conductance, the parameter score is equal to $50 \times \log(p_{max}/p_{min})$ where p_{max} and p_{min} are the maximum and minimum of the parameter range over which the oscillator function. A score of 100 indicates that the oscillator operates from .1 to 10 times the canonical parameter value.

Parameter	Full – Full HCO	Full – R1 HCO	Full – R2 HCO	Full – R3 HCO
$\bar{g}_{\mathrm{Na}}$	63.0	63.0	52.0	56.2
$\bar{g}_{\mathrm{P}}$	4.4	4.9	5.8	2.4
$\bar{g}_{\mathrm{CaF}}$	100.0	97.8	90.6	83.6
$\bar{g}_{\mathrm{CaS}}$	72.7	75.3	96.7	100.0
$\bar{g}_{\mathrm{K1}}$	79.8	57.6	70.7	96.9
$\bar{g}_{\mathrm{K2}}$	12.2	12.2	47.7	63.9
$\bar{g}_{\mathrm{KA}}$	69.0	71.6	96.5	47.1
$\bar{g}_{\mathrm{h}}$	100.0	100.0	100.0	100.0
g_{leak}	11.6	10.2	55.9	53.2

4.2.2 Parameter Variation in Full Model

There is a great degree of variability among living neurons. Even neurons with the same functional role in a network may have significantly different morphologies or ion channel concentrations. In a hybrid system, it is of critical importance the model component of the system function despite variance in the biological component.

We will use our asymmetric model oscillators to assess how the performance of the reduced models might be effected by biological variability in hybrid systems. For each asymmetric half-center oscillator, each maximal conductance in the FULL model is varied from 0 nS to 10 times its canonical value, while keeping all other parameters at their canonical values. We will evaluate the robustness and flexibility of each oscillator in order to determine how the system's function is effected by model reduction.

Robustness

The parameter ranges over which the oscillators function are shown in Figure 35. The robustness scores for the four asymmetric half-center oscillators are shown in Table (Table 3). There is no consistent effect of reducing the complexity of the model on the parameter range where the model produces half-center oscillations. The functional ranges

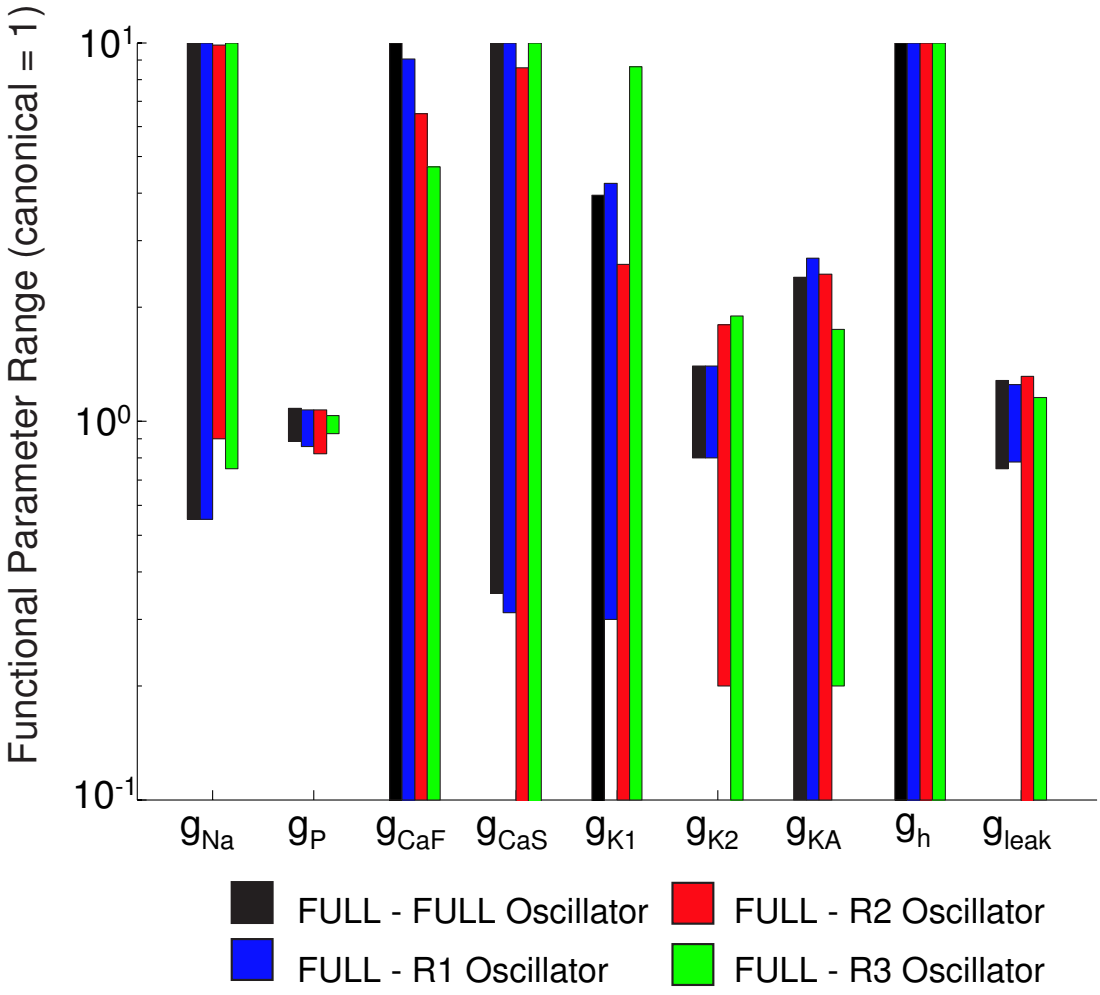

Figure 35: Functional parameter ranges for FULL model in asymmetric oscillators. Each bar shows the functional range of the parameter in the FULL model over which the system produces half-center oscillations.

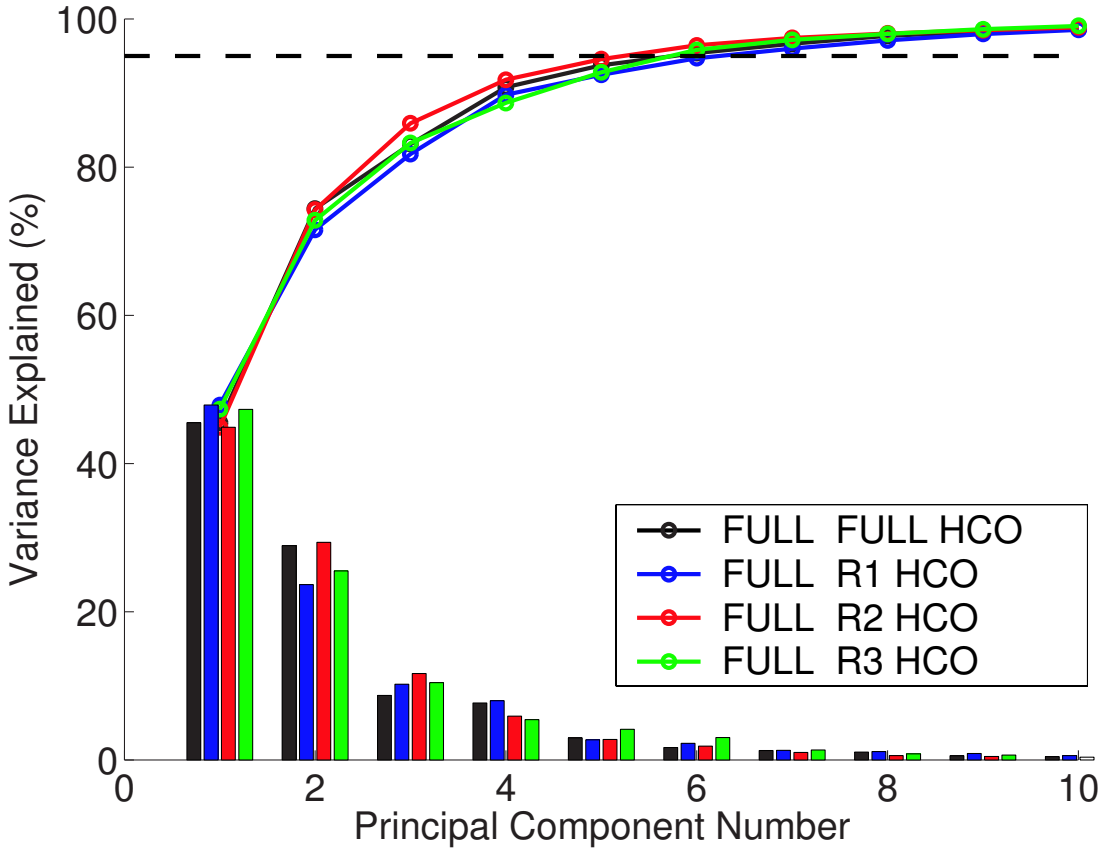

Figure 36: Flexibility assessment for parameter variation in FULL model. Bars represent the percent of variance explained by each principal component; lines indicate the total percent of variance explained by the previous principal components. The dashed line indicates the level where 95% of the variance is explained.

of $\bar{g}_{\mathrm{Na}}$ and $\bar{g}_{\mathrm{CaF}}$ are reduced when the complexity of the opposing cell is reduced. The functional ranges of $\bar{g}_{\mathrm{CaS}}$ and $\bar{g}_{\mathrm{K2}}$ increase as the complexity of the opposing cell is reduced. The functional range of $\bar{g}_{\mathrm{h}}$ is unaffected by model reduction. The functional range of the other maximal conductances constricts or expands at different stages of model reduction. Because there does not appear to be any consistent overall effect of model reduction on the parameter ranges of the FULL model, it stands to reason that all of our reduced models should be able to form hybrid half-center oscillators when coupled to a biological neuron.

Flexibility

The results of our flexibility analysis are shown in Figure 36. For all of the model oscillators, 95% of the variance in the data was explained by six or seven principal components. When the maximal conductances of the FULL model are varied, there is essentially no difference in the results of PCA between the four half-center oscillators oscillators. This finding indicates that although reducing the model can constrict or expand the functional range of the parameters, no significant modes of activity are lost or gained.

Discussion

The results presented here demonstrate that the reduced model neurons are all capable of creating a half-center oscillations when coupled to a FULL model neuron. The overall robustness of the system, as determined by the parameter ranges of the FULL neuron where the model produces half-center oscillations, does not appear to be substantially effected by model reduction.

We must note, however, that the robustness of the system to variation in a single parameter can be substantially effected by model reduction. This affect was most notable in the cases of $\bar{g}_{\mathrm{CaF}}$, whose functional range was decreased as the model complexity was reduced, and $\bar{g}_{\mathrm{K2}}$, whose functional range was increased as the model complexity was reduced. Furthermore, it is very likely that the robustness of the system is dependent upon the location of the canonical parameter point in the system's parameter space. The system can exhibit its canonical activity at different points in its parameter space; a more thorough analysis of the system's robustness would need to examine the system using different canonical parameter sets. Unfortunately, we were not able to examine the system in such detail in these studies.

The overall flexibility of the system, as determined by PCA, did not noticeably increase or decrease as the model complexity was reduced. As with our robustness measurement, a caveat to this finding is that the results may be dependent on the location of the canonical parameter point in the system's parameter space. Another caveat is that we have only analyzed the overall flexibility of the system; the flexibility of the system in the face of $\bar{g}_{\mathrm{h}}$

variation, for example, may be altered as the model complexity is reduced.

Nonetheless, the overall robustness and flexibility of the asymmetric oscillators do not appear to be significantly altered as the model complexity is reduced. This finding indicates that there should be no difficulty in creating hybrid oscillators using our reduced model neurons, and that the functional role of the biological neuron in these hybrid systems will not be significantly altered as the complexity of the model neuron is reduced.

4.2.3 Parameter Variation in Reduced Models

The primary rationale for creating hybrid systems is that the model component provides access to controls that are not accessible through other techniques. In future medical applications, this control will allow the model component to modulate the activity of the biological network, curtailing the affects of traumatic injury or disease. In scientific investigations, this control allows the investigator to examine the functional effects of specific neuronal components. In either of these cases, it is desirable that the model component be both robust and flexible. A high level of robustness means that the system will be able to function over a large range of parameters, and a high level of flexibility means that the system can produce a variety of outputs in order to achieve its function.

We will now use our asymmetric model oscillators to assess the potential for reduced models to produce robust and flexible activity in hybrid half-center oscillators. In the reduced model of each asymmetric half-center oscillator, we individually vary $\bar{g}_{\mathrm{CaS}}$, $\bar{g}_{\mathrm{h}}$, and g_{leak} from zero to ten times their canonical value while keeping all other parameters at their canonical values. We chose these parameters as the focus of our study because they are retained across all three model reductions. After examining the individual effects of each parameter on the network activity, we will compare the effect of parameter variation on the overall robustness and flexibility of system.

Variation of $\bar{g}_{\mathrm{h}}$ in reduced models

The affect of varying $\bar{g}_{\mathrm{h}}$ on the oscillator period, duty cycle, mean spike frequency and escape frequency is shown in Figure 37. There is no significant affect of model reduction on the role of $\bar{g}_{\mathrm{h}}$ in the system. The only difference between the four model oscillators occurs for the FULL – R2 oscillator, where the functional range of $\bar{g}_{\mathrm{h}}$ is noticeably decreased.

This reduction in the range of $\bar{g}_{\mathrm{h}}$ is due to a peculiar interaction of the ionic currents. Large amounts of I_{h} cause the neuron to rapidly overcome inhibition. This rapid escape from inhibition, however, does not allow for sufficient removal of I_{CaS} inactivation before I_{h} deactivates. The lack of removal of I_{CaS} inactivation means that less depolarizing current

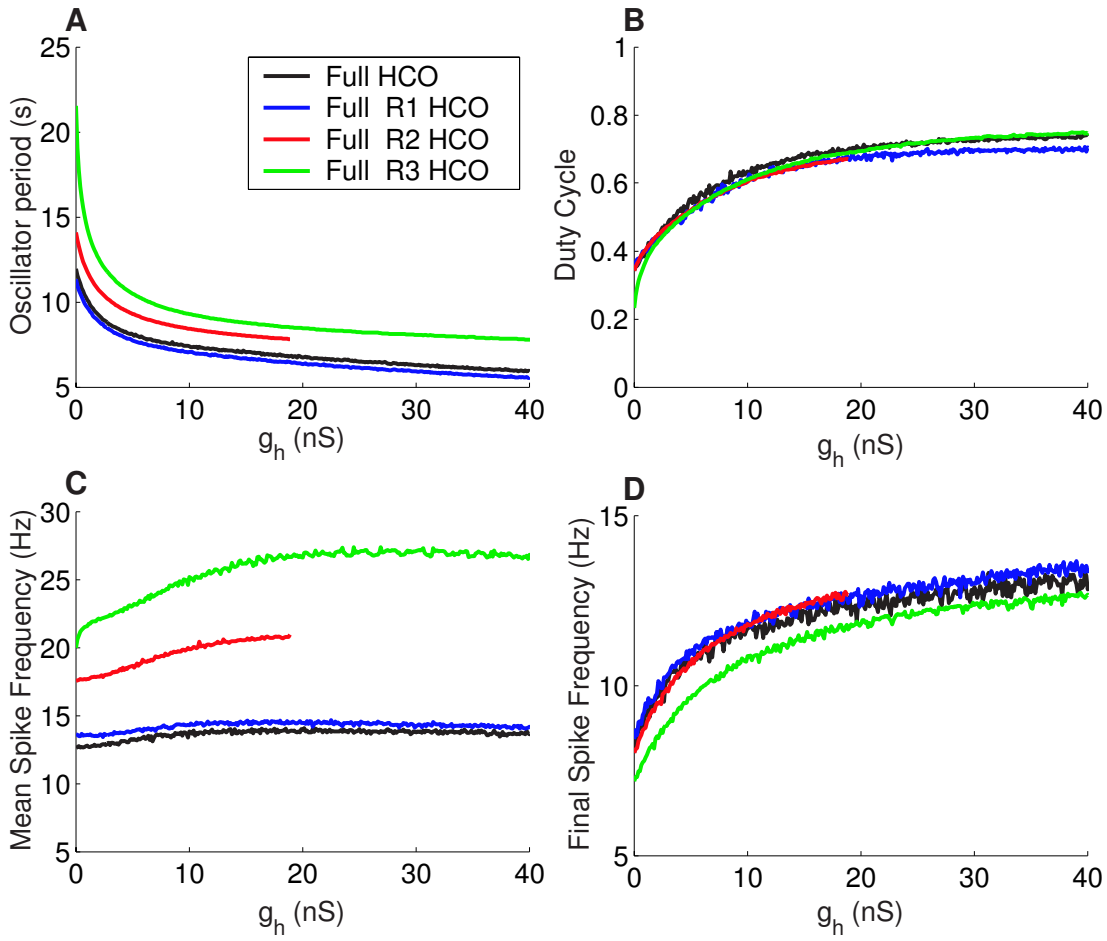

Figure 37: Effect of varying $\bar{g}_{\mathrm{h}}$ in reduced models. **A.**Oscillator period, which is the same for both neurons in a half-center oscillator. **B.** Duty cycle for the reduced model neuron. **C.** Mean spike frequency of the reduced neuron. **D.** Escape frequency of reduced model neuron (the final spike frequency of the FULL model neuron)

is available to drive V_{m} to the firing threshold. These combined effects together cause the R2 neuron to be unable to escape from inhibition. This problem disappears in the R3 model because replacing I_{P} and I_{K2} with a passive current provides a slight decrease in hyperpolarizing current between -45 and -40 mV (Figure 31), which helps the neuron to reach its firing threshold.

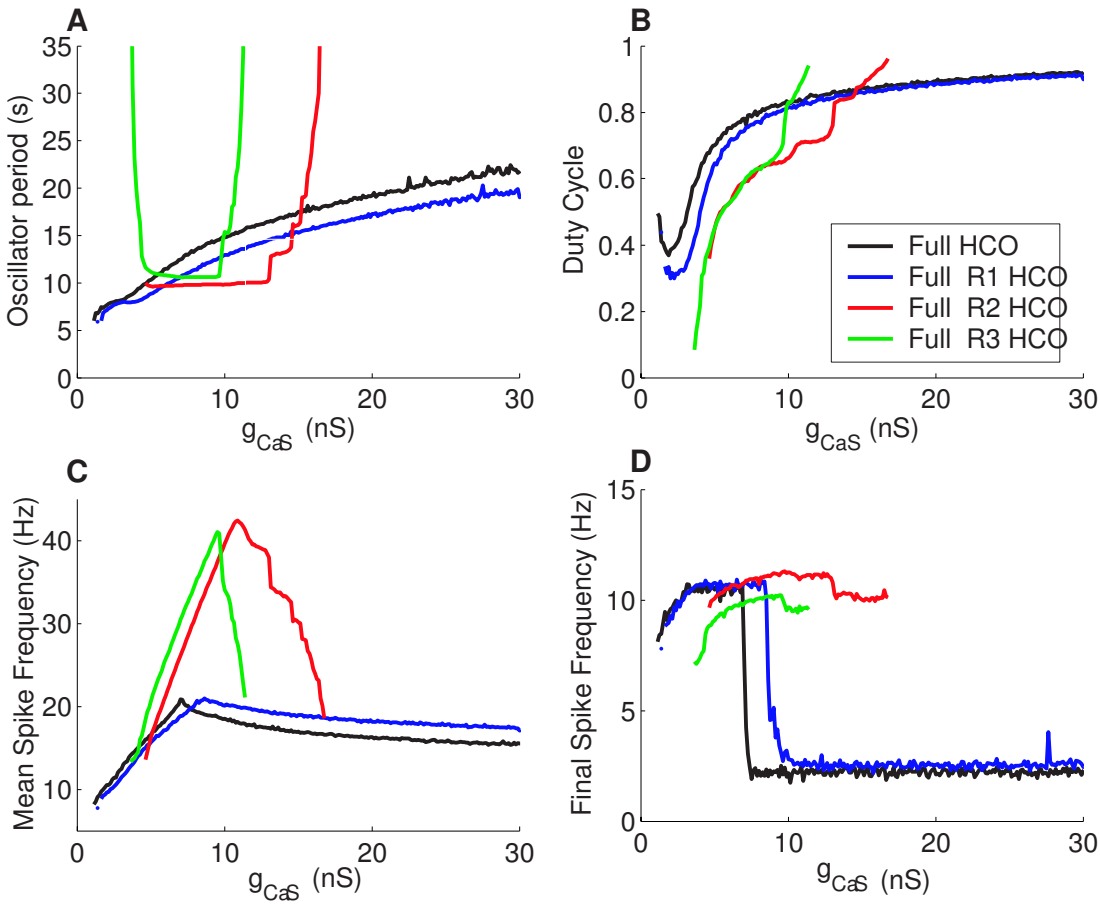

Figure 38: Effect of varying $\bar{g}_{\text{CaS}}$ in reduced models. **A.**Oscillator period, which is the same for both neurons in a half-center oscillator. **B.** Duty cycle for the reduced model neuron. **C.** Mean spike frequency of the reduced neuron. **D.** Escape frequency of reduced model neuron (the final spike frequency of the FULL model neuron)

Variation of $\bar{g}_{\text{CaS}}$ in reduced models

The affect of varying $\bar{g}_{\text{CaS}}$ on the oscillator period, duty cycle, mean spike frequency and escape frequency is shown in Figure 38. There is little difference on how $\bar{g}_{\text{CaS}}$ effects the FULL – FULL and FULL – R1 oscillators. Increasing $\bar{g}_{\text{CaS}}$ causes an increase in the oscillator period and the duty cycle of the modified cell. As $\bar{g}_{\text{CaS}}$ increases, there is an initial increase in the mean spike frequency of the modified neuron, followed by a gradual decrease. The escape frequency of the modified neuron dramatically decreases at a certain point, but otherwise remains constant. This transition is due to the appearance of "plateau-like" oscillations, where the modified neuron becomes severely depolarized and as a result

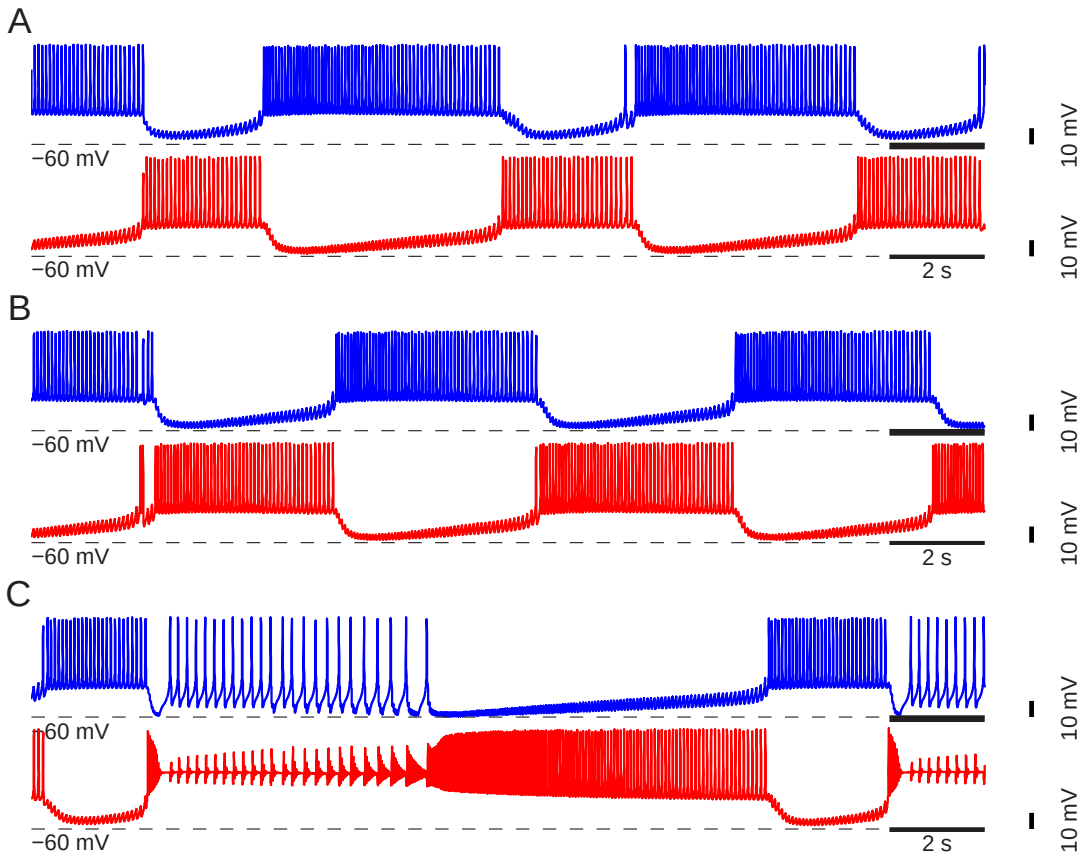

Figure 39: Typical oscillator activity with increasing $\bar{g}_{\text{CaS}}$in FULL—FULL model half-center oscillator. The unmodified neuron ($\bar{g}_{\text{CaS}}$ = 3.2 nS) is shown in blue. The modified neuron is shown in red. The activity in the FULL-R1 half-center was very similar to that of the FULL – FULL model. **A.** $\bar{g}_{\text{CaS}}$ = 2 nS. **B.** $\bar{g}_{\text{CaS}}$ = 3.2 nS (canonical) **C.** $\bar{g}_{\text{CaS}}$ = 10 nS. Note the appearance of "plateau-like" oscillations in the modified neuron.

cannot fire action potentials (Figure 39). In the R2 and R3 models, however, this type of activity is not possible because of the resetting of V_m after a spike event (Figures 40 and 41).

The relationship between $\bar{g}_{\text{CaS}}$ and the oscillator period is dramatically effected by the introduction of IAF mechanisms, as are the duty cycle and spike frequency relationships. Increasing $\bar{g}_{\text{CaS}}$ in the R2 neuron causes an increase in the duty cycle of the R2 neuron with the period initially remaining relatively constant. This change can be seen in the activity traces shown in Figure 40. When $\bar{g}_{\text{CaS}}$ exceeds 13 nS, there is a sharp increase in the period of the oscillator. In the R3 neuron, the duty cycle increases in a manner similar to the R2

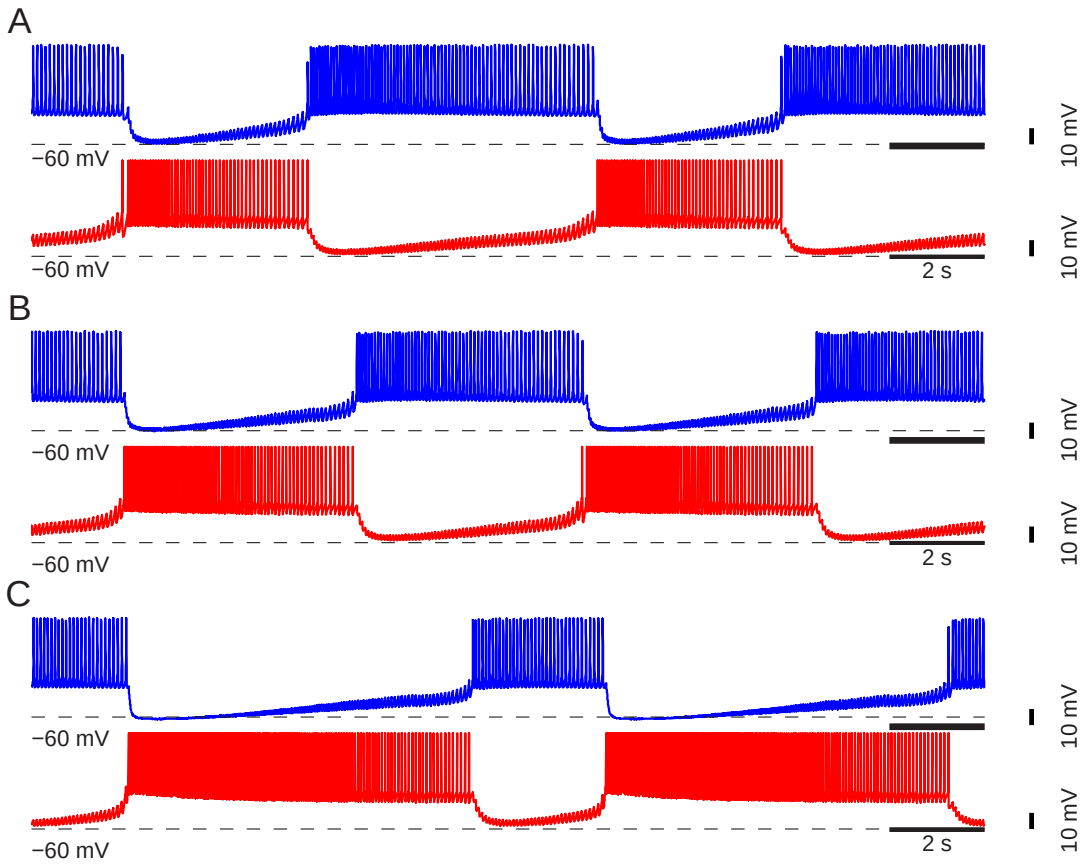

Figure 40: Typical oscillator activity with increasing $\bar{g}_{\text{CaS}}$in FULL—R2 model half-center oscillator. The FULL neuron is shown in blue. The R2 neuron is shown in red. **A.** $\bar{g}_{\text{CaS}} = X$ nS. **B.** $\bar{g}_{\text{CaS}} = 5.375$ nS (canonical) **C.** $\bar{g}_{\text{CaS}} = X$ nS.

model. With low values of $\bar{g}_{\text{CaS}}$, the period is very long. Increasing $\bar{g}_{\text{CaS}}$ initially causes the period of oscillation to decrease. After this initial decrease in period, the R3 model behaves similarly to the R2 model: the period remains relatively constant with increasing $\bar{g}_{\text{CaS}}$, then sharply increases before the oscillations terminate.

In both the R2 and R3 models, large increases in $\bar{g}_{\text{CaS}}$ cause the oscillations to terminate. Even though I_{CaS} inactivates at depolarized membrane potentials, there is still some I_{CaS} present. When $\bar{g}_{\text{CaS}}$ is large, the contribution of I_{CaS} is sufficient to keep the IAF model neurons firing at a rate from which the FULL model can not escape.

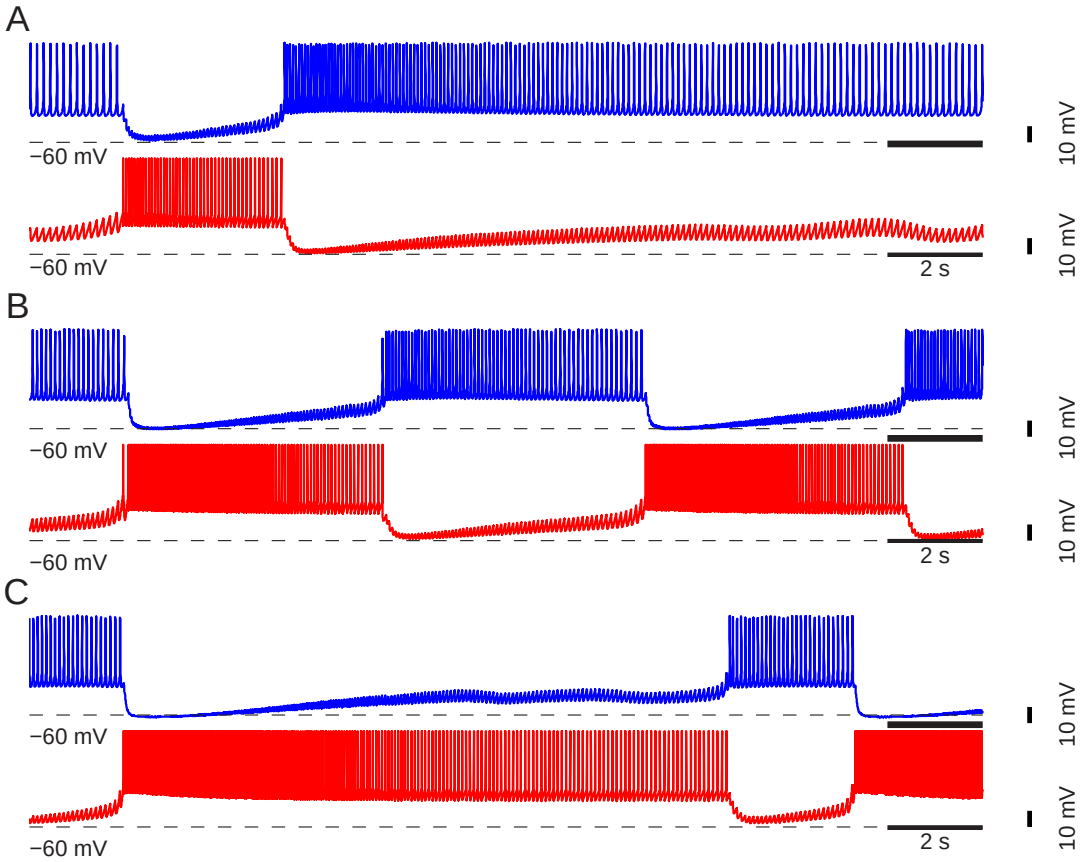

Figure 41: Typical oscillator activity with increasing $\bar{g}_{\text{CaS}}$in FULL—R2 model half-center oscillator. The FULL neuron is shown in blue. The R3 neuron is shown in red. **A.** $\bar{g}_{\text{CaS}} = X$ nS. **B.** $\bar{g}_{\text{CaS}} = 5.375$ nS (canonical) **C.** $\bar{g}_{\text{CaS}} = X$ nS.

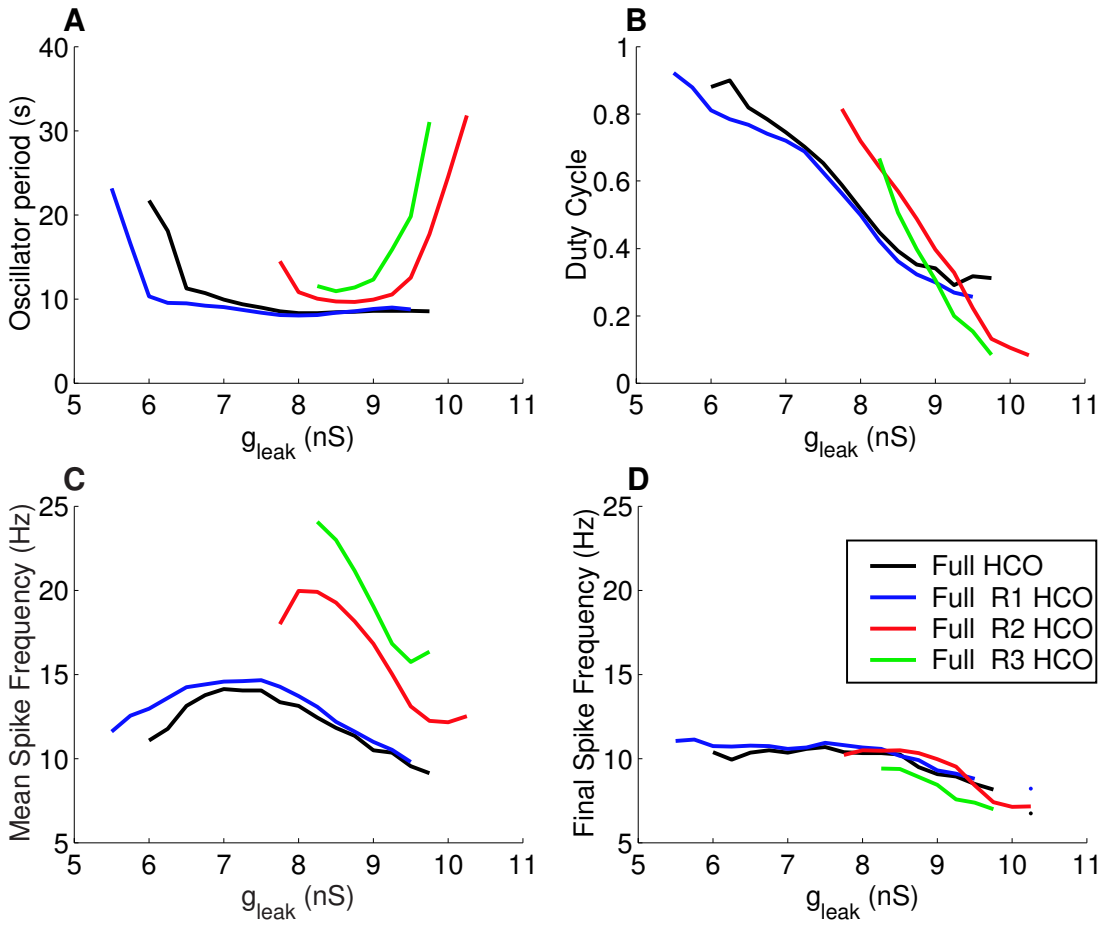

Figure 42: Effect of varying g_{leak} in reduced models. **A.**Oscillator period is the same for both neurons in a half-center oscillator. **B.** Duty cycle for the reduced model neuron. **C.** Mean spike frequency of the reduced neuron. **D.** Escape frequency of reduced model neuron (the final spike frequency of the FULL model neuron)

Variation of g_{leak} in reduced models

The effects of varying g_{leak} on the oscillator period, duty cycle, mean spike frequency and escape frequency are shown in Figure 42. In all models, increasing g_{leak} causes a decrease in the duty cycle and mean spike frequency of the modified neuron. In the FULL and R1 reduced models, these changes are associated with an sharp decrease in the oscillator period at low values of g_{leak}, whereas in the R2 and R3 models these changes are associated with a sharp increase in the oscillator period at high values of g_{leak}. Changes in g_{leak} have little effect on the escape frequency of the neuron.

Robustness

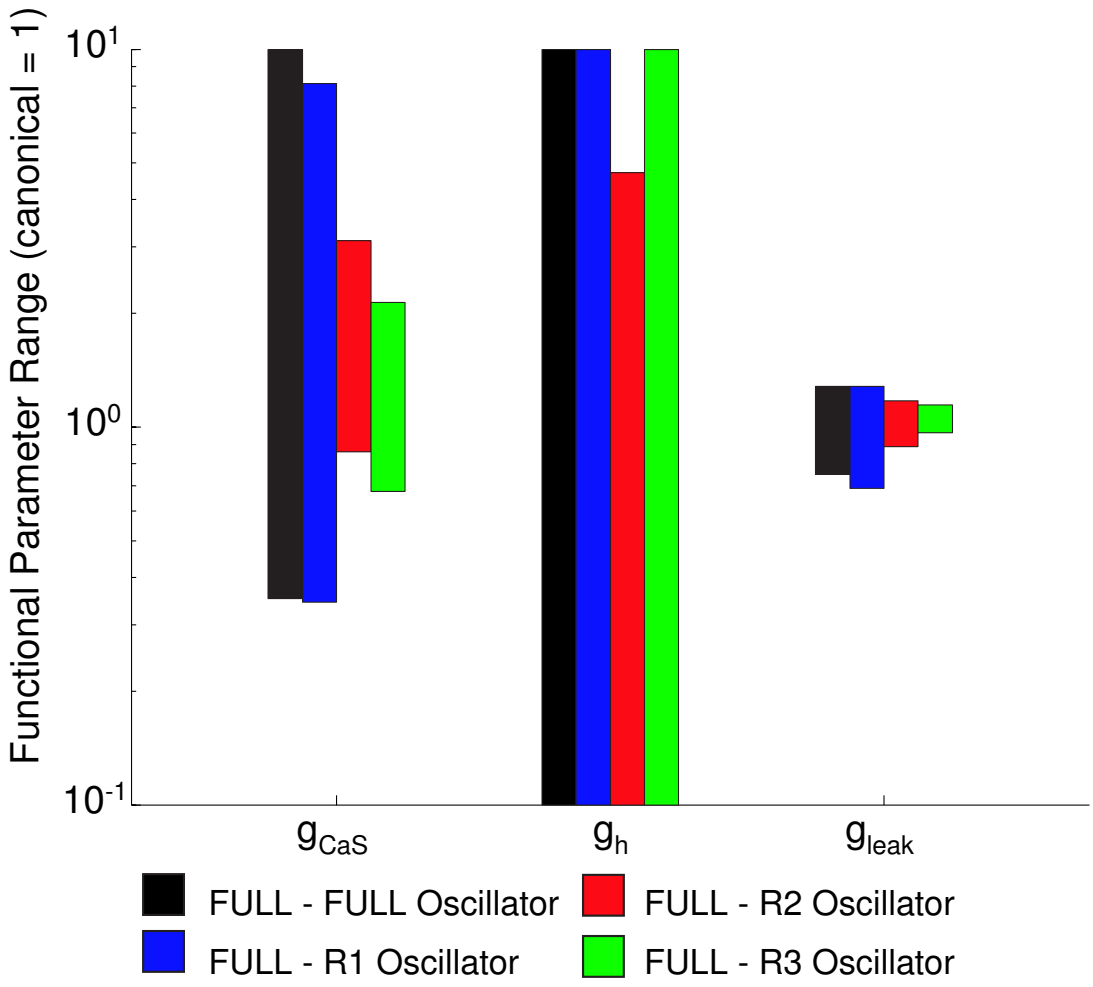

Figure 43: Functional parameter ranges for reduced models in asymmetric oscillators. Each bar shows the functional range of the parameter in the reduced models over which the system produces half-center oscillations.

Table 4: Robustness scores for parameter variation in reduced models. For each conductance, the parameter score is equal to $50 \times \log(p_{max}/p_{min})$ where p_{max} and p_{min} are the maximum and minimum of the parameter range over which the oscillator function. A score of 100 indicates that the oscillator operates from .1 to 10 times the canonical parameter value.

Parameter	Full – Full HCO	Full – R1 HCO	Full – R2 HCO	Full – R3 HCO
$\bar{g}_{\mathrm{CaS}}$	72.7	68.7	27.9	25.1
$\bar{g}_{\mathrm{h}}$	100.0	100.0	83.7	100.0
g_{leak}	11.6	13.5	6.1	3.6

The functional parameter ranges of the reduced models over which the asymmetric oscillators function are shown in Figure 43. The robustness scores for the various parameters are given in Table 4. For both $\bar{g}_{\mathrm{CaS}}$ and g_{leak}, there is a significant decrease in the robustness score as the model complexity is decreased. The most notable change in these robustness scores occurs between the R1 and R2 models, the point at which the conductance-based spiking mechanisms are replaced with integrate-and-fire mechanisms. The functional range of $\bar{g}_{\mathrm{h}}$ fully spans the region from .4 to 40 nS in the FULL – FULL, FULL – R1, and FULL – R3 oscillator; in the FULL – R2 oscillator, the functional range of $\bar{g}_{\mathrm{h}}$ is restricted, due to the interaction explained above. It appears, therefore, that the overall effect of model reduction is to constrict the range of parameters over which the system functions.

Flexibility

The results of our flexibility analysis are shown in Figure 44. In the FULL, R1, and R3 models, 95% or more of the variance in the data is explained by the first six principal components, similar to when the maximal conductances were varied in the FULL model. In the R2 model, 95% of the variance was explained by the first 5 principal components. This decrease in the flexibility of the FULL – R2 oscillator's output is most likely due to the shortened range of $\bar{g}_{\mathrm{h}}$.

This result is somewhat surprising, because we observed that replacing the physiologic spiking mechanisms with IAF mechanisms eliminated a particular mode of oscillation: the "plateau-like" oscillations seen in the FULL and R1 models. If we apply our flexibility

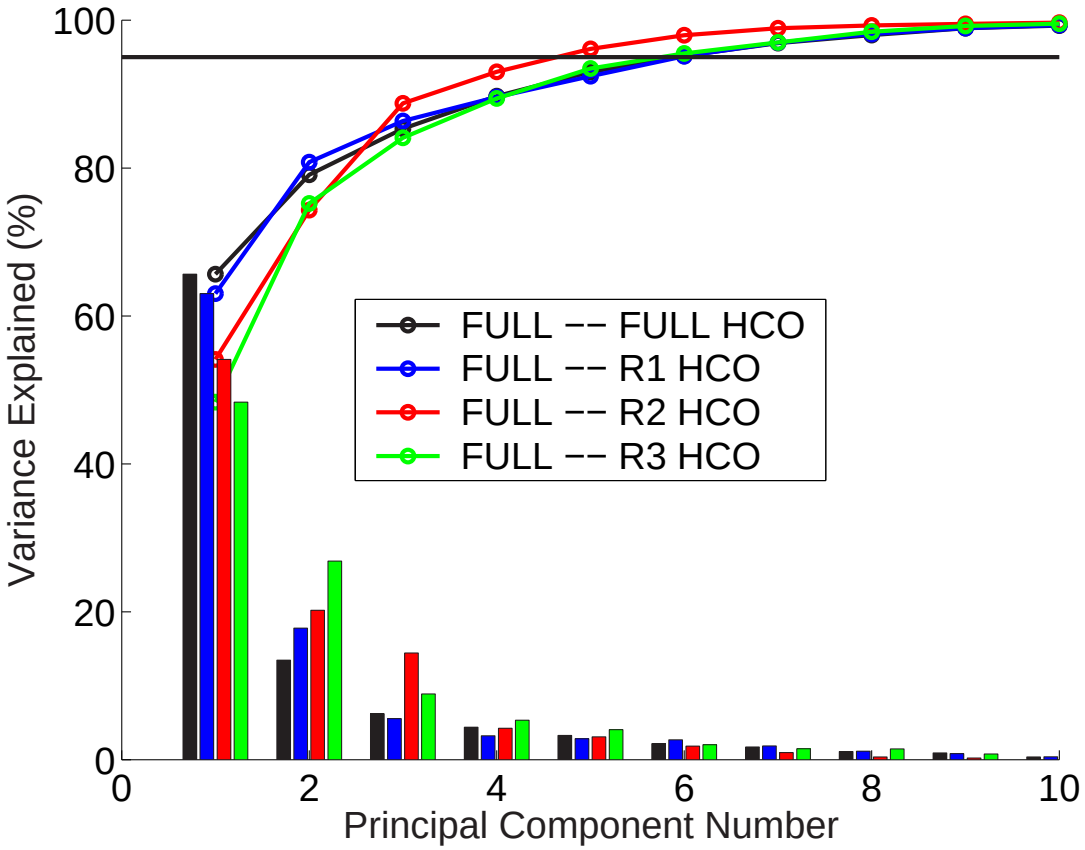

Figure 44: Principal component analysis of half-center oscillation when maximal conductances are varied in the reduced model. Bars indicate the contribution of each principal component to explaining the variance in the data. Lines indicate the total amount of variance explained. The dashed horizontal line indicates where 95% of the variance in the data has been explained.

assessment only to the data from $\bar{g}_{\text{CaS}}$ variation, instead of to the entire data set, we observe that there is a definite reduction in the flexibility of the system in the FULL – R2 and FULL – R3 oscillators (Figure **??**). This alteration in the system's flexibility does not appear in our analysis of the overall system flexibility because it is overshadowed by the variance introduced by g_{leak} and $\bar{g}_{\text{h}}$.

Discussion

As was the case when parameters were varied in the FULL model, it is apparent that we must consider the effect of model reduction on each parameter on a case-by-case basis. Reducing the complexity of the model caused a decrease in the robustness of the system to

variation in $\bar{g}_{\mathrm{CaS}}$ and g_{leak}. The robustness of the system to $\bar{g}_{\mathrm{h}}$ variation was effected only in the R2 model.

As we discussed in the previous section, it would also be advantageous to examine the functional parameter space of the system in a more global fashion. The robustness of the system to variation in a particular parameter is likely effected by our choice of a canonical parameter point; a more global analysis of the model would inform us whether or not the results at this parameter point are typical of the system as a whole.

Although there was a clear restriction in the functional ranges of the inputs $\bar{g}_{\mathrm{CaS}}$ and g_{leak}, there was little overall change in the flexibility of the models as determined by PCA. The notable difference was in the FULL – R2 model, where the restriction of $\bar{g}_{\mathrm{h}}$ appeared to reduce the flexibility of the model somewhat.

4.3 Validation of Reduced Models Using Hybrid Systems

The results from our modeling studies indicate that a reduction in model complexity can effect the robustness of the system to parameter variation in the model. The model studies also demonstrated that the flexibility of such systems may be altered by model reduction. But do these results hold true for actual hybrid systems?

Unfortunately, directly assessing robustness and flexibility within the context of a hybrid system would be impossible. The experimental overhead and limited time available to work with an individual preparation preclude using large-scale parameter sweeps in hybrid systems. Furthermore, the lack of a means to account for the variability among biological neurons severely decreases the utility of our robustness and flexibility metrics.

We can use the hybrid system, however, to validate some of the predictions from our model. We demonstrated this ability in Chapter 2 where we examined the functional role of $\bar{g}_{\mathrm{h}}$ in both the hybrid system and mathematical model oscillator. The effect of $\bar{g}_{\mathrm{h}}$ on the oscillatory characteristics was the same in both the model system and the hybrid system; this similarity validated our ability to apply predictions from the model to the hybrid system.

The effects of $\bar{g}_{\mathrm{h}}$ variation on oscillator period, duty cycle, and spike frequency characteristics was nearly identical in all of our asymmetric model oscillators; the effects were also what we observed and validated in Chapter 2. We can therefore be reasonably well assured that all of our model oscillators correctly describe the role of $\bar{g}_{\mathrm{h}}$ in determining network activity.

In asymmetric model oscillators, the reduction of the HN model had a significant effect on the role of $\bar{g}_{\mathrm{CaS}}$. In the R3 and R4 reduced models, the dynamic range of $\bar{g}_{\mathrm{CaS}}$ is shortened as compared to the FULL and R1 models. The FULL and R1 models have a very similar relationship in how $\bar{g}_{\mathrm{CaS}}$ effects the oscillation characteristics, and the R2 and R3 models have a very similar relationship in how $\bar{g}_{\mathrm{CaS}}$ effects the oscillation characteristics. There is, however, a noticeable difference between the first two and the last two models in how $\bar{g}_{\mathrm{CaS}}$ effects the oscillation characteristics. Notably, the range of $\bar{g}_{\mathrm{CaS}}$ over which the system

operates is constricted in the R2 reduction stage, and the effect of $\bar{g}_{\mathrm{CaS}}$ on oscillator period, duty cycle, and spike frequency characteristics is noticeably different.

In order to validate these modeling results, we created a hybrid half-center oscillator using the R1 and R2 reduced models, and varied $\bar{g}_{\mathrm{CaS}}$ of the model neuron. We chose to utilize only the R1 and R2 models in our hybrid systems because it was at the reduction from R1 to R2 that we observed the most noticeable change in oscillator behavior. We chose to study the effect of $\bar{g}_{\mathrm{CaS}}$ on oscillations because it was the parameter most influenced by the reduction from R1 to R2.

For both the R1 and R2 model neuron, we created four separate hybrid system preparations. In the R1 model hybrid oscillator we vary $\bar{g}_{\mathrm{CaS}}$ over four points: 2, 4, 8, and 16 nS. In the R2 hybrid oscillator we vary $\bar{g}_{\mathrm{CaS}}$ over these points as well as 5.375 nS, the canonical value of $\bar{g}_{\mathrm{CaS}}$ for the R2 model.

4.3.1 Using FPGAs in Hybrid Systems

The creation of hybrid systems requires the model used to operate in real-time. In real-time operation, a simulation step size of 1×10^{-4} s must take 1×10^{-4} s to compute. Otherwise, the model will run to fast or too slow for its output to correlate with the physical system with which the model interacts. In order to achieve real-time performance with the FPGA, several modifications to our previous methods were necessary.

Second, because the lowest possible FPGA clock frequency (20 MHz) provides performance far in excess of real-time it was necessary to modify the FPGA model neuron architecture.

First, the FPGA was no longer run with a single-stepped clock. As stated previously, the hardware co-simulation functionality provided with the Xilinx XtremeDSP package was necessary in order to run scripted simulations with the neuron models. It was also necessary to run the model using a single-stepped clock; that is, the Simulink clock and the FPGA clock needed to be synchronized. Othewise, we did not obtain correct output from

the neuron model. This synchronization is accomplished by having Simulink generate the clock signals for the FPGA. Unfortunately, this method means that the user of the model has no control over the clocking speed of the FPGA. Additionally, the clock speed can vary greatly as the resource load on the PC changes. Therefore, in order to obtain true-real time operation the FPGA was run in *free-running* clock mode, where the clock frequency of the FPGA is explicitly set before the model is run.

Second, because the lowest possible FPGA clock frequency provides performance far in excess of real-time it was necessary to modify the FPGA model neuron architecture. The minimum possible free-running clock frequency is 20 MHz. This limitation is built into the FPGA development system, and cannot be overcome. At this frequency, the model, with a simulation step size of 1×10^{-4} s, will run at approximately 2000 times real-time. There are several possible ways to modify the model in order to obtain real-time performance. One would be to reduce to the simulation step size to 5×10^{-8}. This method, however, would require significant changes to the precisions of time constants and state variables within the model, so we did not pursue it. Instead, we modified the state variable integrators so that they were enabled for only 1 out of every 2000 clock cycles. This method proved very simple to implement, and produced true real-time results from the FPGA.

Third, because we wanted only one model to interact with a living neuron at a time, we no longer pipelined multiple models through the FPGA.

Finally, in order to interface with the electrophysiology equipment, we added the DACs and ADCs to our model. The membrane potential of the living neuron was input to the model through one of the two dedicated ADCs. The membrane potential and the synaptic current signal for the living neuron were output using the two dedicated DACs.

A schematic depiction of the FPGA-based hybrid system is shown in Figure 45. All electrophysiology, data acquisition, and data analysis methods are the same as those used in Chapter 2.

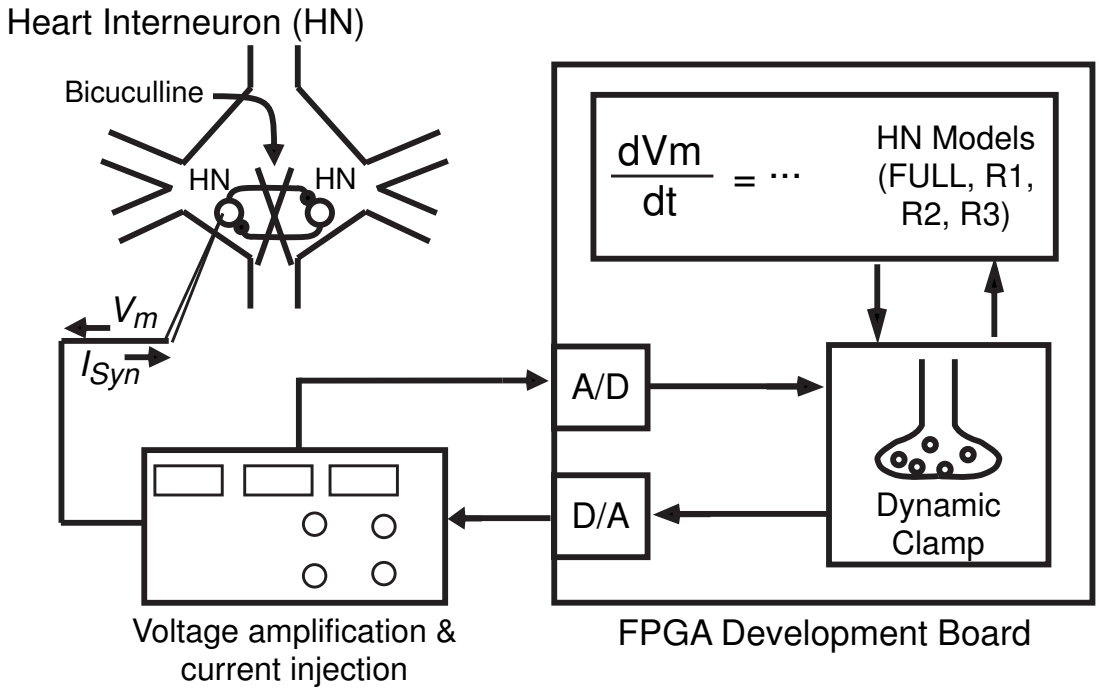

Figure 45: FPGA-based hybrid system design.

4.3.2 $\bar{g}_{CaS}$ in the R1 model.

With canonical parameters ($\bar{g}_{CaS}$ = 4 nS), the R1 hybrid half-center oscillator produced rhythmic oscillations in all four experiments. The period was 6.6 ± 2.2 s, the duty cycle was 0.47 ± 0.17, and the mean spike frequency was 20.9 ± 3.5 Hz. The escape frequency was 7.9 ± 3.8 Hz.

As predicted by our modeling studies, increasing $\bar{g}_{CaS}$ shows a consistent increase in the oscillator period (Figure 46), although only the first group (at 2 nS) was significantly different from the others ($p < .05$). Also, the oscillator period is significantly shorter for the hybrid half-center oscillator than for the model half-center. This phenomenon was observed in the silicon neuron hybrid system used in Chapter 2; as we discussed then, this shortening of the period is most likely due to the effects of sharp microelectrode penetration, which decreases the membrane time constant and limits the efficacy of spike mediated synaptic transmission.

Increasing $\bar{g}_{CaS}$ from 2 to 4 nS causes a slight decrease in the duty cycle of the model; this difference, however, was not statistically significant. The increase in duty cycle between 4 and 8 nS was both significant and similar to the increase predicted from our modeling studies, although the range of duty cycles observed was smaller than that predicted from modeling.

There was a significant increase in mean spike frequency from 2 to 4 nS, and from 4 to 8 nS. There was no significant change in mean spike frequency from 8 to 16 nS. This change was similar to that predicted by modeling, although we did not see the decrease in spike frequency from 8 to 16 nS as we saw in the model half-center. Additionally, the mean spike frequency was noticeably higher in the hybrid half-center than they were predicted by modeling.

Finally, increasing $\bar{g}_{CaS}$ from 4 to 8 nS caused a significant decrease in the escape frequency of model neuron. The trend of this result is very similar to that predicted by modeling, although the escape frequency is lower in the hybrid system.

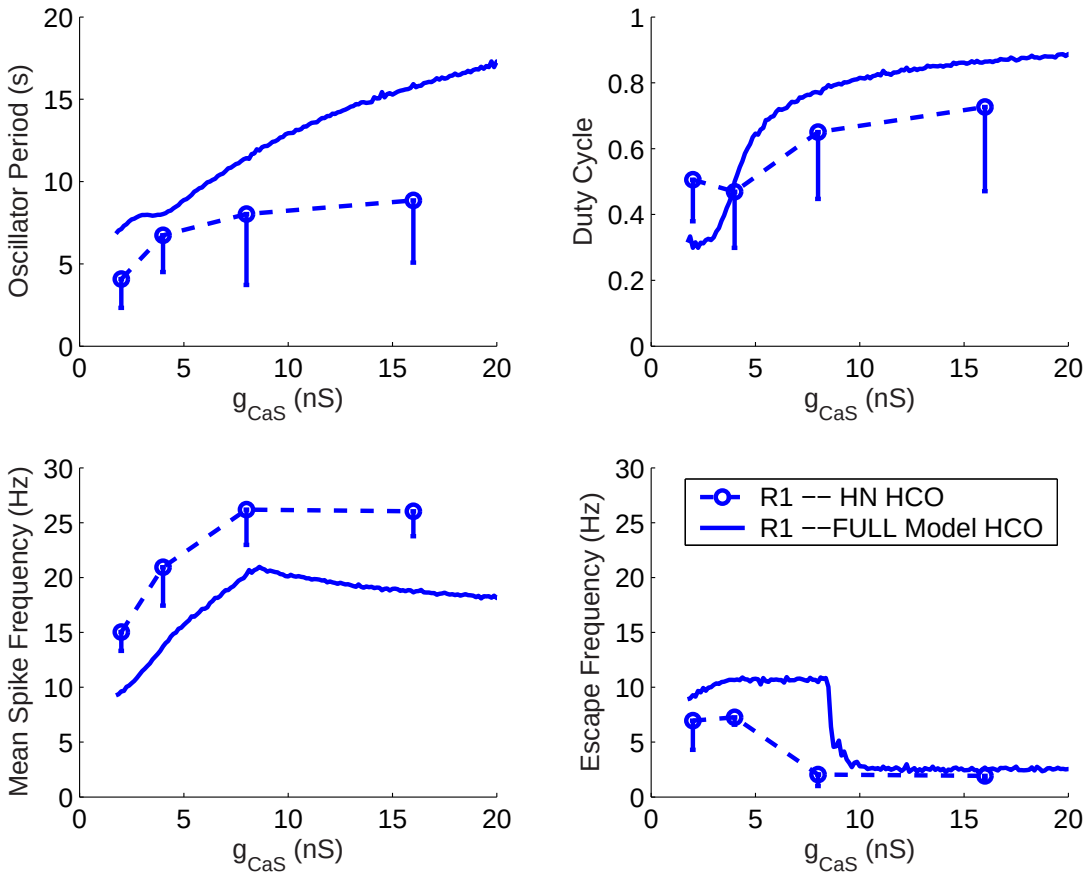

Figure 46: $\bar{g}_{CaS}$ in R1 hybrid HCO.

The activity observed in the hybrid system is similar to that observed in the modeling studies (Figure 47). As in the model, large values of $\bar{g}_{CaS}$ cause the "plateau-like" oscillations in the model, where the model becomes so depolarized that it cannot fire.

Overall, the results from our HN – R1 hybrid system are very similar to what we expect from our modeling studies of the FULL – R1 model oscillator.

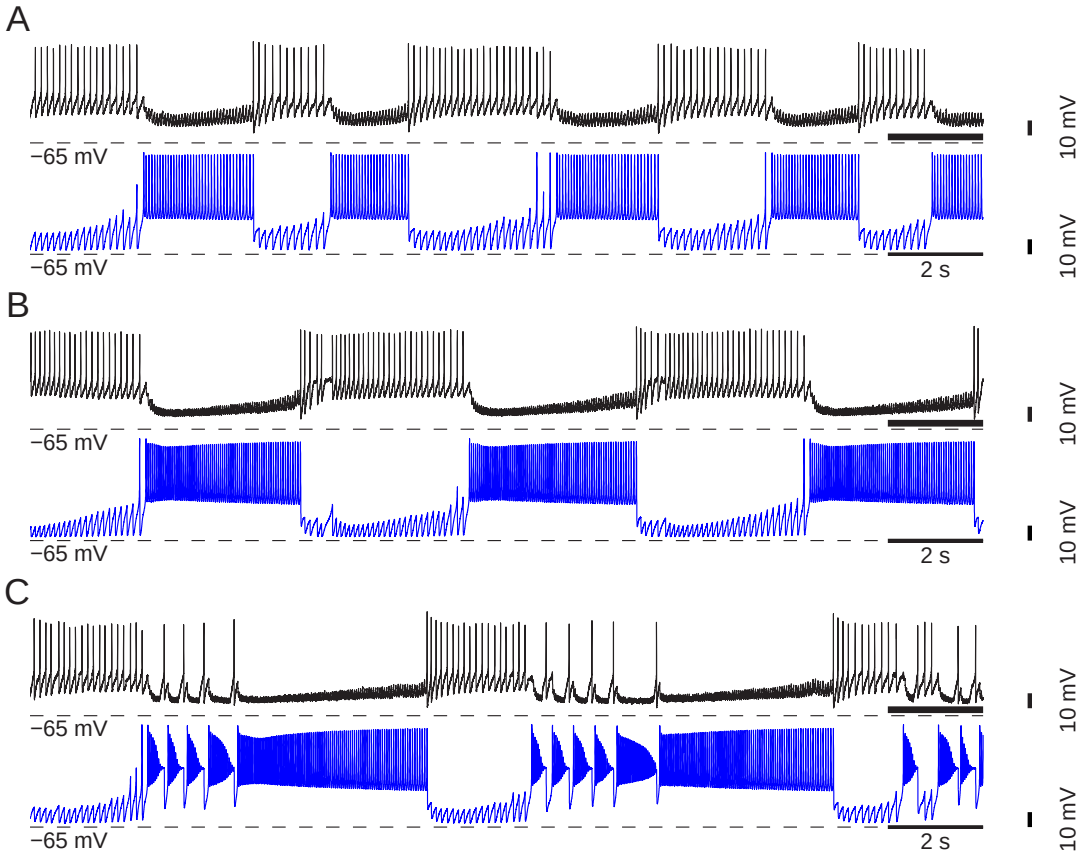

Figure 47: Hybrid oscillations with the R1 model. V_m of the heart interneuron is shown in black. V_m of the R1 model neuron is shown in blue. **A.** $\bar{g}_{CaS}$ = 2nS **B.** $\bar{g}_{CaS}$ = 4 nS (canonical value for R1 model) **C.** $\bar{g}_{CaS}$ = 8 nS.

4.3.3 $\bar{g}_{CaS}$ in the R2 model.

With canonical parameters ($\bar{g}_{CaS}$ = 5.375 nS), the R2 hybrid half-center oscillator produced rhythmic oscillations in all four experiments. The period was 9.7 ± 2.7 s, the duty cycle was 0.59 ± 0.11, and the mean spike frequency was 32.5 ± 3.2 Hz. The escape frequency of the R2 neuron was 6.2 ± 1.4. The period and mean spike frequency were all significantly higher in the HN – R2 oscillator than in the HN – R1 hybrid oscillator; this increase, however, is predicted by modeling. The mean duty cycle was higher for the HN – R2 hybrid oscillator than in the HN – R1 hybrid oscillator, and the escape frequency was lower; these differences, however, were not statistically significant.

The R2 hybrid half-center oscillator behaved very differently from the R1 hybrid half-center (Figure 48). As predicted by the modeling studies, the R2 hybrid system did not produce half-center oscillations when $\bar{g}_{CaS}$ = 2 nS. Increasing $\bar{g}_{CaS}$ from 4 to 5.375 nS caused a slight decrease in the period of oscillations, and increasing $\bar{g}_{CaS}$ to 8 nS caused a slight increase in the oscillator period; neither of these changes were statistically significant, however. In the model oscillator, increasing $\bar{g}_{CaS}$ from 8 to 16 nS, caused a large increase in the oscillator period. In the hybrid oscillator the oscillations also increased, but not to the extent predicted by modeling.

As $\bar{g}_{CaS}$ was increased from 4 to 8 nS, the duty cycle of the R2 neuron increased, in a manner very similar to the duty cycle predicted by our modeling studies. Increasing $\bar{g}_{CaS}$ from 4 to 5.375 nS and from 5.375 to 8 nS caused a statistically significant increase in the duty cycle. There was no statistically significant change in the duty cycle between 8 and 16 nS.

Increasing $\bar{g}_{CaS}$ caused a large increase in the mean spike frequency of the R2 neuron. As in the HN – R1 hybrid oscillator, the mean spike frequency of the reduced model neuron in the hybrid oscillator was much higher than that predicted by the model oscillator. This difference is especially noticeable for $\bar{g}_{CaS}$ = 16 nS. This very high spike frequency is undoubtedly due to the fact that, in the R1 model, the conductance-based spiking mechanisms

place a limit on the maximum firing rate the neuron; without sufficient time to remove inactivation from I_{Na}, there is no way the neuron can fire another spike. This firm limit in the inter-spike interval is often referred to as the *absolute refractory period* of the neuron. When the conductance-based spiking mechanisms are replaced by IAF mechanisms, however, there is no such limit to the spike frequency; V_{m} only needs to exceed V_{thresh} in order for a spike to occur. Thus, with an large increase in the depolarizing current I_{CaS}, the neuron fires at a very high frequency, and the mean spike frequency of the R2 neuron increases substantially with increasing $\bar{g}_{\mathrm{CaS}}$.

Overall, the escape frequency of the R2 neuron is lower than that predicted by modeling. Overall, there is little change in the escape frequency as $\bar{g}_{\mathrm{CaS}}$ is increased. Although, increasing $\bar{g}_{\mathrm{CaS}}$ from 4 to 5.375 nS does cause a significant increase in the escape frequency of the R2 neuron, there was no statistically significant difference in the escape frequency when $\bar{g}_{\mathrm{CaS}}$ was increased above 5.375 nS.

Overall, the oscillations observed in the HN – R2 hybrid oscillator were very similar to what we observed in the FULL – R2 model oscillator (Figure 49). The period remains relatively constant as $\bar{g}_{\mathrm{CaS}}$ increases, while the duty cycle of the R2 model neuron noticeably increases.

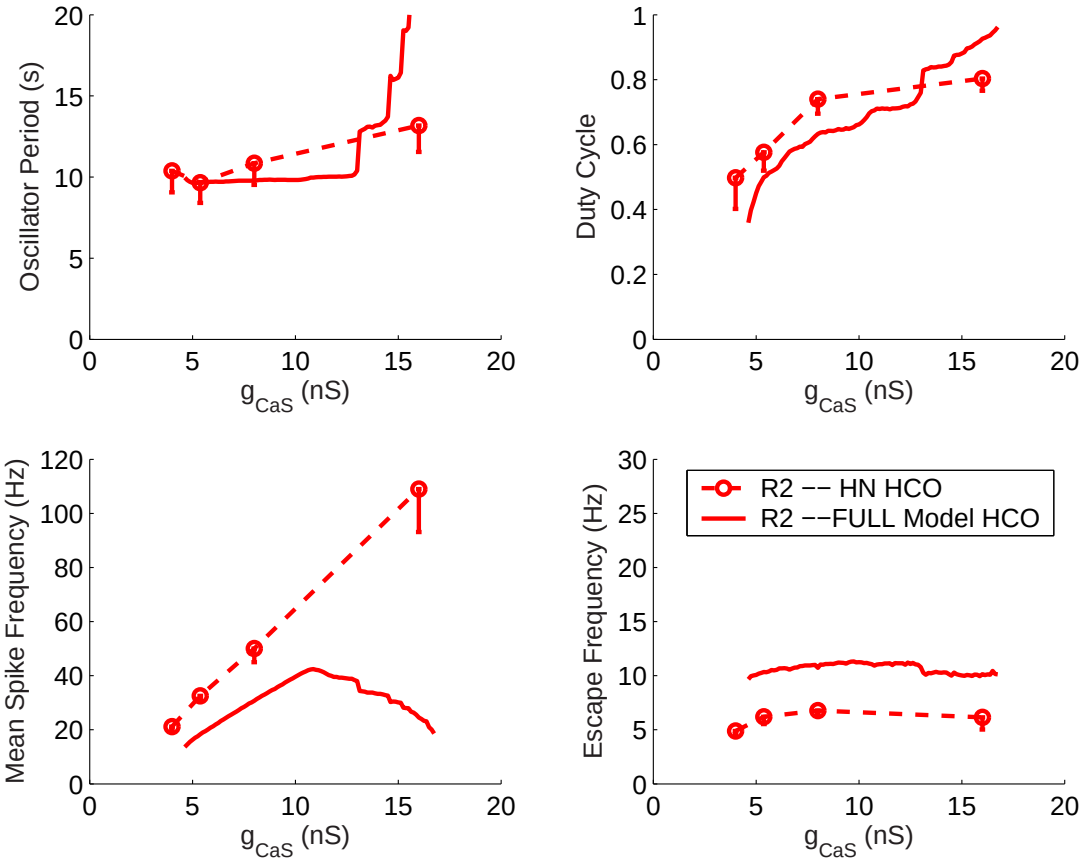

Figure 48: $\bar{g}_{\mathrm{CaS}}$ in R2 hybrid HCO.

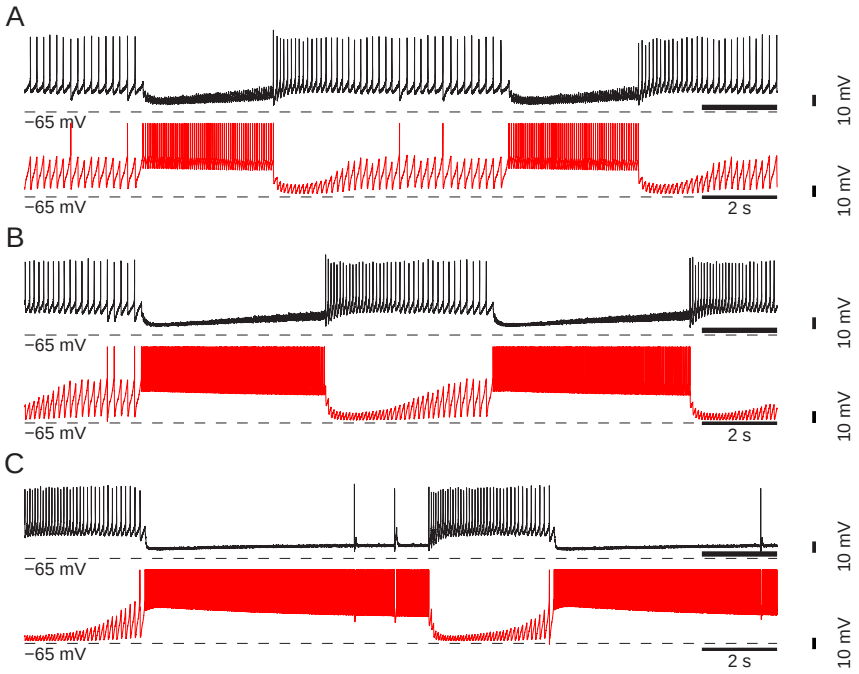

Figure 49: Hybrid oscillations with the R2 model. V_{m} of the heart interneuron is shown in black. V_{m} of the R2 model neuron is shown in red. Unlike the R1 model, half-center oscillations were not produced when $\bar{g}_{\mathrm{CaS}} = 2\mathrm{nS}$. **A.** $\bar{g}_{\mathrm{CaS}} = 4\mathrm{nS}$ **B.** $\bar{g}_{\mathrm{CaS}} = 5.375$ nS (canonical value for R2 model) **C.** $\bar{g}_{\mathrm{CaS}} = 8$ nS.

4.3.4 Discussion

These experiments provide validation of our reduced models. As was predicted from our modeling studies, both the R1 and R2 model neuron were able to create realistic half-center oscillations when coupled to a living neuron. Furthermore, the relationships between $\bar{g}_{\text{CaS}}$ and oscillator period, duty cycle, and spike frequency characteristics were correctly predicted by our modeling studies.

The R1 hybrid oscillator functioned when $\bar{g}_{\text{CaS}}$ of the R1 model was set to 2 nS; the R2 hybrid oscillator did not. This result indicates that there is indeed some constriction of the system's input space when the model is reduced. As was the case with our modeling studies, however, we must admit that our experiments did not address the parameter space in holistic fashion. $\bar{g}_{\text{CaS}}$ was the sole parameter varied; the parameters of the heart interneuron are, of course, unknown.

As we observed in our hybrid experiments in Chapter 2, the absolute values for the period, duty cycle, and spike frequency characteristics in our hybrid system are not what we expect from our modeling studies. The *trend* of the these characteristics as $\bar{g}_{\text{CaS}}$ is varied, however, is correctly predicted by the modeling studies. It appears, therefore, that the functional role of $\bar{g}_{\text{CaS}}$ in the hybrid oscillators is correctly represented by our model oscillators.

4.4 Symmetric Half-Center Oscillators

The asymmetric half-center oscillators used in the previous studies are a useful tool to analyze and understand how reduced neuron models might behave in a hybrid half-center oscillator. The asymmetric parameter variation showed that model reduction had little effect on the functional range of parameters in the FULL model of the asymmetric oscillator, but did reduce the functional range of $\bar{g}_{\text{CaS}}$ and $\bar{g}_{\text{leak}}$ parameters in the reduced model of the asymmetric oscillators. The overall flexibility of the model, however, did not noticeably change as the model was reduced.

There is a seeming contradiction in this result: although the size of the input space is noticeably reduced by model reduction, the apparent size of the output space is not. It is therefore possible that the presence of the FULL model neuron in the asymmetric model oscillators acts to maintain the flexibility of the oscillators as its partner is reduced.

In order to test this hypothesis, we constructed three *symmetric* half-center oscillators for each of the three reduced models; we then asymmetrically varied $\bar{g}_{\mathrm{CaS}}$, $\bar{g}_{\mathrm{h}}$, and g_{leak}, as we did with the asymmetric half-center oscillators. Although these models do not provide a direct comparison with hybrid oscillators, they provide an insight into the functional role of complexity that is important in development of hybrid systems: if the presence of additional complexity in a model system helps to stabilize the robustness and flexibility of that system, that additional complexity provided by a biological neuron may serve to accomplish the same function in a hybrid system.

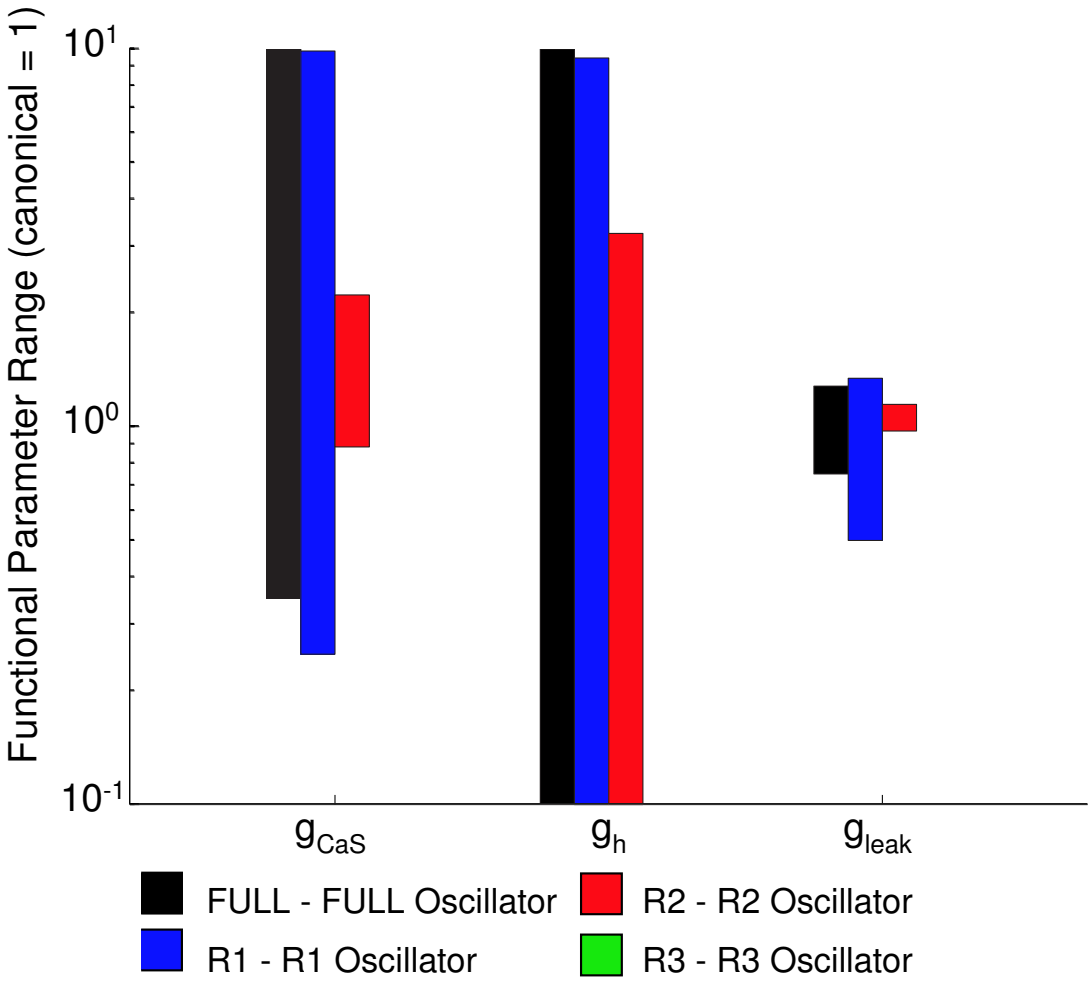

Figure 50: Functional parameter ranges for symmetric oscillators. Each bar shows the functional range of the parameter in the reduced models over which the system produces half-center oscillations.

Robustness

The parameter ranges over which the symmetric reduced oscillators produce oscillations are shown in Figure 50. Robustness scores are given in Table 5. In the case of the R3 – R3 model network, half-center oscillations were not produced with canonical parameter values. It was possible to produce half-center oscillations by increasing g_{leak} in both neurons of the oscillator, but because this change would be a departure from our previous studies we chose not to do so.

As was the case with parameter variation in the reduced model of the asymmetric half-center oscillators, decreasing model complexity from the R1 to the R2 model causes an

Table 5: Robustness scores for parameter variation in symmetric oscillator models. For each conductance, the parameter score is equal to $50 \times \log(p_{max}/p_{min})$ where p_{max} and p_{min} are the maximum and minimum of the parameter range over which the oscillator function. A score of 100 indicates that the oscillator operates from .1 to 10 times the canonical parameter value.

Parameter	Full – Full HCO	R1 – R1 HCO	R2 – R2 HCO	R3 – R3 HCO
$\bar{g}_{\text{CaS}}$	72.7	79.8	20.1	—
$\bar{g}_{\text{h}}$	100.0	100.0	75.6	—
g_{leak}	11.6	21.4	3.5	—

overall decrease in the ranges of the parameters where the model produces half-center oscillations. Interestingly, the R1 – R1 oscillator appears to be slightly more robust than the FULL – R1 osicllator. Furthermore, the robustness of the oscillator to variations in $\bar{g}_{\text{CaS}}$ and g_{leak} increases in the R1 – R1 oscillator as compared to the FULL – FULL oscillator. In the R2 – R2 oscillator, the robustness of the system to $\bar{g}_{\text{CaS}}$, $\bar{g}_{\text{h}}$, and g_{leak} are all decreased with respect to the FULL – R2 oscillator, indicating that for the R2 model, the presence of the FULL model in the oscillator serves to increase the robustness of the system.

Flexibility

The results our flexibility assessment are shown in Figure 51. In the FULL – FULL oscillator, six principal components were needed to account for 95% of the variance data. In the R1 – R1 oscillator, five principal components were needed to account for 95% of the variance in the data. In the R2 – R2 oscillator, 95% of the data were explained by slightly more than four principal components. These results are noticeably different than for the asymmetric reduced oscillators. In the asymmetric reduced oscillators, there was little change in the flexibility of the model as the model was reduced. In the symmetric oscillators, however, decreasing model complexity causes a noticeable decrease in the number of principal components needed to explain 95% of the variance in the data; the flexibility of the model is noticeably reduced for the reduced model oscillators. In addition, the flexibility of the R1 – R1 and R2 – R2 oscillators are lower than their asymmetric counterparts.

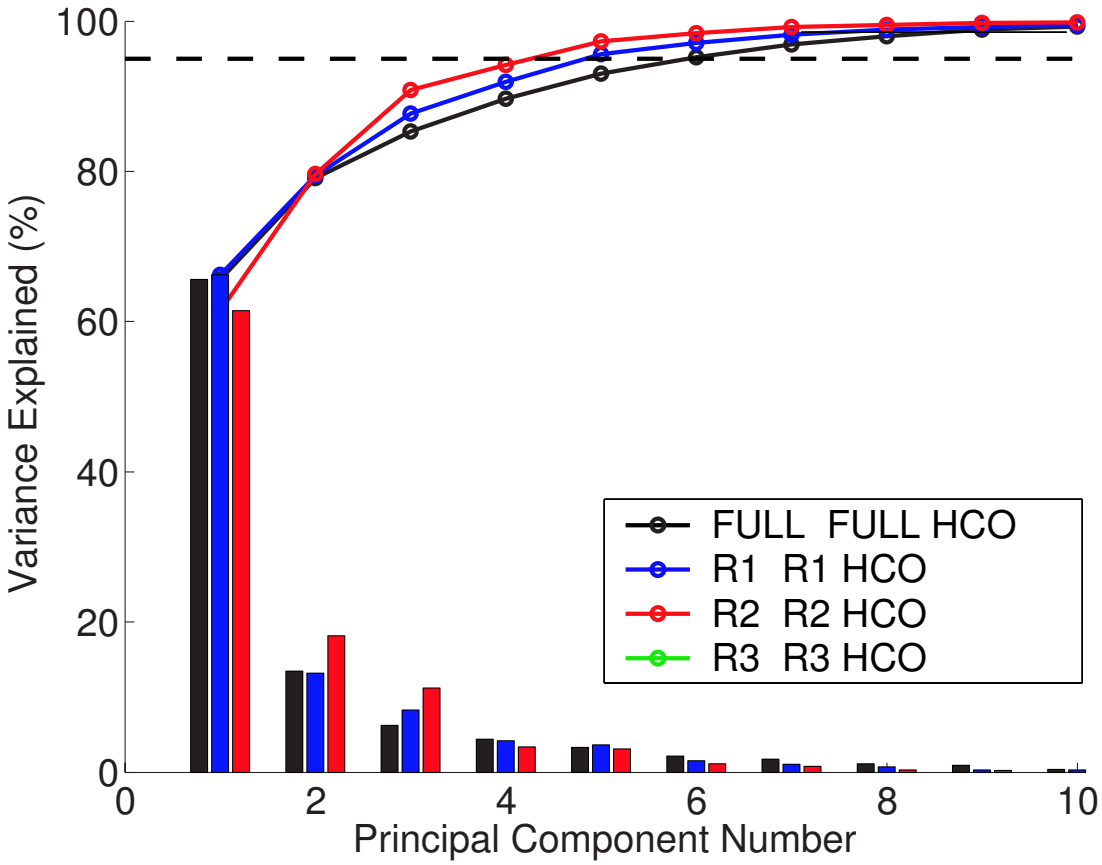

Figure 51: Flexibility assessment for parameter variation in FULL model. Bars represent the percent of variance explained by each principal component; lines indicate the total percent of variance explained by the previous principal components. The dashed line indicates the level where 95% of the variance is explained.

Discussion

The functional affects of model complexity are more apparent in the symmetric oscillators than in the asymmetric oscillators. Replacing the physiologic spiking mechanisms with IAF mechanisms causes a significant decrease in the robustness of the system. In the case of the R3 – R3 oscillator, this decrease in robustness is so severe that the canonical parameter point no longer lies within the system's functional input space. It is interesting to note, however, that the R1 – R1 oscillator is more robust than both the FULL – FULL oscillator and the FULL – R1 oscillator. In this case, model reduction appears to increase the size of the system's functional input space.

CHAPTER V

CONCLUSIONS

The goal of hybrid systems research is to develop systems that reproduce the function of biological neural networks, either for the treatment of injury or disease, or for the creation of engineered constructs that use neural properties for computation or interaction with the physical world. In these systems, the living neurons provide the complex dynamics and functionality that are necessary to reproduce biological phenomena, whereas the model provides a means to manipulate and control the system. In order for these systems to function, however, the the engineered component must be able to correctly interpret signals from the nervous system, and produce signals that are functionally relevant to the nervous system.

We have developed a hybrid half-center oscillator that consists of a single model neuron coupled to a single biological neuron. The relative simplicity of this system allowed us to ask fundamental questions regarding the role of neuronal mechanisms and model complexity in the generation of neuronal activity. We have shown how a single neuronal property can be used to control the activity of the system. We have shown how the hybrid system can be used to validate neuronal models. Finally, we have shown how the complexity of the model affects the robustness and flexibility of the system. These three findings are important for the development of next-generation hybrid systems in which neuronal models will interact with larger-scale neural networks.

5.1 Regulation of Neuronal Network Activity by an Intrinsic Current

Biological neural networks regulate their activity through numerous mechanisms. Ionic currents, 2nd-messenger systems, and the transcription of proteins all play a role in determining how the nervous system behaves. In order to create engineered constructs that can be used to modulate or control the activity of biological neural networks, it is critical to understand how biological neural modulate and control their own activity.

Our hybrid system provides a novel method for investigating the role of neuronal properties in the generation of neural activity. The model provides a degree of control over neuronal properties that is not possible with traditional techniques. The biological component, however, provides a degree of realism and relevance that is much greater than with modeling alone. By utilizing a physiologically realistic model in our hybrid system, we can draw very strong conclusions about how neural networks can modulate their activity using neuronal properties.

We investigated how the ionic current I_{h} regulates the activity of a half-center oscillator. Increasing $\bar{g}_{\mathrm{h}}$, the maximal conductance of I_{h}, caused the period of oscillations to decrease. The decrease in oscillator period was caused by a decrease in the inhibited phase of the modified neuron, indicating that I_{h} preferentially affects the inhibited phase of the oscillation. Furthermore, we demonstrated that $\bar{g}_{\mathrm{h}}$ determines the frequency of spike-mediated synaptic inhibition at which an inhibited cell escapes from inhibition; this finding demonstrates how I_{h} can be used to regulate the relationship between two cells in a half-center oscillator.

The findings of this study are important both to biologists and engineers. Identifying the effects of neuronal properties on the activity of neural networks improves our understanding of the nervous system. Identifying mechanisms that can be used to modulate or control the activity of neural networks improves our ability to develop functionally useful hybrid systems.

5.2 Validation of Neuronal Models with Hybrid Systems

Much of our understanding of the nervous system is based on studies using mathematical neuron models. A neural model provides a degree of access and controllability that is impossible with a biological neuron or neural network. Of course, the mathematical model simplifies many properties of the biological system; a critical concern in neural modeling is whether or not the model is valid representation of the biological system.

Hybrid systems are an invaluable tool for validating neuronal models. In a traditional modeling paradigm, a model is validated by reproducing a particular characteristic of the biological system; the model is then used to make predictions about the biological system itself. Hybrid systems provide a means to further validate the predictions of the model. By operating the model system in concert with a biological system, the idealizations of modeling are tempered by the reality of biology. If a particular mechanism effects both the model system and the hybrid system in a similar fashion, we can be reasonably well assured that the model correctly describes the function of that mechanism.

We validated the results of modeling in three separate hybrid systems protocols. In the first set of experiments, we examined the effect of $\bar{g}_{\mathrm{h}}$ in a mechanistic mathematical model of a half-center oscillator, and validated this study using a hybrid half-center that incorporated a silicon model neuron that was a reduced version of the mathematical model. In addition, we induced changes in the living neuron to demonstrate that the model neuron and the living neuron were operating in symmetry. In the second set of experiments, we examined the role of $\bar{g}_{\mathrm{CaS}}$ in an asymmetric model half-center oscillator; in these studies, a reduced mechanistic neuron model was coupled to a more complex mechanistic model. We then validated these studies using a hybrid half-center oscillator composed of a living neuron and the reduced mechanistic model neuron. In our final set of experiments, we studied the affect of $\bar{g}_{\mathrm{CaS}}$ in an asymmetric model half-center oscillator that was composed of a complex mechanistic model neuron and a simplified, semi-empirical model neuron. We then validated these studies using a hybrid half-center oscillator composed of a living

neuron and the simplified semi-empirical model neuron.

All of our hybrid systems experiments validated the results of modeling. Although the absolute values of certain oscillator characteristics (such as period, duty cycle, and spike frequencies) were different in our hybrid experiments and modeling studies, the effect of parameter variations on these characteristics was the same. For example, although the period of the hybrid oscillator was less than the period of the mathematical model oscillator, increasing $\bar{g}_{\mathrm{h}}$ caused the period to decrease in each of these systems. This validation increases our confidence in the conclusions drawn from our models.

5.3 The Functional Role of Model Complexity

One of the most critical decisions in developing a hybrid system is the decision of how complex the model component needs to be in order to produce a functional system when coupled to the biological component. A more complex model might accurately reproduce the behavior of biology, but may be so complex as to render it unusable. A simple model, however, might be easily understood, yet may not provide enough accuracy to create an effective system.

Biological neural systems are presumed to be both robust and flexible. Robustness describes the ability of the system to function despite variable inputs. For example, the presence of increased levels of nicotine in the brain does not affect the ability of a person to perform motor functions. The motor system could therefore be said to be robust to changes in nicotine concentration. Flexibility describes the ability of the system to produce different outputs in order to achieve its function. For example, a person's motor system produces different patterns of muscle activation depending on whether or not the person is walking, jogging, or running. The function of the system, moving the person forward, can be achieved using different outputs.

In order to evaluate how model complexity might effect the robustness and flexibility of hybrid systems, we created three asymmetric model half-center oscillators; in each of

these model oscillators, a complex mechanistic model neuron was coupled to a reduced model neuron. In addition, in order to evaluate the effects of model complexity in model systems, we created three symmetric model half-center oscillators; in each of these model oscillators, a reduced model neuron was coupled to an identical reduced model neuron.

We assumed that the function of a half-center oscillator is to produce half-center oscillations. We assessed the robustness of these oscillators by determining the parameter ranges of the maximal conductances over which the model systems produced half-center oscillations. We assessed the flexibility of our oscillators by performing a principal component analysis on the output measures of oscillator activity. We judged that the more variance there was between the measures of oscillator activity, the more flexible the system was.

Although decreasing model complexity did not appear to have any consistent effect on the robustness of the asymmetric oscillators when parameters were varied in the complex model, it did reduce the robustness of system when parameters were varied in the simplified models. In the symmetric oscillators, reducing the model complexity caused a reduction in the system's robustness. In our asymmetric oscillators, there was little change in the overall flexibility of the system as the model complexity was reduced. In our symmetric oscillators, however, decreasing the model complexity caused a decrease in the overall flexibility of the system.

Our original hypothesis was that model complexity serves to increase system robustness and flexibility. Our modeling studies appear to support our original hypothesis. There are, however, several caveats to this conclusion.

5.4 Future Research Directions

The findings reported here bode well for the development of hybrid systems. They demonstrate the utility of these systems for biological investigations. They demonstrate that the findings of neural modeling can be confidently applied to hybrid systems. Finally, they demonstrate that even simplified models can be used to create realistic activity in hybrid

systems, although their is a trade-off in system performance as model complexity is decreased. We envision that this research can be refined through two developments: a more global analysis of neuronal models, and improved metrics for evaluating model performance.

The studies presented here investigated only a small portion of the systems' parameter space. All of our parameter sweeps were conducted in one dimension off of a single canonical parameter point. To more fully gauge the effect of model reduction on the model's parameter space, we would either need to map out a set of canonical parameter points — distinct points in parameter space where the model produces the canonical output — or conduct a multi-dimensional parameter sweep — simultaneously varying the parameters of the oscillator instead of one parameter at a time. Either of these approaches, however, would require more computational resources than we were provided in this study. Future research studies should develop the computational resources that will allow a more global analysis of the system to be performed.

The metrics we utilized to evaluate system robustness and flexibility were useful as a first-order measure of system performance. Improved metrics are possible, however. Of primary importance is the development of methods to assess what features of the activity are important to the system. For example, we evaluated flexibility based on the relationships between measures of spike timing and membrane potential. It is likely, however, that other measures, such as the shape of spikes or slow-wave potentials, are more important to the functionality of the system. More work will need to be done in order to evaluate what features are most important to the functionality of the system.

The research presented here has provided a critical step in the development of hybrid systems for biomedical and neuromorphic applications. Continued research will serve to increase the applicability and importance of these systems.

REFERENCES

[1] Angstadt, J. and Calabrese, R., "A hyperpolarization-activated inward current in heart interneurons of the medicinal leech.," *J Neurosci*, vol. 9, no. 8, pp. 2846–57, 1989.

[2] Breen, B., Gerken, W., and Butera, R., "Hybrid Integrate-and-Fire Model of a Bursting Neuron," *Neural Computation*, no. 15, pp. 2843–2862, 2003.

[3] Butera, Jr, R., Clark, Jr, J., and Byrne, J., "Dissection and reduction of a modeled bursting neuron.," *J Comput Neurosci*, vol. 3, no. 3, pp. 199–223, 1996.

[4] Cymbalyuk, G. S., Gaudry, Q., Masino, M. A., and Calabrese, R. L., "Bursting in Leech Heart Interneurons: Cell-Autonomous and Network-Based Mechanisms," *J. Neurosci.*, vol. 22, no. 24, pp. 10580–10592, 2002.

[5] Cymbalyuk, G., Sorensen, M., Simoni, M., DeWeerth, S., and Calabrese, R., "Software tools for hybrid systems analysis.," *Society for Neuroscience Annual Meeting*, 2002.

[6] Derjean, D., Bertrand, S., Le Masson, G., Landry, M., Morisset, V., and Nagy, F., "Dynamic balance of metabotropic inputs causes dorsal horn neurons to switch functional states.," *Nat Neurosci*, vol. 6, no. 3, pp. 274–81, 2003.

[7] Douglas, R. and Rasche, C., *Silicon Neurons*. MIT, 2002.

[8] Fitzhugh, R., "Impulses and physiological stages in theoretical models of nerve membrane.," *Biophys J*, vol. 1, pp. 445–466, 1961.

[9] Goldman, M., Golowasch, J., Marder, E., and Abbott, L., "Global structure, robustness, and modulation of neuronal models.," *J Neurosci*, vol. 21, no. 14, pp. 5229–38, 2001.

[10] Golomb, D., Guckenheimer, J., and Gueron, S., "Reduction of a channel-based model for a stomatogastric ganglion LP neuron.," *Biological Cybernetics*, vol. 69, pp. 129–137, 1993.

[11] Golowasch, J., Goldman, M., Abbott, L., and E, M., "Failure of averaging in the construction of a conductance-based neuron model.," *J Neurophysiol*, no. 87, pp. 1129–1131, 2002.

[12] Graas, E., Brown, E., and Lee, R., "An fpga-based approach to high-speed simulation of conductance-based neuron models.," *Neuroinformatics*, vol. 2, no. 4, 2004.

[13] Graas, E., "Exploration of alternative to general-purpose computers in neural simulation," master's thesis, Georgia Institute of Technology, 2003. methods.

[14] Hill, A., Lu, J., Masino, M., Olsen, O., and Calabrese, R., "A model of a segmental oscillator in the leech heartbeat neuronal network.," *J Comput Neurosci*, vol. 10, no. 3, pp. 281–302, 2001.

[15] Hill, A., Masino, M., and Calabrese, R., "Model of intersegmental coordination in the leech heartbeat neuronal network.," *J Neurophysiol*, vol. 87, no. 3, pp. 1586–602, 2002.

[16] Hodgkin, A. and Huxley, A., "A quantitative description of membrane current and its application to conduction and excitation in nerve," *J. Physiol.*, vol. 117, pp. 500–544, 1952.

[17] Izhikevich, E., "Resonate-and-fire neurons.," *Neural Netw*, vol. 14, no. 6-7, pp. 883–94, 2001.

[18] Kepler, T., Abbott, L., and Marder, E., "Reduction of conductance-based neuron models.," *Biol Cybern*, vol. 66, no. 5, pp. 381–7.

[19] Lapicque, L., "Recherches quantitatives sur l'excitation electriquedes nerfs traitee comme une polarization.," *J Physiol (Paris)*, vol. 9, pp. 620–635, 1907. This is the original integrate-and-fire paper.

[20] Le Masson, G., Le Masson, S., and Moulins, M., "From conductances to neural network properties: analysis of simple circuits using the hybrid system method.," *Prog. Biophys. molec. Biol.*, vol. 64, no. 2/3, pp. 201–220, 1995.

[21] Le Masson, G., Renaud-Le Masson, S., Debay, D., and Bal, T., "Feedback inhibition controls spike transfer in hybrid thalamic circuits.," *Nature*, vol. 417, no. 6891, pp. 854–8.

[22] LeMasson, G. and Maex, R., *Introduction to Equation Solving and Parameter Fitting*. Boca Raton: CRC Press, 2001.

[23] Luthi, A. and McCormick, D., "H-current: properties of a neuronal and network pacemaker.," *Neuron*, vol. 21, no. 1, pp. 9–12.

[24] MacLean, J., Zhang, Y., Johnson, B., and Harris-Warrick, R., "Activity-independent homeostasis in rhythmically active neurons.," *Neuron*, vol. 37, no. 1, pp. 109–20.

[25] Mahowald, M. and Douglas, R., "A silicon neuron," *Nature*, vol. 354, no. 6354, pp. 515–518, 1991.

[26] Manor, Y. and Nadim, F., "Synaptic depression mediates bistability in neuronal networks with recurrent inhibitory connectivity.," *J Neurosci*, vol. 21, no. 23, pp. 9460–70.

[27] Marder, E. and Calabrese, R., "Principles of rythmic motor pattern generation," *Physiol. Review*, vol. 76, pp. 687–717, 1996.

[28] Morris, C. and Lecar, H., "Voltage oscillations in the barnacle giant muscle fiber.," *Biophys J*, vol. 35, no. 1, pp. 193–213.

[29] Nadim, F. and Manor, Y., "Frequency regulation demonstrated by coupling a model and a biological neuron," *Neurocomputing*, vol. 38-40, pp. 269–278, 2001.

[30] Nagumo, J., Arimito, S., and Yoshizawa, S., "An active pulse transmission line simulating nerve axon.," *Proc IRE*, vol. 50, pp. 2061–2070, 1962.

[31] Olsen, O. and Calabrese, R., "Activation of intrinsic and synaptic currents in leech heart interneurons by realistic waveforms.," *J Neurosci*, vol. 16, no. 16, pp. 4958–70.

[32] Pape, H., "Queer current and pacemaker: the hyperpolarization-activated cation current in neurons.," *Annu Rev Physiol*, vol. 58, pp. 299–327.

[33] Patel, G. and DeWeerth, S., "Analogue vlsi moris-lecar neuron," *Electronics Letters*, vol. 33, no. 12, pp. 997–998, 1997.

[34] Patel, G. and DeWeerth, S., "Bifurcation analysis of a silicon neuron.," *Advances in Neural Information Processing Systems*, 2000.

[35] Potter, S. and DeMarse, T., "A new approach to neural cell culture for long-term studies.," *J. Neurosci. Methods*, vol. 110, pp. 17–24, 2001.

[36] Prinz, A., Billimoria, C., and Marder, E., "Alternative to hand-tuning conductance-based models: construction and analysis of databases of model neurons.," *Journal of Neurophysiology*, vol. 90, pp. 3998–4015, 2003.

[37] Prinz, A., Bucher, D., and Marder, E., "Similar network activity from disparate circuit parameters.," *Nature Neuroscience*, pp. 1345–1352, November 2004.

[38] Renaud-LeMasson, S., LeMasson, G., Marder, E., and Abbott, L., "Hybrid Circuits of Interacting Computer Model and Biological Neurons," in *Neural Information Processing Systems 5*, (San Mateo, CA), pp. 813–819, Morgan Kauffman, 1993.

[39] Robinson, R. and Siegelbaum, S., "Htperpolarization-activated cation currents: from molecules to physiological function.," *Annu Rev Physiol*, vol. 65, pp. 453–80.

[40] Selverston, A., Rabinovich, M., Abarbanel, H., Elson, R., Szucs, A., Pinto, R., Huerta, R., and Varona, P., "Reliable circuits from irregular neurons: a dynamical approach to understanding central pattern generators.," *J Physiol Paris*, vol. 94, no. 5-6, pp. 357–74.

[41] Sharp, A., O'Neil, M., Abbott, L., and Marder, E., "Dynamic clamp: computer-generated conductances in real neurons.," *J Neurophysiol*, vol. 69, no. 3, pp. 992–5.

[42] Sharp, A., Skinner, F., and Marder, E., "Mechanisms of oscillation in dynamic clamp constructed two-cell half-center circuits.," *J Neurophysiol*, vol. 76, no. 2, pp. 867–83.

[43] Simoni, M. F., Cymbalyuk, G. S., Sorensen, M. E., Calabrese, R. L., and DeWeerth, S. P., "A Multiconductance Silicon Neuron With Biologically Matched Dynamics," *IEEE Trans. Biomed. Eng.*, vol. 51, pp. 342–354, 2004.

[44] Simoni, M. F., Cymbalyuk, G. S., Sorensen, M. Q., Calabrese, R. L., and DeWeerth, S. P., "Development of Hybrid Systems: Interfacing a Silicon Neuron to a Leech Heart Interneuron," in *Neural Information Processing Systems 13*, (Cambridge, MA), MIT Press, 2000.

[45] Skinner, F., Kopell, N., and Marder, E., "Mechanisms for oscillation and frequency control in reciprocally inhibitory model neural networks.," *J Comput Neurosci*, vol. 1, no. 1-2, pp. 69–87.

[46] Sorensen, M., Cymbalyuk, G., DeWeerth, S., and R, C., "Using a hybrid neural system to reveal regulation of neuronal network activity by an intrinsic current," *Journal of Neuroscience*, vol. 24, no. 23, pp. 5427–5438, 2004.

[47] Szucs, A., Varona, P., Volkovskii, A., Abarbanel, H., Rabinovich, M., and Selverston, A., "Interacting biological and electronic neurons generate realistic oscillatory rhythms.," *Neuroreport*, vol. 11, no. 3, pp. 563–9.

[48] Yarom, Y., "Rhythmogenesis in a hybrid system–interconnecting an olivary neuron to an analog network of coupled oscillators.," *Neuroscience*, vol. 44, no. 2, pp. 263–75.

VITA

Michael Sorensen was born in Lakeland, FL. He lived in Utah, British Columbia, and Arizona before finally settling down in Roswell, GA at the age of eight. There he spent a magical childhood surrounded by a loving family and several wonderful dogs. He attended Roswell High School from 1991-1995, and failed to do anything there that warranted any attention whatsoever. He left Roswell in 1995 to attend Rice University in Houston, TX. He served as the president of Jones College at Rice from 1998-1999, and also worked as a research assistant at Baylor College of Medicine. He graduated Rice in 1999 with a BS in electrical engineering. He began his post-graduate career in 1999 at Georgia Institute of Technology in Atlanta, GA. He received his PhD in bioengineering from Georgia Tech in 2005. On August 4, 2001, he somehow managed to convince a beautiful, intelligent, and charming woman to spend the rest of her life with him. At the time of this writing they live in Asheville, NC, where they have a house and a dog named Molly.